NASA TECHNICAL NOTE

NASA TN D-7935

BUCKLING TESTS OF THREE 4.6 METER DIAMETER ALUMINUM HONEYCOMB SANDWICH CONICAL SHELLS LOADED UNDER EXTERNAL PRESSURE

James Kent Anderson and Randall C. Davis

Langley Research Center
Hampton, Va. 23665

NATIONAL AERONAUTICS AND SPACE ADMINISTRATION • WASHINGTON, D. C. • JULY 1975

1. Report No. NASA TN D-7935	2. Government Accession No.	3. Recipient's Catalog No.
4. Title and Subtitle BUCKLING TESTS OF THREE 4.6-METER-DIAMETER ALUMINUM HONEYCOMB SANDWICH CONICAL SHELLS LOADED UNDER EXTERNAL PRESSURE		5. Report Date July 1975 6. Performing Organization Code
7. Author(s) James Kent Anderson and Randall C. Davis		8. Performing Organization Report No. L-9936
9. Performing Organization Name and Address NASA Langley Research Center Hampton, Va. 23665		10. Work Unit No. 505-02-42-01 11. Contract or Grant No.
12. Sponsoring Agency Name and Address National Aeronautics and Space Administration Washington, D.C. 20546		13. Type of Report and Period Covered Technical Note 14. Sponsoring Agency Code

15. Supplementary Notes

16. Abstract

Three aluminum honeycomb sandwich conical shells with a 120^{o} apex angle and a 4.6-m (15.0-ft) base diameter were loaded to failure by a uniform external pressure. The cones differed from one another only in the thickness of their respective face sheets. Test specimen details, test procedure, and test results are discussed. Both buckling and prebuckling data are compared with appropriate theoretical predictions. Good agreement was obtained between test and theory. Extensive imperfection measurements were made and reported on the three cones in the "as fabricated" condition.

17. Key Words (Suggested by Author(s)) Shells Buckling Cones Honeycomb sandwich Aluminum Imperfections Ring-stiffened cones	18. Distribution Statement Unclassified – Unlimited New Subject Category 39		
19. Security Classif. (of this report) Unclassified	20. Security Classif. (of this page) Unclassified	21. No. of Pages 100	22. Price* $4.75

*For sale by the National Technical Information Service, Springfield, Virginia 22151

BUCKLING TESTS OF THREE 4.6-METER-DIAMETER ALUMINUM HONEYCOMB SANDWICH CONICAL SHELLS LOADED UNDER EXTERNAL PRESSURE

James Kent Anderson and Randall C. Davis
Langley Research Center

SUMMARY

Three aluminum honeycomb sandwich conical shells with a 120° apex angle and a 4.6-m (15.0-ft) base diameter were loaded to failure by a uniform external pressure. The cones differed from one another only in the thickness of their respective face sheets. Test specimen details, test procedure, and test results are discussed. Both buckling and prebuckling data are compared with appropriate theoretical predictions. Good agreement was obtained between test and theory. Extensive imperfection measurements were made and reported on the three cones in the "as fabricated" condition.

INTRODUCTION

Results of structural tests on three large aluminum honeycomb sandwich conical shells are presented and compared with contemporary theoretical predictions. The size, mass, and configuration of these shells are such as to be applicable to space missions where large, lightweight, blunt-shaped structures are needed for deceleration in a thin atmosphere such as that of the planet Mars.

The test specimens are truncated conical shell structures which have an apex angle of 120° and a base diameter of 4.6 m (15.0 ft). The overall shape and design loadings of the cones are shown in figure 1. The base and truncated edges are supported by stiff magnesium toroidal rings. The shell wall is of sandwich construction, the inside and outside surfaces are equal-thickness aluminum skin, and the core is aluminum honeycomb of constant thickness. The three cones differ from one another only in the thickness of their face sheets. The cones are loaded by a uniform external pressure with the load being supported or reacted at the ring near the truncated end.

Tests on two magnesium, ring-stiffened cones of similar dimensions and under the same loading conditions were reported in a previous publication by the authors. (See ref. 1.) Tests on two aluminum, ring-stiffened cones (Viking structural aeroshells) with somewhat smaller dimensions but loaded under similar conditions are reported in

reference 2. Also, a test program is reported in reference 3 where small conical structures are tested under similar loading conditions; otherwise, little test information is available on conical structures under this loading.

This paper describes the geometry and fabrication of the specimens, the test setup, and test procedure, and discusses and compares the test results with theoretical predictions. Test results include the prebuckling strain distributions in the shell wall and the cone buckling phenomenon. In order to characterize the buckling behavior, this paper reports the buckling and collapse external pressure loads, apparent buckling-mode shape, deflection of the base ring at buckling, and the pressure-strain history in an area of maximum wall deflection. Also included is an extensive initial imperfection survey of the surface of each cone. These imperfection measurements are given in appendix A. Appendix B discusses the analyses to which the test data were compared.

SYMBOLS

The units used for physical quantities defined in this paper are given in the International System of Units (SI) with the U.S. Customary Units in parentheses. An exception is made in figures 6 to 9, 13 to 16, and 21 to 23 where only SI units are used. Correlation between this system of units and U.S. Customary Units is given in reference 4.

E	modulus of elasticity, N/m^2 (psi)
G	shear modulus of elasticity, N/m^2 (psi)
h	height of core, cm (in.)
n	number of full circumferential buckling waves
p_{cr}	critical buckling pressure, N/m^2 (psi)
p_{ult}	ultimate pressure, N/m^2 (psi)
R	radius, cm (in.)
s	meridional coordinate with origin at the cone base, cm (in.)
s_L	meridional length between the base edge and truncated edge, cm (in.)
t	thickness, cm (in.)

x	axial coordinate, cm (in.)
y	radial coordinate, cm (in.)
z	normal coordinate, cm (in.)
ϵ_{s_i}	inside surface meridional strain
ϵ_{s_o}	outside surface meridional strain
ϵ_{θ_i}	inside surface circumferential strain
ϵ_{θ_o}	outside surface circumferential strain
ϵ_{θ_r}	circumferential strain in stiffening rings
μ	Poisson's ratio

TEST SPECIMENS

The test specimens consisted of three aluminum honeycomb sandwich conical shells which were essentially identical except for the thickness of their face sheets. Honeycomb-core thickness and edge-supporting rings were the same for all the cones. The face sheets of the honeycomb walls for cones 1, 2, and 3 were 0.051 cm (0.020 in.), 0.038 cm (0.015 in.), 0.025 cm (0.010 in.) thick, respectively. A general overall view of the test cones is shown in figure 2. Construction details with nominal dimensions are shown in figure 3 with the actual measured dimensions given in table I.

Cone Fabrication Procedure

Each cone was fabricated from 12 equal-size aluminum honeycomb sandwich panels. For each cone assembly, one extra panel was fabricated for study in the "as fabricated" or never-loaded condition.

Each sandwich panel was manufactured from four basic parts: (1) inside and outside face sheets; (2) honeycomb core; (3) attachment ring inserts at each end of the panel; and (4) inside and outside scalloped doublers located at each end of the panel. All components were incorporated into the finished panel by suitable structural adhesives.

The face sheets were chem-milled to the desired thickness from 0.0635-cm (0.025-in.) thick stock of 7075-T6 aluminum alloy. The 54.5-kg/m^3 (3.4-lbf/ft^3) alumi-

num honeycomb core had 0.64-cm (0.25-in.) hexagonal cells with perforated, 0.0038-cm (0.0015-in.) thick, 5052 aluminum alloy walls and had a depth of 1.27 cm (0.50 in.). The meridional orientation of the core ribbon, because of available stock, necessitated one core splice for each panel. The 1.27-cm (0.50-in.) thick solid attachment ring inserts (fig. 3) were fabricated from 7075-T651 aluminum alloy plate by machining to the required curvature.

The panels were fabricated using conventional autoclave bonding procedures. Face sheets were bonded to the core and attachment ring inserts using American Cyanamide-Bloomingdale tape adhesive FM 123-2 and Bloomingdale's BR 123 primer. The honeycomb core splice that was necessary for each panel was made with American Cyanamide-Bloomingdale FM-37, a modified epoxy form. Ultrasonic methods verified the integrity of the bonds of each panel.

Scalloped doublers were subsequently bonded to the ends, inside and outside, of each panel using FM 123-4 tape adhesive, BR 123 primer, and a conventional autoclave procedure. The FM 123-4 tape adhesive was similar to FM 123-2 except for the carrier employed. The doublers were cut from the same chem-milled sheets as the face sheets. After removal from the autoclave, bonds were ultrasonically inspected.

Each cone was preassembled from 12 panels on a large assembly fixture that permitted panel attachment and support for practically all necessary operations. After proper fit was assured, the panels were removed and the meridional edges of each panel were filled and sealed with Shell's Epon 912 epoxy, a room temperature curing sealer, to assure a clean and smooth mating surface for bonding together the butt edges of adjacent panels. Also, the honeycomb core near the meridional butt joint was compacted to insure sufficient strength in the joint area. After the panels were reassembled on the fabrication fixture, adjacent panels were joined together by a modified epoxy RADM 73040 along the smooth butting surface and with rivets at the attachment insert ring joints. The assembly was allowed to cure at room temperature and then the inner and outer edges of the cones were machined to the required dimensions. To attach the inside and outside meridional doublers at the panel joints, a room temperature adhesive was used. This adhesive was the modified epoxy AVCO system RADM 73040 with J. P. Stevens scrim cloth no. 2530/44 A1100 to eliminate voids. These test cones were manufactured by the Avco Corporation.

End Ring Attachment and Edge Reinforcement

The last major fabrication step was the attachment of large stiffening rings to the edges of the cones. The stiffening ring attached at the large edge, or base ring, was a 4.6-m (15.0-ft) diameter, magnesium tube with a 15.2-cm (6.0-in.) diameter cross section. The ring was attached using 0.64-cm (0.25-in.) rivets. A structural membrane,

used as a pressure seal in the test setup, was attached to the cone at the base ring and held in place by rivets and an adhesive at the junction of the base ring and shell. The stiffening ring attached at the small edge (termed payload ring if the structure is to be used as a decelerator on a space mission) was a 2.0-m (6.67-ft) diameter, magnesium tube with a 6.4-cm (2.5-in.) diameter cross section. The ring was attached using 0.64-cm (0.25-in.) rivets. The tubes were extruded from ZK60A magnesium alloy and were the same tubes used in the tests of reference 1.

One other modification on the cones was necessary before they were ready for testing. A preliminary stress analysis indicated that the shell wall at the small end would be subjected to high circumferential tensile stresses if the cones were loaded to the expected test pressures. The analysis showed that while the shell wall in each panel in this area was sufficiently strong, the riveted splices at the attachment ring insert joints were deemed inadequate. This situation was remedied by attaching reinforcing plates (fig. 3) at each of the 12 joints. These plates were made of 7075-T6 aluminum alloy.

TEST PROCEDURE

Each cone was instrumented with 138 strain gages to provide a comprehensive strain survey for evaluation of cone response to applied external surface pressure. The base ring was instrumented to measure vertical and horizontal displacements during the buckling tests. Additional gages were used to record circumferential strains in the payload and base rings.

A schematic view of the test setup is shown in figure 4. The inner steel conical test fixture, the test cone, and a membrane-like skirt at the base ring form an airtight chamber. By creating a partial vacuum in this chamber, a uniform external pressure is exerted on the test cone and is reacted by the payload ring resting on the flat machined surface at the top of the conical test fixture. The membrane-like skirt which seals the chamber is intended to provide minimal restraint to the shell during loading by restricting the loading from the membrane to a small meridional load applied tangentially to the inside surface of the shell. Loading pressure was controlled by manually operated valves and the resulting pressure-strain response for selected gages was monitored on two oscilloscopes. Test data were recorded automatically by the Langley central digital data recording facility. Figure 5 shows a photograph of the major components of the test setup without the test cone.

An extensive imperfection survey was made of each test cone in the "as fabricated" or no-load condition. Measurements were made along meridional lines at 7.5° intervals around the circumference with a straight edge and with the base ring and payload ring as end reference points. Normal departures of the conical surface from a straight line were

measured with an electrical device and autographically recorded on a continuous plotter. These measurements are presented in appendix A and show that each cone was of good quality and adhered closely to the prescribed geometry. Several diameter measurements were made on each base ring to verify circularity.

Three types of tests were conducted on each cone: The first to determine the prebuckling strain distribution as a function of pressure, the second to determine the buckling pressure, buckling mode, base ring displacements and strain at buckling, and the third to determine the postbuckling strength. Thus, after reaching what was deemed the buckling pressure, each cone was unloaded to zero pressure and then reloaded to complete failure. The prebuckling strain distribution tests were made with pressures up to 13.8 kN/m^2 (2.0 psi) (0.136 atmosphere) which were considerably less than the predicted buckling pressure. For these tests, 3 of the 12 panels, 120^o apart, were extensively instrumented with strain gages, the number of gages being limited by the number that could be recorded in one test. For the buckling tests, strain gages were located at points of expected maximum buckling deflections around the test cones to record back-to-back, inside and outside circumferential strains, and thus indicate the buckling mode. One panel on each of the cones was also instrumented with a sufficient number of strain gages to indicate the circumferential and meridional strain profiles at buckling. The horizontal and vertical displacements of the base ring were also measured during the buckling tests; for this purpose, displacement transducers were placed at two locations 180^o apart on the base ring. The same procedure was used for the failure test.

Photographs were taken during buckling and after each cone had been loaded to failure. The cones were then cut into three sections and coupons removed along the meridional cuts for thickness and weight measurements and for further structural testing to determine the honeycomb stiffness properties used in the stress analysis. Also, the extra panel for each cone was cut into coupons for similar measurements. The thickness measurements are given in table I and the material properties are given in appendix B.

TEST RESULTS AND DISCUSSION

Prebuckling Strain Distribution Tests

A comparison of the measured and predicted prebuckling strain distributions in the conical shells is presented in figures 6 to 9. Two computer programs, BOSOR 2 (Buckling Of Shells Of Revolution) and SALORS (Structural Analysis of Layered Orthotropic Ring-Stiffened Shells of Revolution), were used to compute the theoretical strain values. These programs are discussed briefly in appendix B.

In figures 6 and 7 outside and inside surface circumferential strains on the honeycomb sandwich shell walls are plotted against the dimensionless meridional distance

s/s_L, where s/s_L is measured such that the outer edge of the conical sandwich shell is at $s/s_L = 0$ and the inner edge of the shell is at $s/s_L = 1.0$. The base ring is attached near the midspan of a rectangular-sectioned aluminum attachment ring insert built into the edge of the sandwich shell (fig. 3) at the station $s/s_L = 0.01678$. A similar construction is used at the inner edge with the payload ring attached at $s/s_L = 0.9832$. Test strain measurements were taken from three panels 120^o apart. The location of these panels and their imperfection measurements are given in appendix A.

In general, there is good agreement between the two computer programs and the test data for the circumferential strains in all three cones. The largest discrepancies between test and theoretical strains exist near the inner edge of each cone where theory indicates the largest circumferential bending moments occur. The test results near the inner edge in all three cones fall between the two computed results. Throughout the rest of the shell, the differences between the two programs are small.

Although the highest circumferential moments occur at the inner edges, their effects on the circumferential strains are small compared to the high tensile strains produced by the circumferential stress resultants. These curves reflect a phenomenon peculiar to this type of shell, wherein the shell is loaded by external pressure and supported at the payload ring. Under these conditions, the payload ring rotates and expands outwardly thereby creating high tensile hoop forces at the inner edge of the shells.

The prebuckling strains in the meridional direction along a meridional generator are shown in figures 8 and 9. The agreement between the programs and the test data is generally good except near the inner edges where the maximum meridional bending moments occur.

The discontinuities in the theoretical curves predicted by BOSOR 2 are caused by using discontinuous wall construction near the ends and in the doubler region of the shell. In BOSOR 2, the doubler region was divided into equal segments, with each segment having a constant thickness obtained by averaging the thickness of adjacent segments. (See appendix B.) However, in SALORS, the thickness was varied linearly across the doubler region; hence, there are no jump discontinuities in the shell thickness and therefore no resulting jump discontinuities in the predicted strain curves. The discontinuities at $s/s_L = 0.01678$ and 0.9832 in both curves are caused by the attachment of the base ring and payload ring, respectively.

The circumferential strains produced in the base ring and payload ring at the prebuckling pressure load of 13.8 kN/m^2 (2.0 psi) for each cone are given in table II. Strain gages A and B were attached to the rings along the same meridional generator that was used in figures 6 to 9 for strain data on the cone walls, each generator being 120^o apart. The panel number and gage are noted on table II. The location of these panels with respect to each cone is given in appendix A.

Buckling Tests

The buckling character of all three cones was essentially the same with the development of a six full-wave buckle pattern (general instability) about the circumference of each cone. The buckling phenomenon was not catastrophic as the development of the buckles occurred smoothly and the shell remained intact. After each cone was buckled, the pressure loading was reduced to zero and each cone visually inspected on the outside. There appeared to be no damage to any of the cones from the buckling loading. Figures 10 and 11 show cones 2 and 3 at buckling. The depth of the buckles can be seen by the separation of the sandwich wall from the straight edges.

Test procedure for the buckling test called for all 12 panels of each cone to be instrumented with a sufficient number of strain gages to determine wall bending and to anticipate the onset of buckling. These gages were placed back-to-back (outside and inside surface of sandwich walls) midway between panel seams and at the meridional station in the vicinity of expected maximum deflection to measure circumferential strains. The strains in the panel exhibiting the most wall bending in each cone during the buckling tests are shown in figure 12.

The onset of buckling is defined in this report as that pressure at which there is strain reversal (or more exactly, a strain-rate reversal) in the circumferential strains in the buckling region. Sometimes the buckling load and collapse load (that is, that state at which no additional load can be carried) of a structure occur simultaneously or so very close to each other that the collapse load, which is obviously easy to define, is assumed to be the same as the buckling load. An easily defined buckling load is not the case in the tests of the structures of this report. None of the cones collapsed at buckling but continued to carry additional load. Examination of figure 12 shows that at a certain pressure for each cone, a pressure plateau exists where a sizable change in strain occurs with little increase in pressure. This pressure plateau is at the same pressure level no matter what panel is examined around the cone and does not depend upon the relative magnitude of the wall bending between panels. These pressure levels for cones 1, 2, and 3 are 41.7 kN/m^2 (6.046 psi), 33.1 kN/m^2 (4.800 psi), and 23.2 kN/m^2 (3.371 psi), respectively. While the pressure plateau is easily identified from test results, a consistent strain-reversal pressure is difficult to determine. The average value of the strain-reversal pressure as determined from test pressure-strain plots was about 8.5 percent below the plateau value for each cone. The buckling pressure was therefore assumed to be 8.5 percent below this plateau for each cone.

The buckling pressure determined by this reduction procedure for cone 1 was 38.1 kN/m^2 (5.53 psi), and the apparent buckling mode contained six circumferential waves. The horizontal or radial displacement of the base ring at buckling was only a few thousandths of a centimeter inward; however, the vertical displacement was between

1.17 cm (0.46 in.) and 1.30 cm (0.51 in.) downward. The buckling pressure of cone 2 was 30.3 kN/m^2 (4.39 psi) with six circumferential waves and with a base-ring displacement of 1.12 cm (0.44 in.) to 1.17 cm (0.46 in.) downward and only a slight inward radial displacement. Cone 3 buckled at 21.2 kN/m^2 (3.08 psi) and also had six circumferential waves with a base-ring displacement of 0.84 cm (0.33 in.) to 0.86 cm (0.34 in.) downward and again only slight inward displacement.

One panel on each cone was instrumented with a sufficient number of strain gages to indicate the strain profile at buckling. Figures 13 and 14 present the outside and inside circumferential strains for the three cones and figures 15 and 16 present outside and inside meridional strains. Profiles are given for the buckling pressure and also at several lower pressures for trend comparison. Test data are plotted at discrete points as shown; however, a continuous curve was faired through these points to indicate the approximate strain levels at points where data were not taken.

Theoretical buckling predictions from BOSOR 2 and SALORS are given in table III along with test values. All three cones buckled into an apparent general instability mode of six circumferential waves, although both buckling computer programs (BOSOR 2 and SALORS) predicted buckling modes of seven waves. Fabrication details of the test cones may be responsible for the difference in the theoretically predicted mode and apparent test mode because of the closeness of the buckling pressures for the buckling modes of six and seven waves. (See appendix B.) Each cone was built from 12 panels and buckled into six circumferential waves; the node points of the waves were in close proximity to the seams joining adjacent panels.

Theoretical buckling predictions for shells are usually higher than actual test results. The BOSOR 2 analysis predicts a buckling pressure that must be reduced by about 29 percent for cone 1 and by about 24 percent for cones 2 and 3. The SALORS analysis predicts a buckling pressure that must be reduced by about 24, 20, and 19 percent for cones 1, 2, and 3, respectively. These reduction percentages are comparable to the 25-percent reduction recommended in reference 5 for this type of structure. These values are also comparable to the 20-percent reduction obtained from tests in reference 1.

The tests also verified that the base rings were sufficiently stiff to prevent inextensional shell buckling. This problem had been studied earlier by Cohen. (See ref. 6.)

Postbuckling Tests

While the buckling of the three honeycomb cones was of a mild nature, the failure was of a violent, almost explosive nature. The buckling and failure tests consisted of two separate loading cycles; that is, after buckling, the cones were completely unloaded and then reloaded to failure. The pressure-strain curves of figure 12 indicate the reaction

of the selected panels on each cone to the two load cycles, buckling and failure. The buckling mode remained unchanged during the test from the initiation of strain reversal until failure.

Each cone maintained the ability to carry additional pressure loading after buckling, as much as 48 percent more for cone 2 and as little as 18 percent more for cone 1, although both cones failed at approximately the same pressure. Cone 3 carried 30 percent more pressure after buckling. Figures 17 to 19 show photographs of the failed cones. All the cones were still able to withstand some load after failure with the exception of cone 2 which was ruptured at failure.

CONCLUDING REMARKS

The test results from an investigation to determine the buckling phenomenon and structural response caused by applied uniform external pressure on three honeycomb aluminum conical shells have been presented. These shells have dimensions applicable to space missions involving structural decelerators or aeroshells. Imperfection measurements were made on each cone and should be of benefit for further research into the effect of shell imperfections on the buckling of shells.

Test results were compared with two contemporary sophisticated shell-of-revolution analyses. The prebuckling strains agreed well with theory except in the region of the payload ring (small radius edge); there the test data generally fell between the two predicted strain curves. All three cones buckled into a general instability mode with six circumferential waves.

Both analysis programs predicted a buckling mode of seven waves for each cone, compared with six circumferential waves in the tests; however, construction details of the cones may be responsible for this discrepancy. The BOSOR 2 analysis predicted a critical buckling pressure that should be reduced by about 30 percent for cone 1 (honeycomb walls with the thickest face sheets) and by about 25 percent for cones 2 and 3 for adequate agreement with tests. The SALORS analysis predicted critical pressures that must be reduced by 25 percent for cone 1 and 20 percent for cones 2 and 3.

The cones exhibited a substantial postbuckling strength carrying loads from 18 to 48 percent above the initial buckling loads; also there was no evidence of inextensional buckling at any load level.

Langley Research Center,
National Aeronautics and Space Administration,
Hampton, Va., April 16, 1975.

APPENDIX A

SHELL SURFACE IMPERFECTION MEASUREMENTS

The conical shell surfaces of all three cones were measured extensively to determine the geometric imperfections present in an "as fabricated" and no-load condition. The distances from a straight meridian to the surface of the cones were established along meridional lines between the scalloped shell doublers located at each end of the cones. Measurements were taken at 7.5^{o} intervals around the circumference in a counterclockwise direction. Figure 20 shows locations on the panels where imperfection measurements were made and also shows meridional locations where strain gages were installed for the prebuckling and buckling tests.

Figures 21, 22, and 23 present the imperfection measurements for each panel of the three cones. Each panel is numbered for reference in the text and figures.

Figure 24 shows the imperfection measurements around each cone circumference at the meridional station, $s = 75.18$ cm (29.60 in.). This is the same station location that was used in figure 12, the station of expected maximum deflection. The panels on each cone are bowed out between seams, with the seams being nearly on the nominal circle of zero imperfections.

APPENDIX B

PREBUCKLING AND BUCKLING ANALYSES FOR TEST CONES

Two computer programs, SALORS and BOSOR 2, were used to analyze the cones discussed in the text. A discussion and comparison of these programs are given in reference 7. Both systems employ finite-difference solution procedures; however, BOSOR 2 applies the difference approximations to the energy expression, whereas the SALORS program applies the difference approximations to the differential equations of equilibrium.

The theoretical predictions given in the text are based on the analytical models of the cones shown in figure 25. In the SALORS program a nonlinear analysis was used to compute the prebuckling strain distributions, whereas a linear prebuckling stress state was used in the stability analysis. The SALORS nonlinear stress analysis option is unpublished, but the theory and user's manual for the linear stress analysis option is described in detail in reference 8. The external pressure loading was considered live (load remains normal to the deformed surface). The BOSOR 2 program is described in detail in reference 9. A nonlinear analysis was used to compute the prebuckling strain distribution and also to compute the prebuckling stress state in the stability analysis. External pressure loading was not considered to be live.

Numerical values used in the computations are given in tables I and IV. Table I contains the measured thicknesses obtained from many coupons cut from each cone. The adhesive was chemically dissolved and each coupon weighed. One layer of the uncured adhesive had a weight of 2.969 N/m^2 (0.062 lbf/ft^2) and a thickness of 0.030 cm (0.012 in.). The weight measurements showed that the average weight of one layer of the cured adhesive was about 2.825 N/m^2 (0.059 lbf/ft^2). To determine the actual thickness of the adhesive in the test specimens, photomicrographs were taken of the sandwich wall cross section for each cone. These are shown in figure 26. The bond thickness for each cone was approximately 0.025 cm (0.010 in.).

The mechanical properties used in the analysis are shown in table IV. The in-plane stiffness for the wall of each cone was determined by tests on many compression coupons. The contribution of the core and adhesive was considered to be the difference between the total stiffness of the coupon and that of the two face sheets. The adhesive was assumed to have an isotropic Young's modulus of 3.45 GN/m^2 (0.5×10^6 psi) and a Poisson's ratio of 0.35. (See ref. 10.) The nonwoven synthetic fabric adhesive carrier, upon inspection, was considered ineffective in carrying load. Because of its small extensional stiffness, the honeycomb core was also considered to be isotropic with the same Poisson's ratio as that of the adhesive.

Figure 27 is a plot of the buckling pressure as a function of buckling mode number as computed by BOSOR 2 for its analytical model. The closeness in the buckling pressures for the buckling modes of 6 and 7 was apparent, thus lending credibility to the assumption that the construction details of the test cones may have affected the buckling modes.

Stiffness measurements of the compression coupons also indicated that there was no discernible difference between the coupons cut from the failed cones and the coupons from the unloaded extra panel.

REFERENCES

1. Anderson, James Kent; and Davis, Randall C.: Buckling Tests of Two 4.6-Meter-Diameter, Magnesium Ring-Stiffened Conical Shells Loaded Under External Pressure. NASA TN D-7303, 1973.

2. Heard, Walter L., Jr.; Anderson, Melvin S.; Anderson, James Kent; and Card, Michael F.: Design, Analysis, and Tests of a Structural Prototype Viking Aeroshell. J. Spacecraft & Rockets, vol. 10, no. 1, Jan. 1973, pp. 56-65.

3. Williams, Jerry G.; and Davis, Randall C.: Experiments on Stiffened Conical Shell Structures Using Cast Epoxy Models. Paper No. 2268A, Soc. Exptl. Stress Analysis, Oct. 1973.

4. Metric Practice Guide. E 380-72, Amer. Soc. Testing & Mater., June 1972.

5. Buckling of Thin-Walled Truncated Cones. NASA SP-8019, 1968.

6. Cohen, Gerald A.: The Effect of Edge Constraint on the Buckling of Sandwich and Ring-Stiffened 120 Degree Conical Shells Subjected to External Pressure. NASA CR-795, 1967.

7. Anderson, M. S.; Fulton, R. E.; Heard, W. L., Jr.; and Walz, J. E.: Stress, Buckling, and Vibration Analysis of Shells of Revolution. Computers & Structures, vol. 1, nos. 1/2, Aug. 1971, pp. 157-192.

8. Heard, Walter L., Jr.; Anderson, Melvin S.; and Chen, Ming M.: Computer Program for Structural Analysis of Layered Orthotropic Ring-Stiffened Shells of Revolution (SALORS) – Linear Stress Analysis Option. NASA TN D-7179, 1973.

9. Bushnell, David: Buckling and Vibration of Segmented, Ring-Stiffened Shells of Revolution – User's Manual for BOSOR 2. LMSC 6-78-68-40 (Contract N00014-67-C-0256), Lockheed Missiles & Space Co., Sept. 1968. (Available from DDC as AD 863 453.)

10. Ashton, J. E.; Halpin, J. C.; and Petit, P. H.: Primer on Composite Materials: Analysis. Technomic Pub. Co., Inc., c.1969.

TABLE I.- MEASURED STRUCTURAL DIMENSIONS

Cone	Stiffening rings				Honeycomb wall					
	Payload ring wall thickness		Base ring wall thickness		Face sheets average thickness		Honeycomb core height		Honeycomb wall, total thickness	
	cm	in.	cm	in.	cm	in.	cm	in.	cm	in.
1	0.323	0.127	0.399	0.157	0.0498	0.0196	1.270	0.500	1.379	0.543
2	0.323	0.127	0.399	0.157	0.0363	0.0143	1.270	0.500	1.356	0.534
3	0.323	0.127	0.399	0.157	0.0244	0.0096	1.270	0.500	1.331	0.524

TABLE II.- CIRCUMFERENTIAL STRAINS IN THE END RINGS

AT 13.8 kN/m^2 (2.00 psi)

Cone	Base ring			Payload ring		
	Panel	Gage	ϵ_{θ_r}	Panel	Gage	ϵ_{θ_r}
1	7	A	-0.000004	7	A	-0.000491
		B	.000083		B	.000789
	11	A	-.000006	11	A	-.000162
		B	.000071		B	.000787
	3	A	.000005	3	A	-.000190
		B	.000073		B	.000832
2	2	A	0.000013	2	A	-0.000221
		B	.000086		B	.000821
	13	A	.000003	13	A	-.000106
		B	.000089		B	.000695
	10	A	.000010	10	A	-.000055
		B	.000084		B	.000829
3	2	A	0.000019	2	A	-0.000100
		B	.000128		B	.000675
	6	A	.000023	6	A	-.000317
		B	.000123		B	.000870
	10	A	.000011	10	A	-.000122
		B	.000113		B	.000814

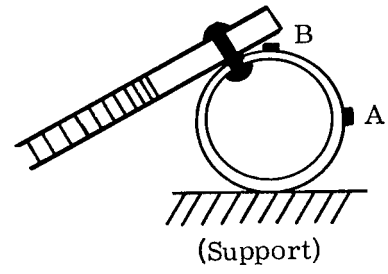

Payload ring

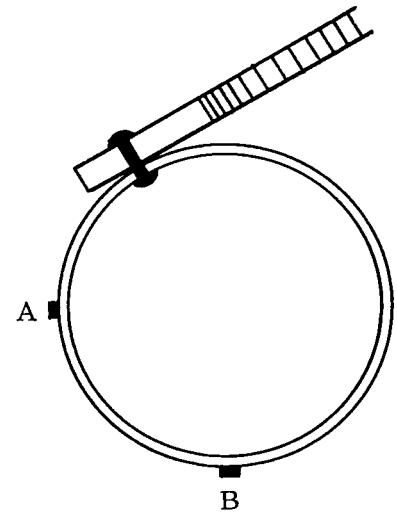

Base ring

TABLE III.- BUCKLING RESULTS FROM TESTS AND THEORY

Cone	Tests			SALORS			BOSOR 2		
	n	p_{cr}		n	p_{cr}		n	p_{cr}	
		kN/m^2	psi		kN/m^2	psi		kN/m^2	psi
1	6	38.13	5.53	7	50.06	7.26	7	53.78	7.80
2	6	30.27	4.39	7	37.99	5.51	7	39.85	5.78
3	6	21.24	3.08	7	26.20	3.80	7	27.79	4.03

TABLE IV.- MECHANICAL PROPERTIES USED IN THE CONE ANALYSIS

[Young's modulus for the magnesium rings was taken to be 44.8 GN/m^2 $(6.5 \times 10^6$ psi)]

Property	Material		
	Face sheets	Adhesive [a]	Honeycomb core [b]
E, GN/m^2 (psi)	71.7 (10.4×10^6)	3.45 (0.50×10^6)	0.262 (0.038×10^6)
G, GN/m^2 (psi)	27.2 (3.94×10^6)	1.28 (0.185×10^6)	.097 $(.014 \times 10^6)$
μ	.32	.35	.35

[a] Reference 10.

[b] The experimentally determined total stiffness of the core (adhesive and honeycomb core) was the same for each cone, that is, 4.90 MN/m $(28 \times 10^3$ lb/in.).

Cone	t cm (in)	h cm (in)
1	.051 (.020)	1.270 (.500)
2	.038 (.015)	1.270 (.500)
3	.025 (.010)	1.270 (.500)

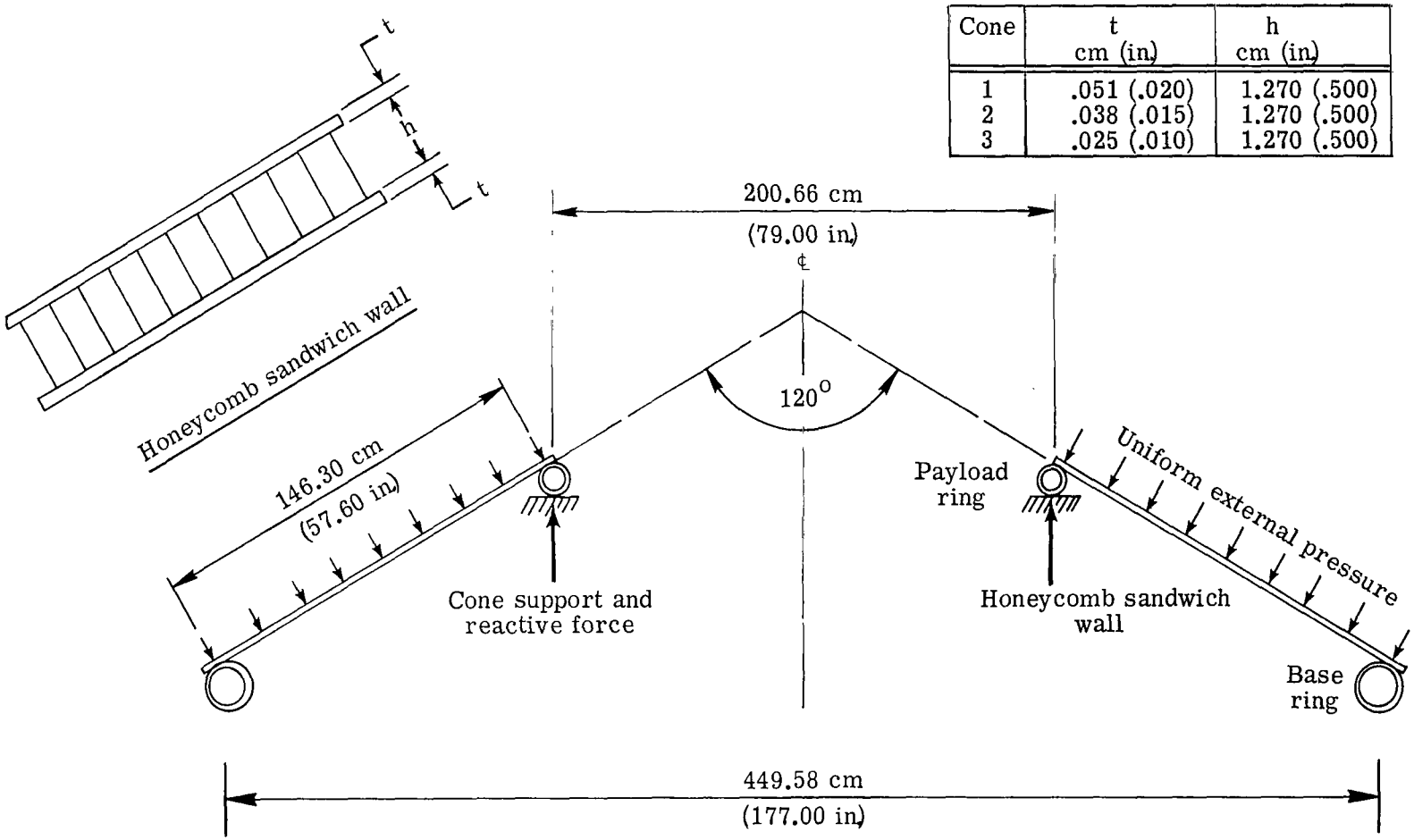

Figure 1.- Cross section of test cones showing shape and design test loading.

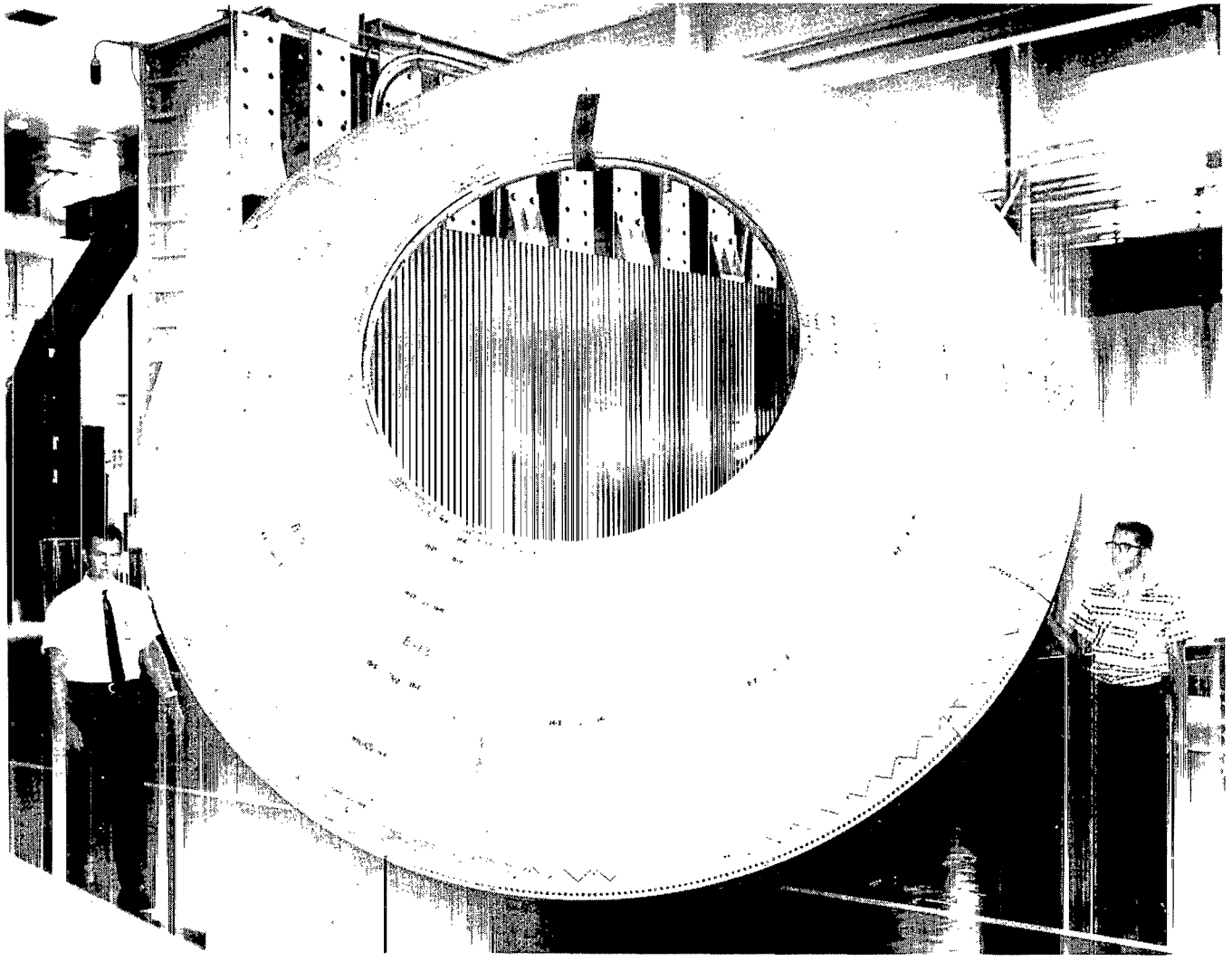

L-69-5235

(a) Outside view of cone 2.

Figure 2.- Overall view of test cone.

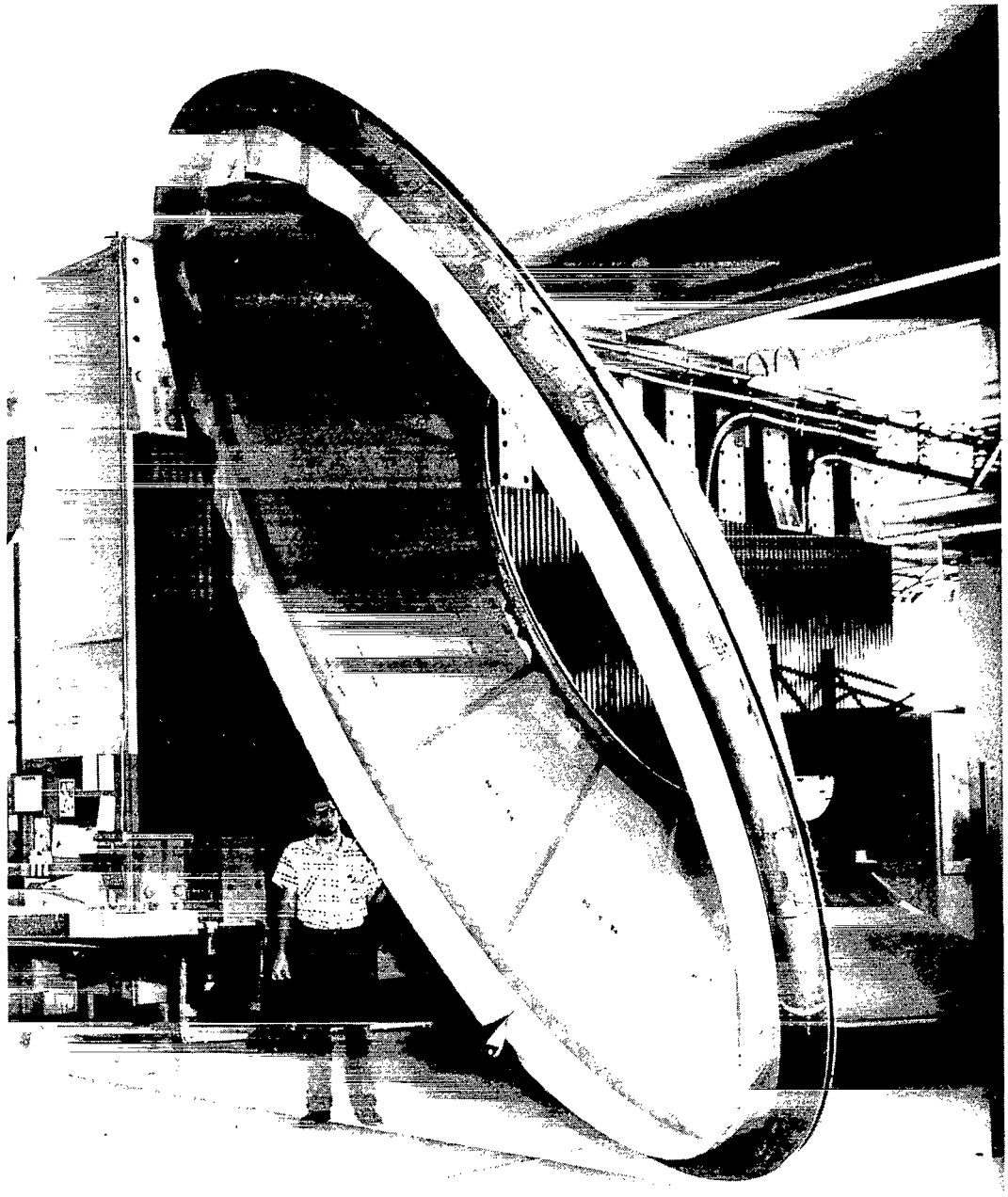

L-69-5234

(b) Inside view of cone 2.

Figure 2.- Concluded.

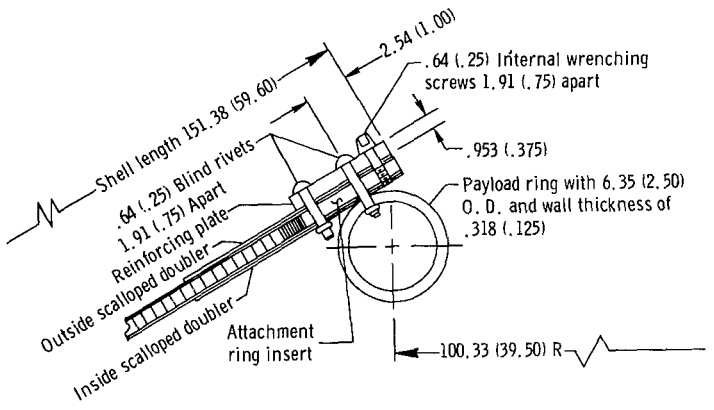

Section A-A

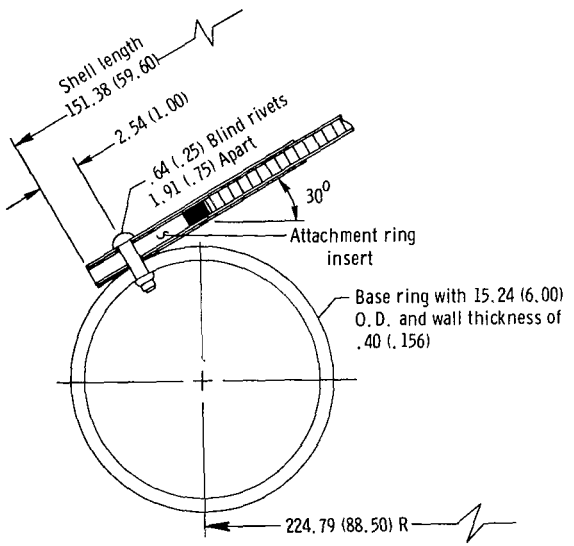

Section B-B

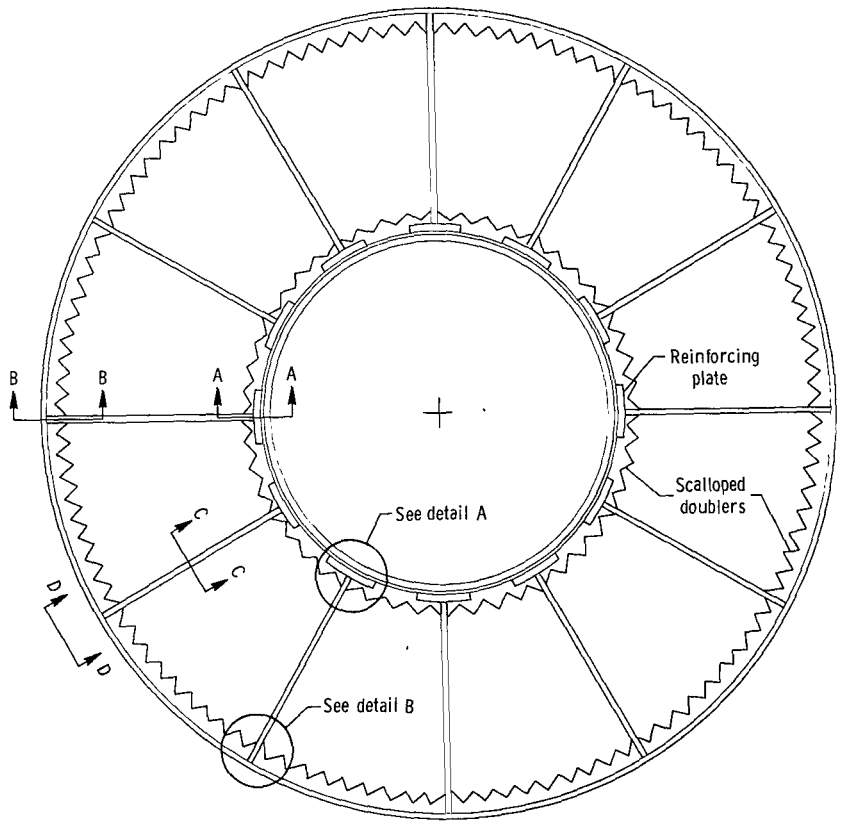

Top View

Honeycomb sandwich cone

Cone	Skin thickness, t
1	.051 (.020)
2	.038 (.015)
3	.025 (.010)

7075-T6 Aluminum alloy

Figure 3.- Construction details of test cones. Dimensions given in cm (in.).

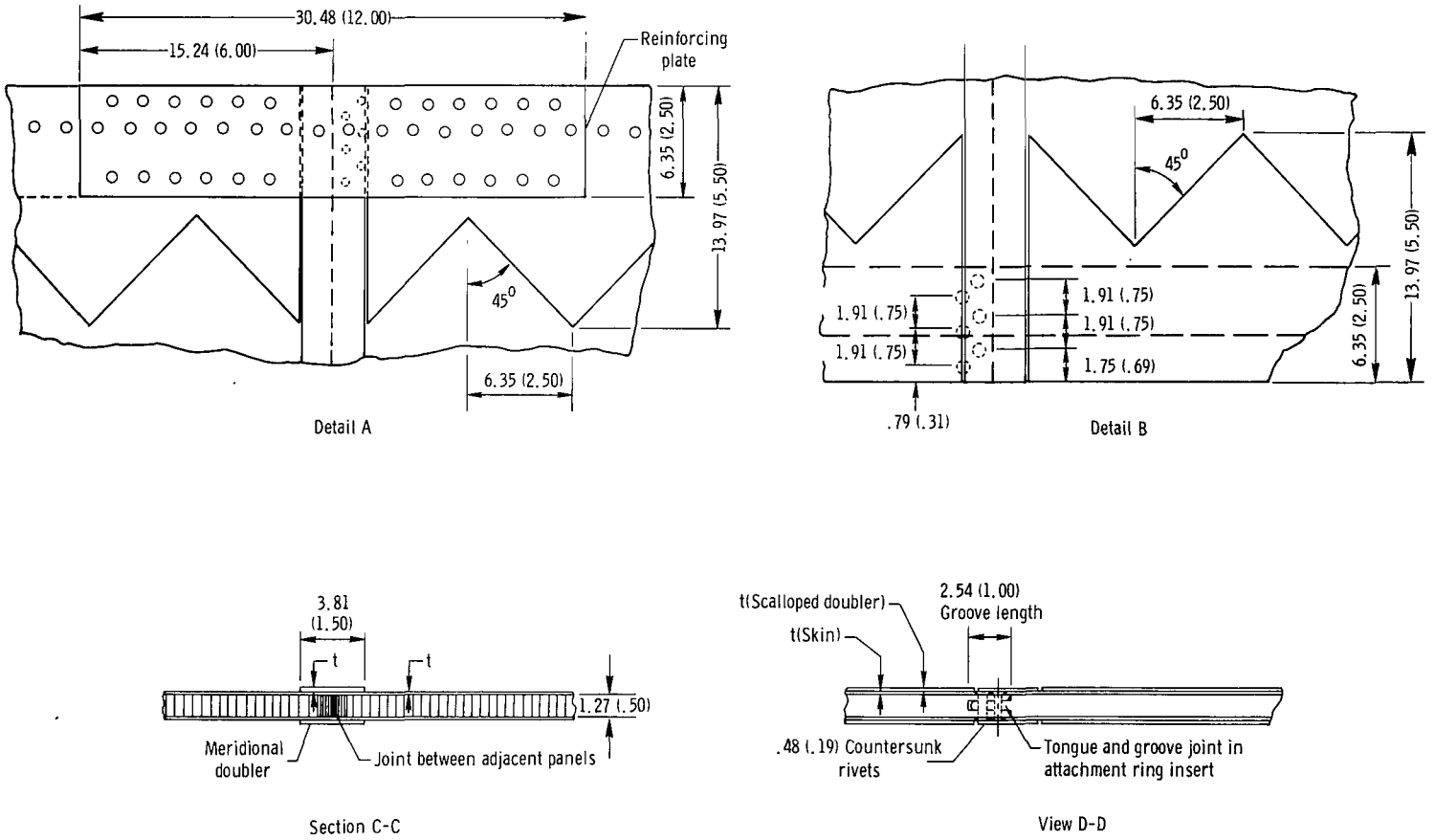

Figure 3.- Concluded.

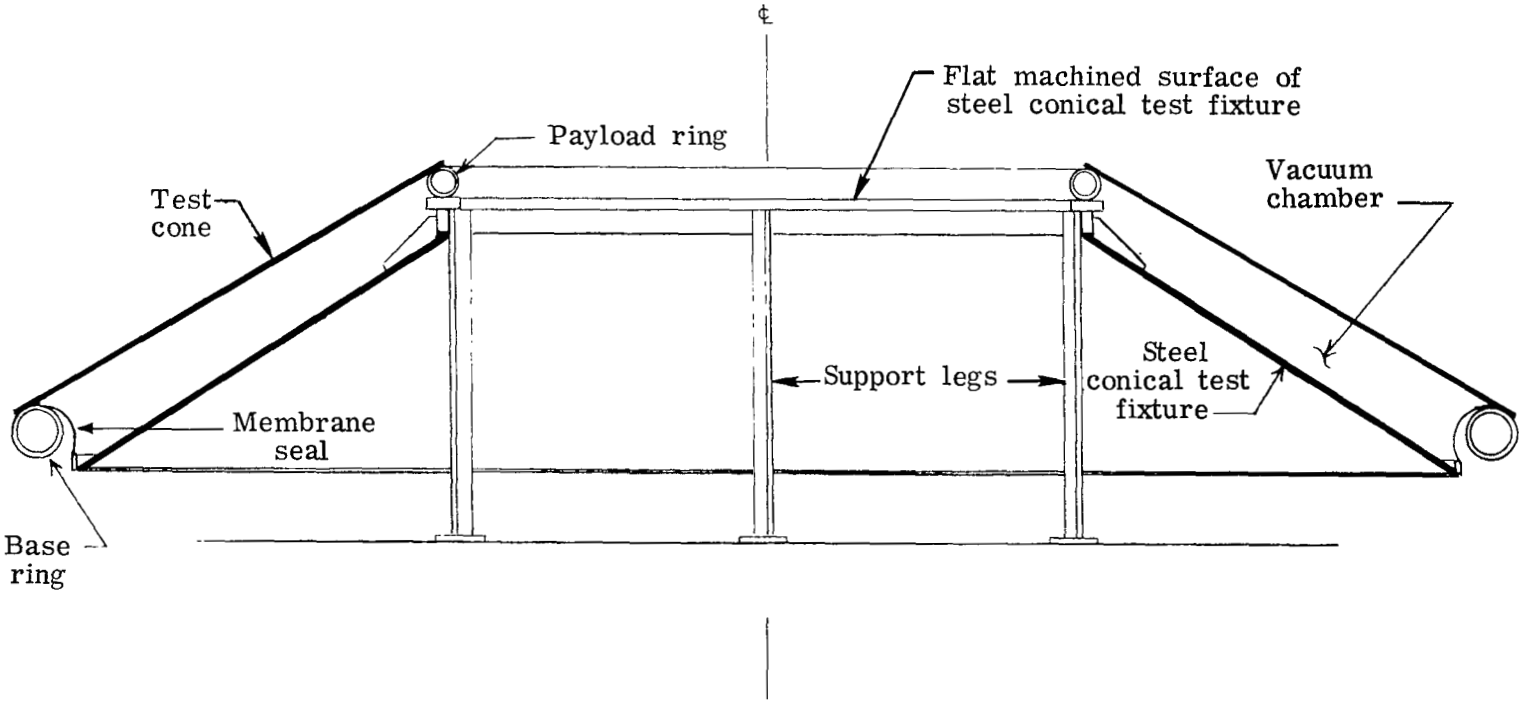

Figure 4.- Cross-section schematic view of test setup.

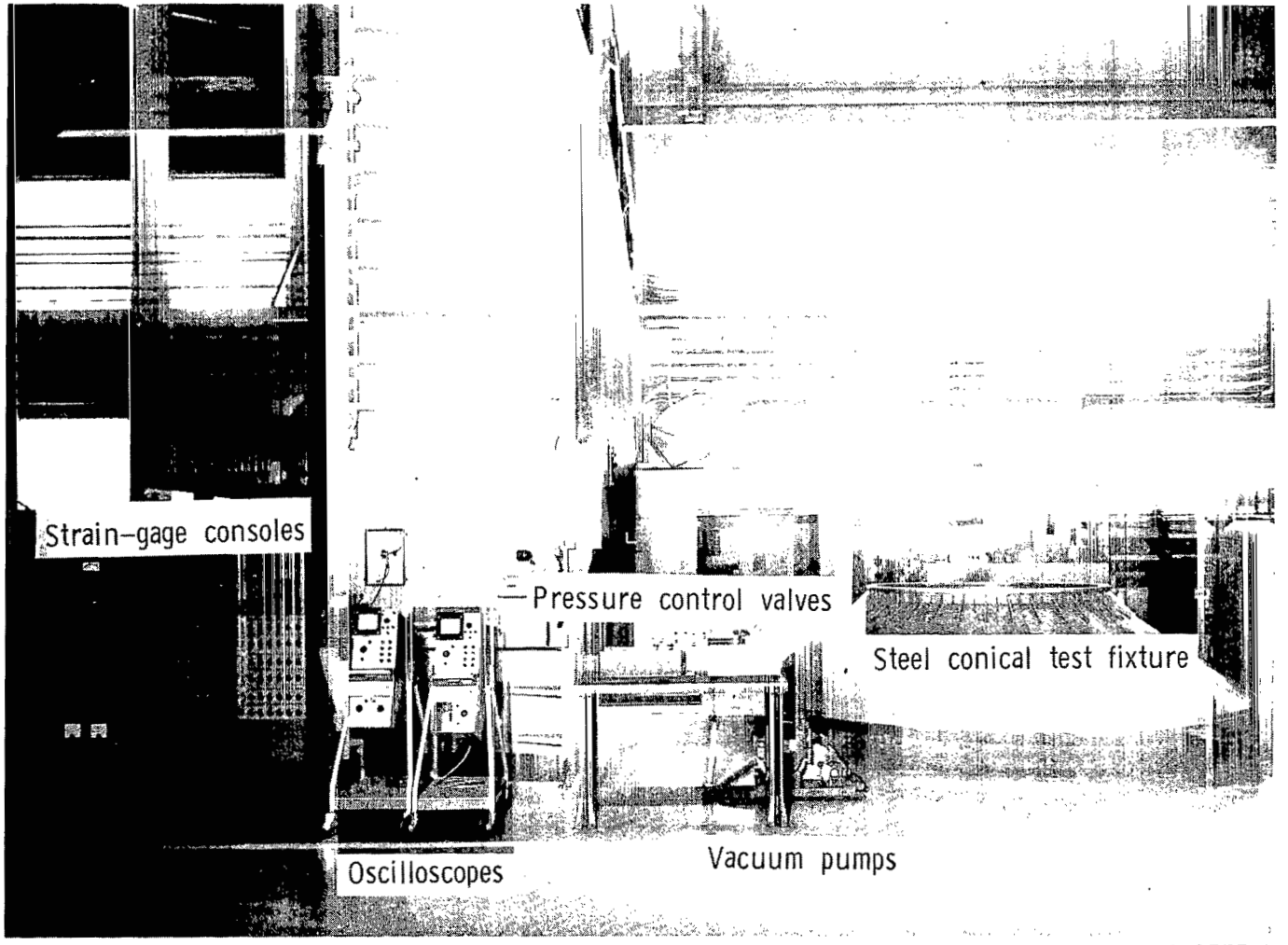

L-69-8555.1

Figure 5.- Test setup components excluding test cones.

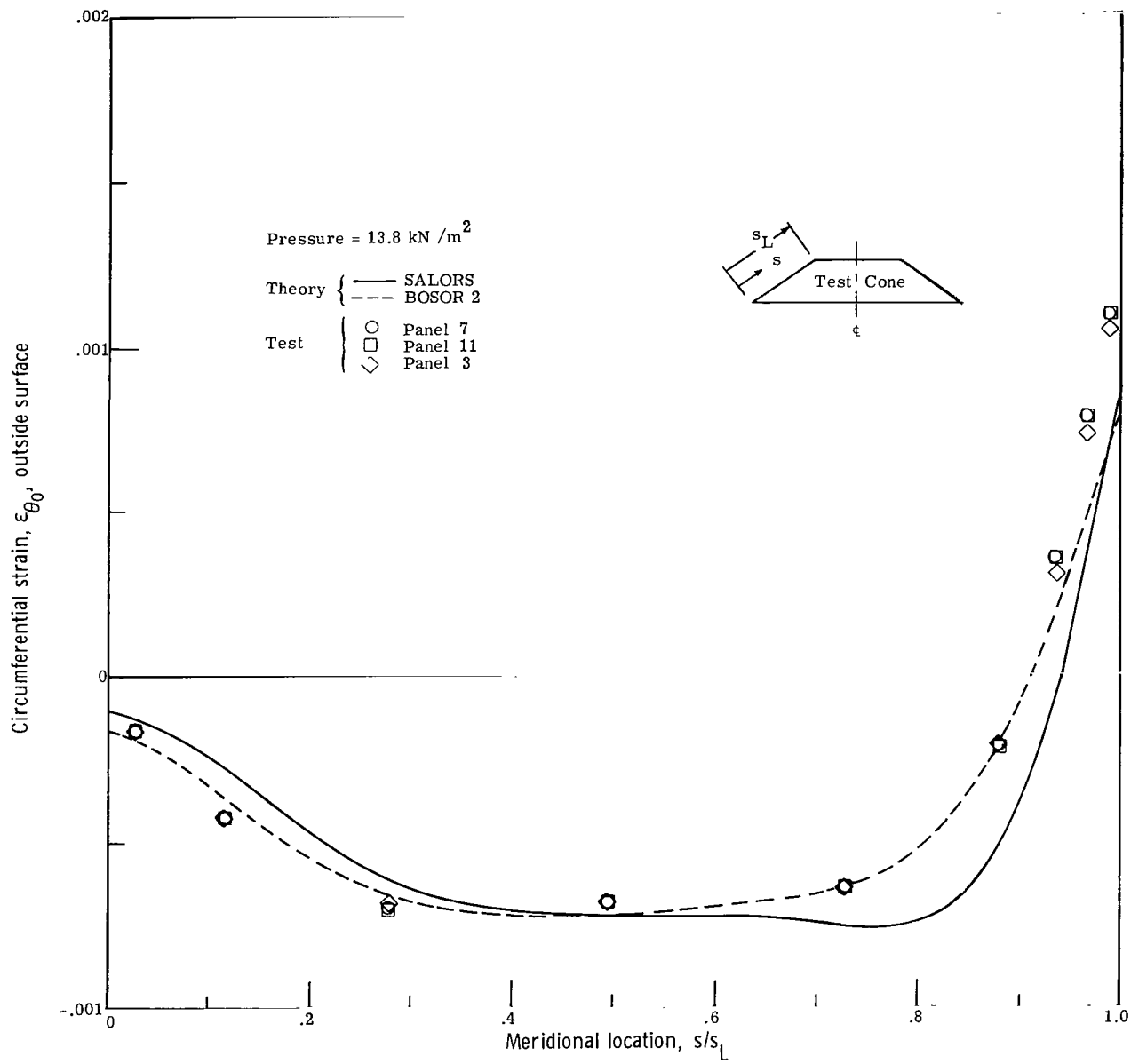

(a) Cone 1.

Figure 6.- Comparison of test and theoretical circumferential strains on outside surface. (See fig. 20 for panel numbering system.)

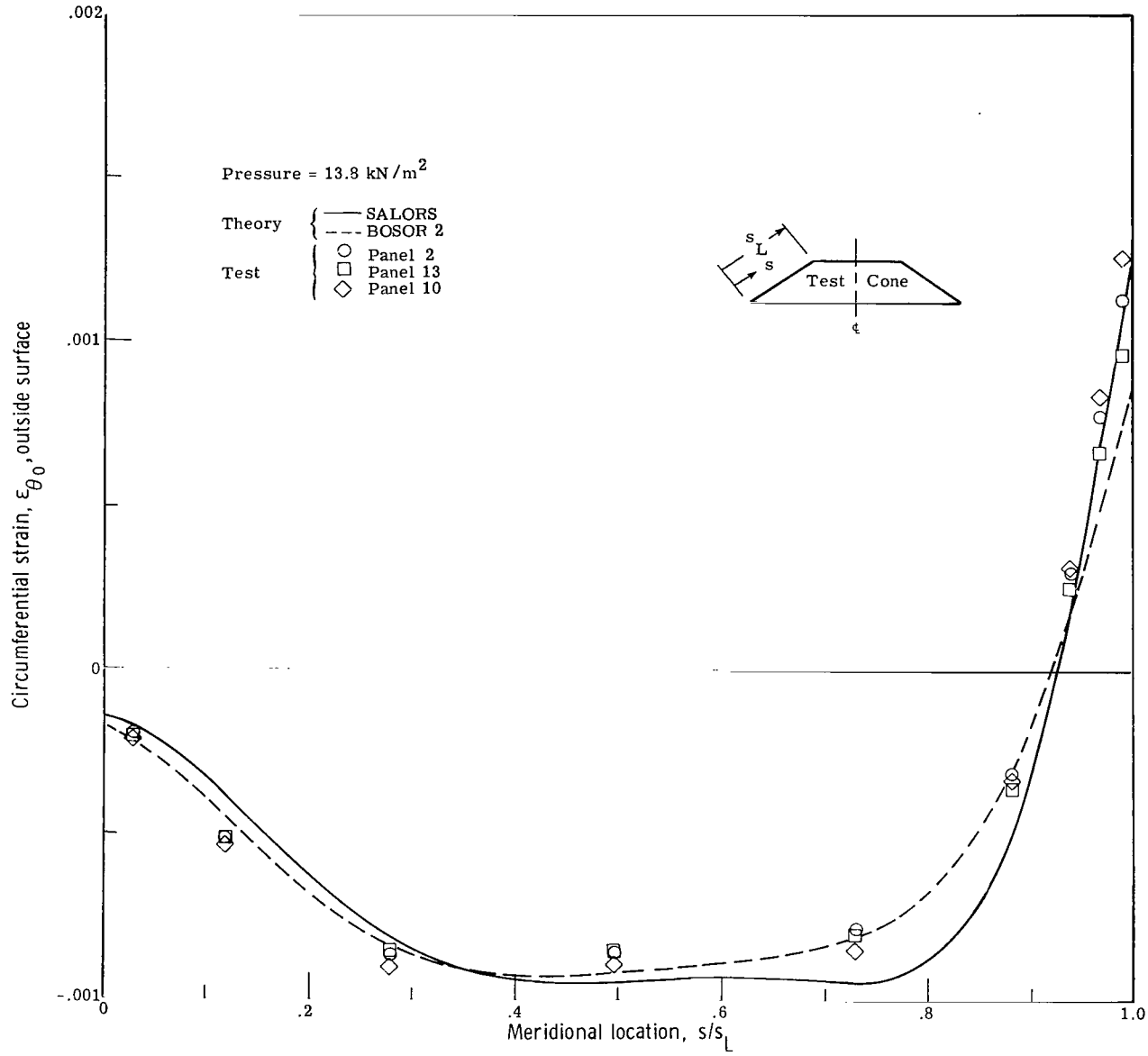

(b) Cone 2.

Figure 6.- Continued.

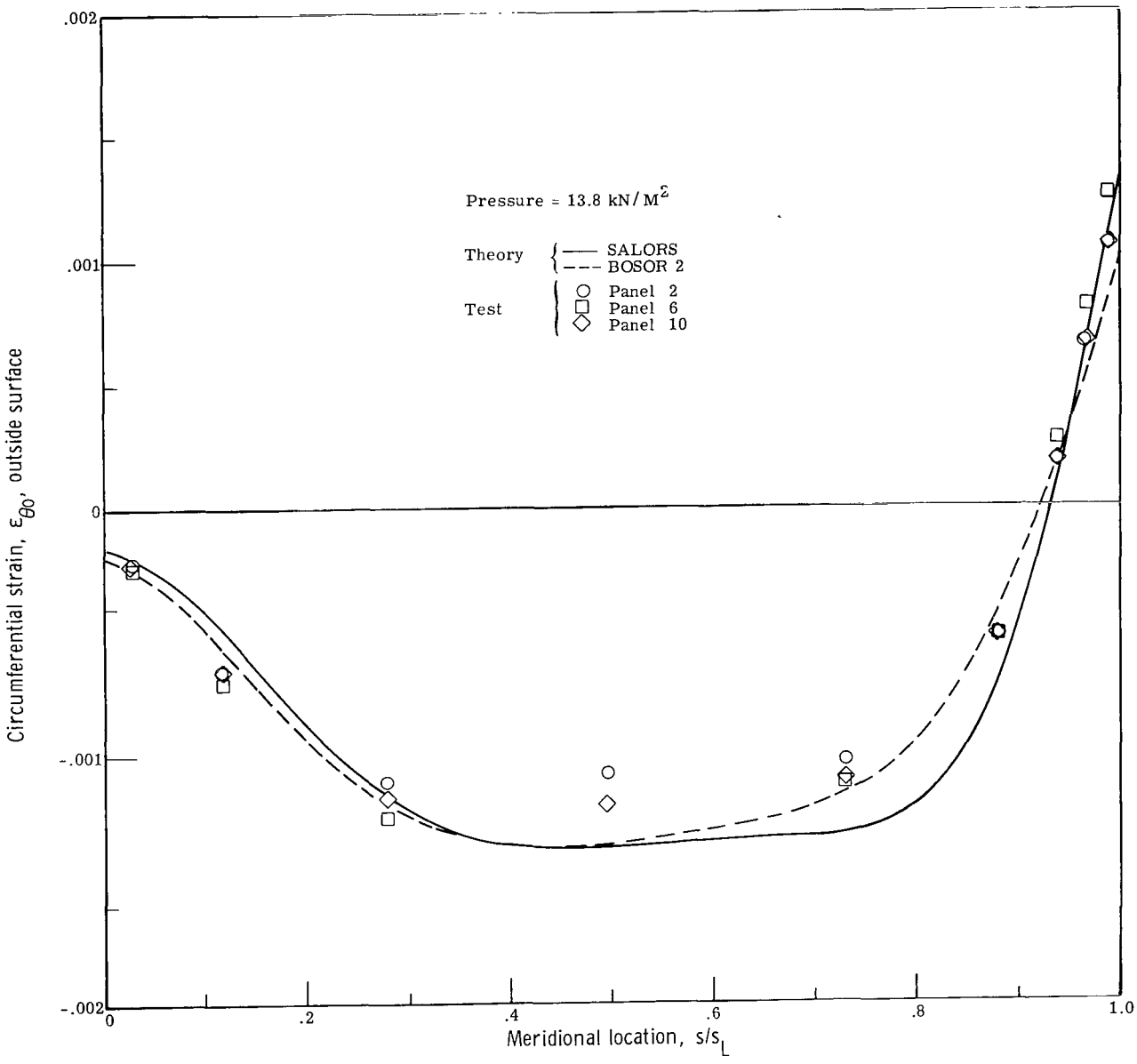

(c) Cone 3.

Figure 6.- Concluded.

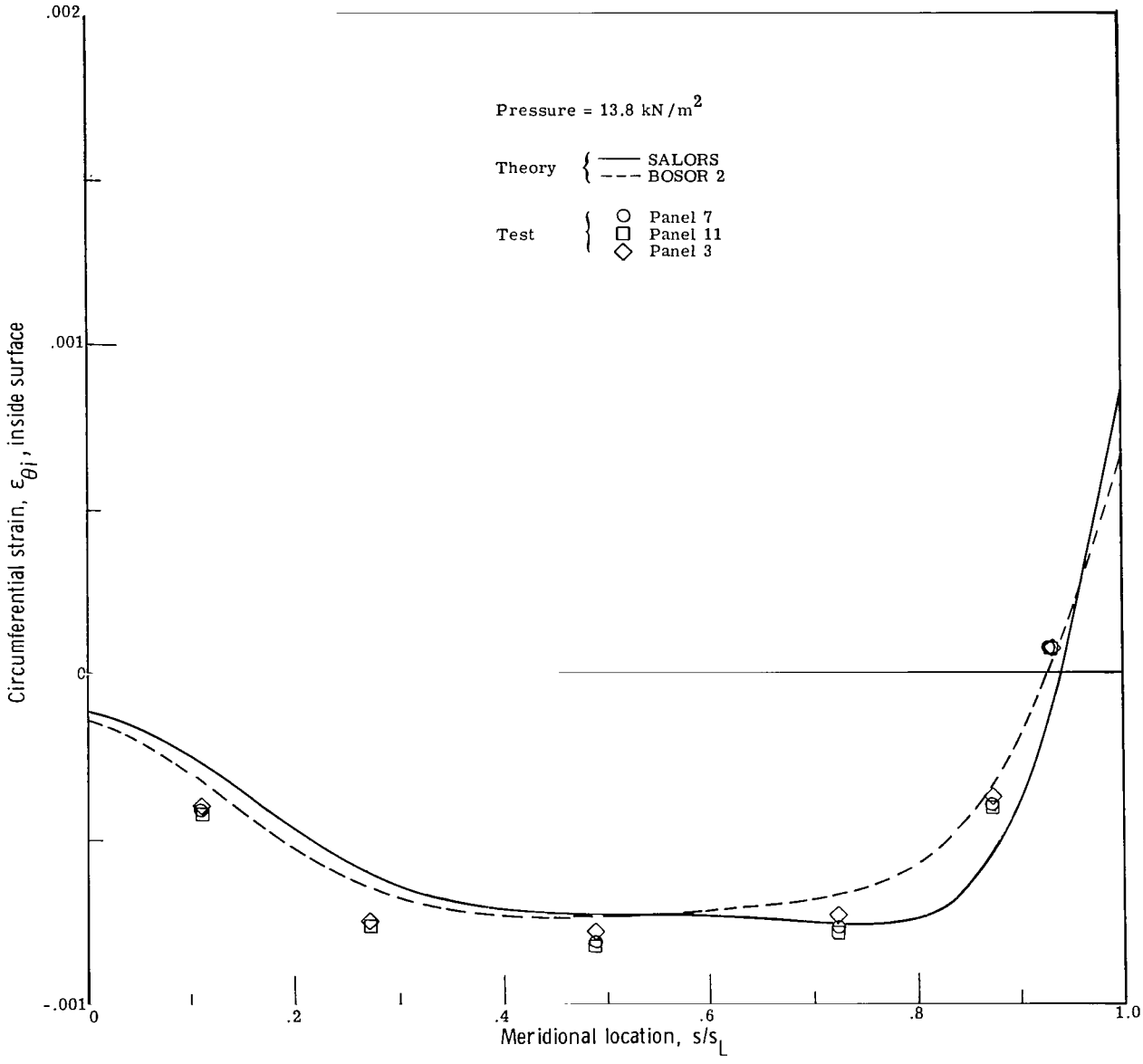

(a) Cone 1.

Figure 7.- Comparison of test and theoretical circumferential strains on inside surface.

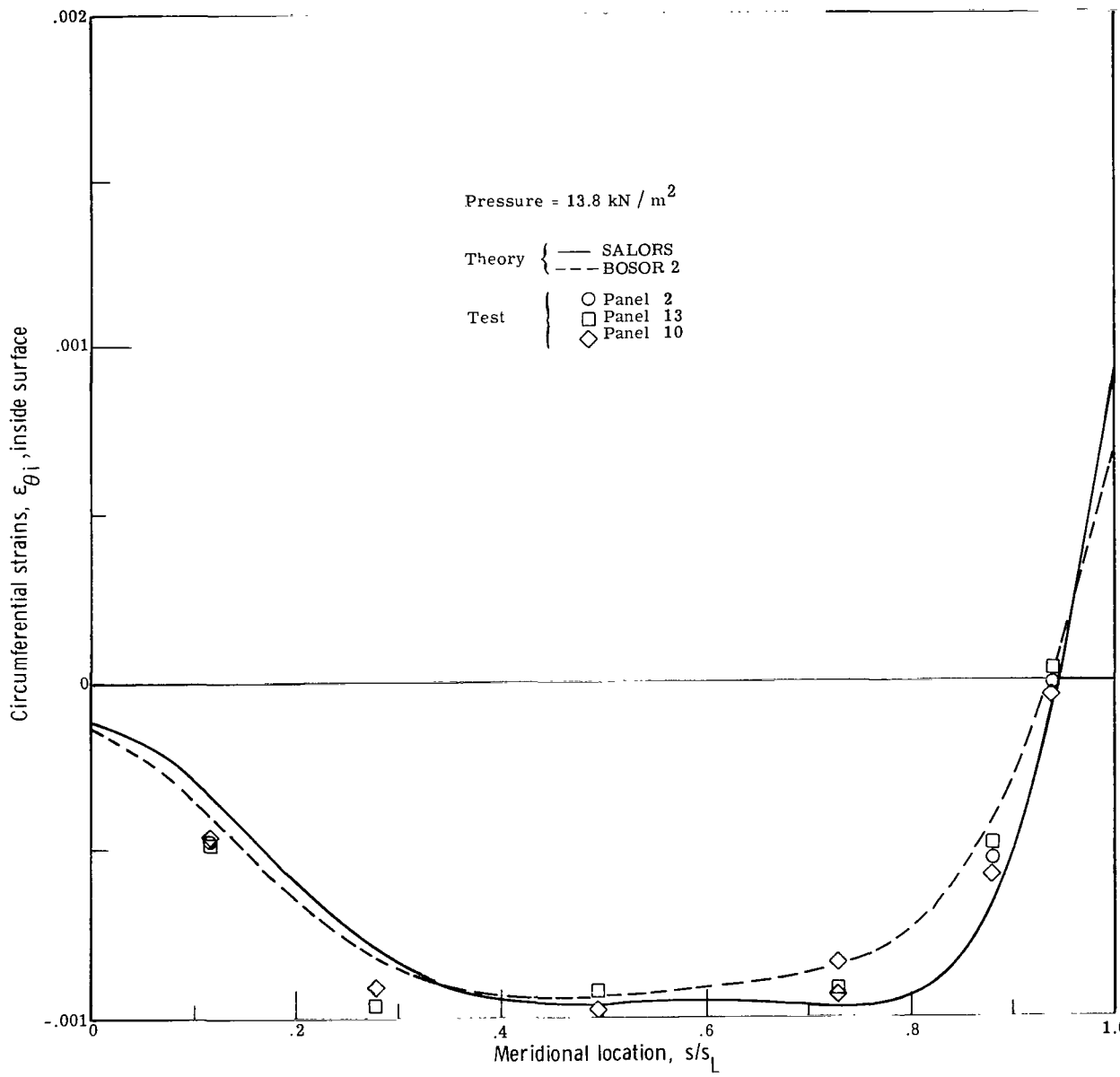

(b) Cone 2.

Figure 7.- Continued.

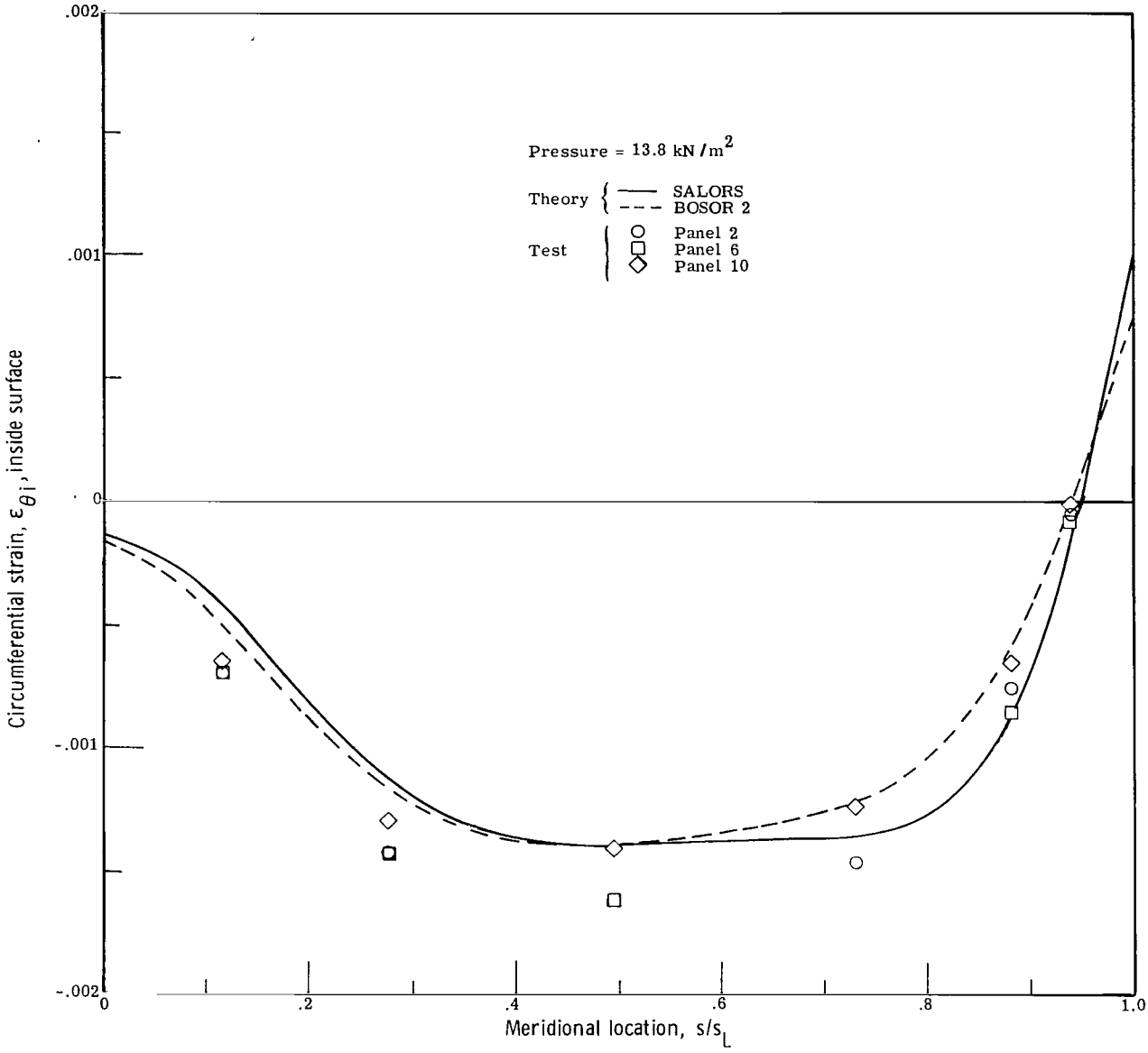

(c) Cone 3.

Figure 7.- Concluded.

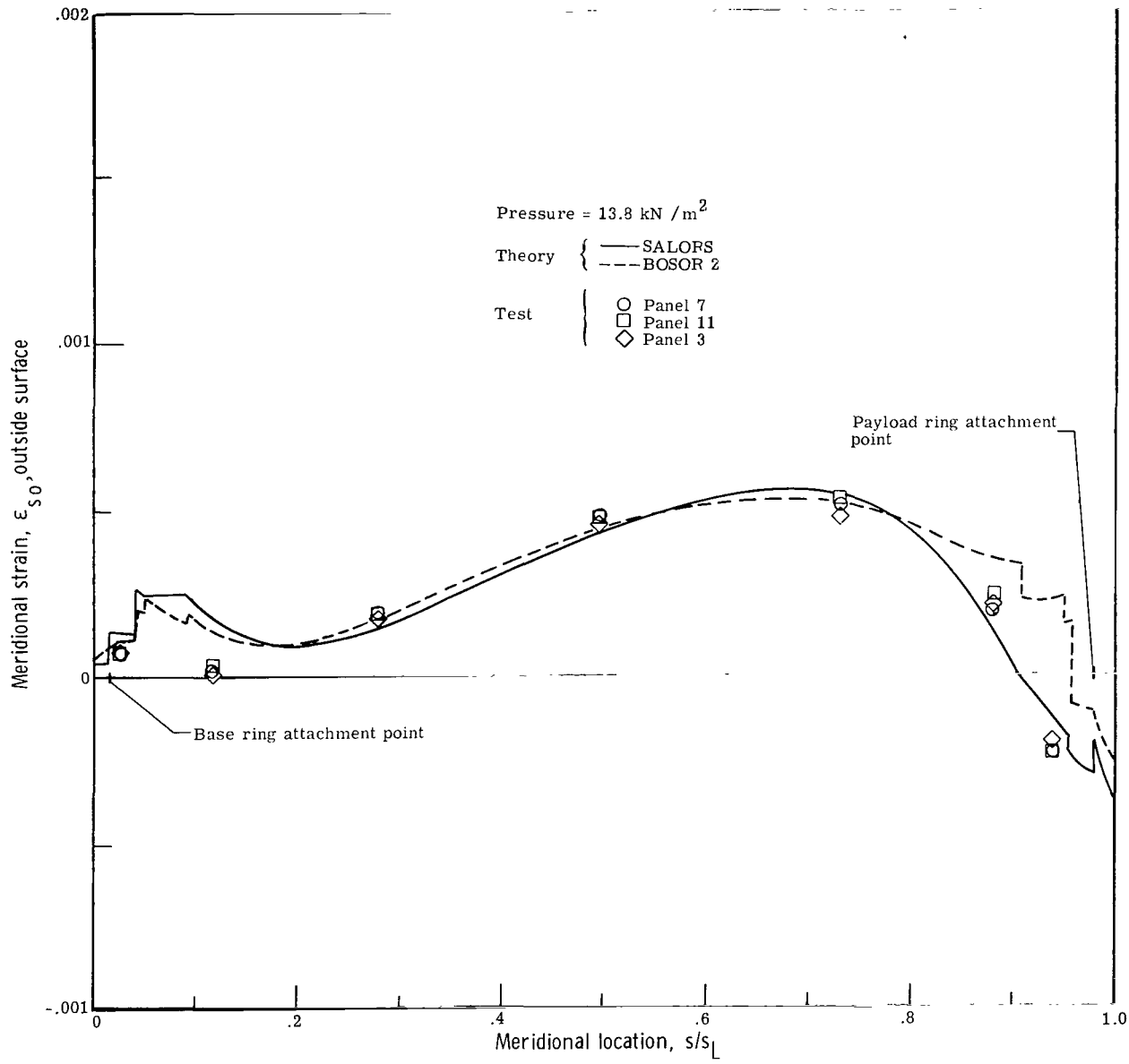

(a) Cone 1.

Figure 8.- Comparison of test and theoretical meridional strains on outside surface.

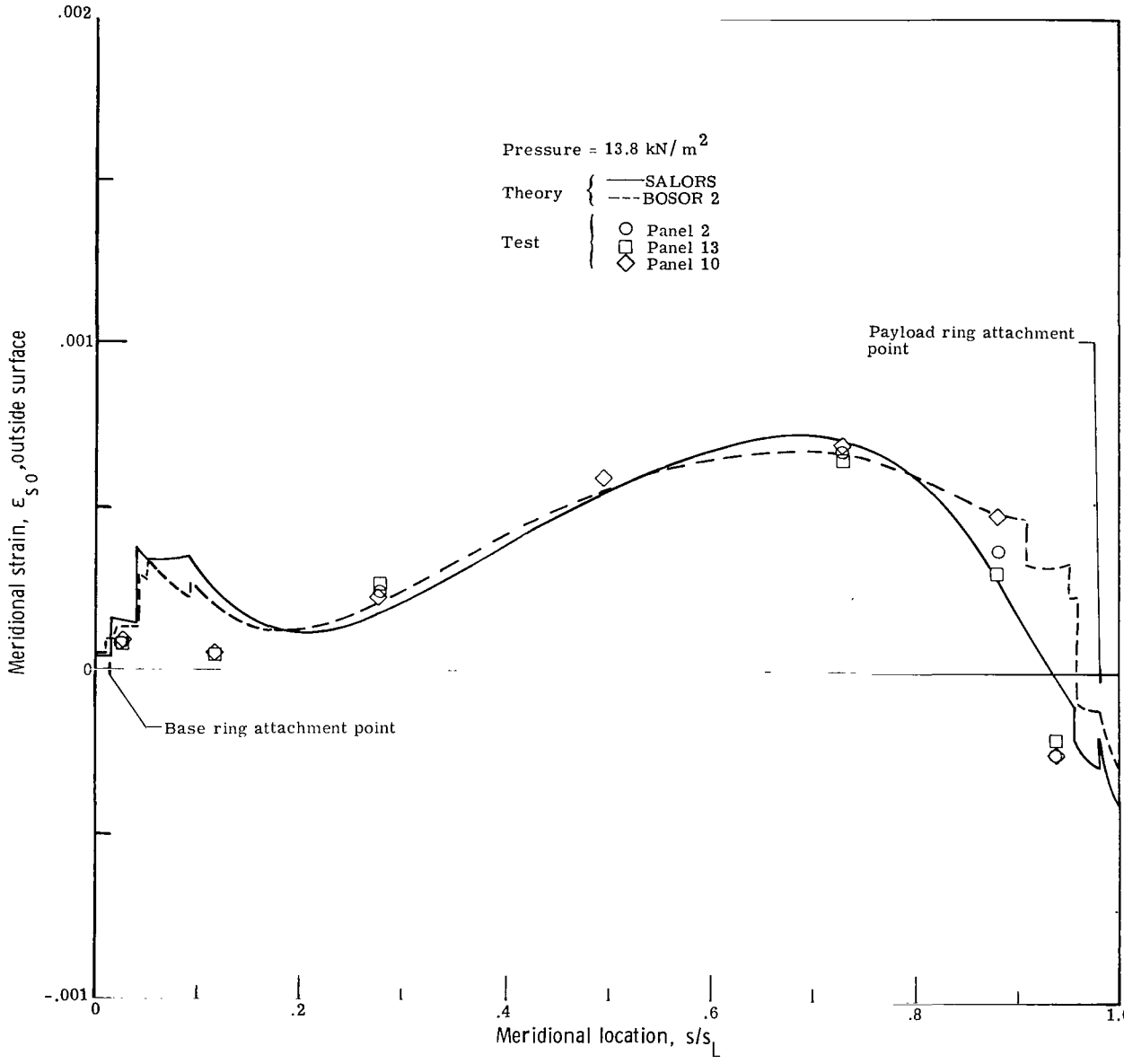

(b) Cone 2.

Figure 8.- Continued.

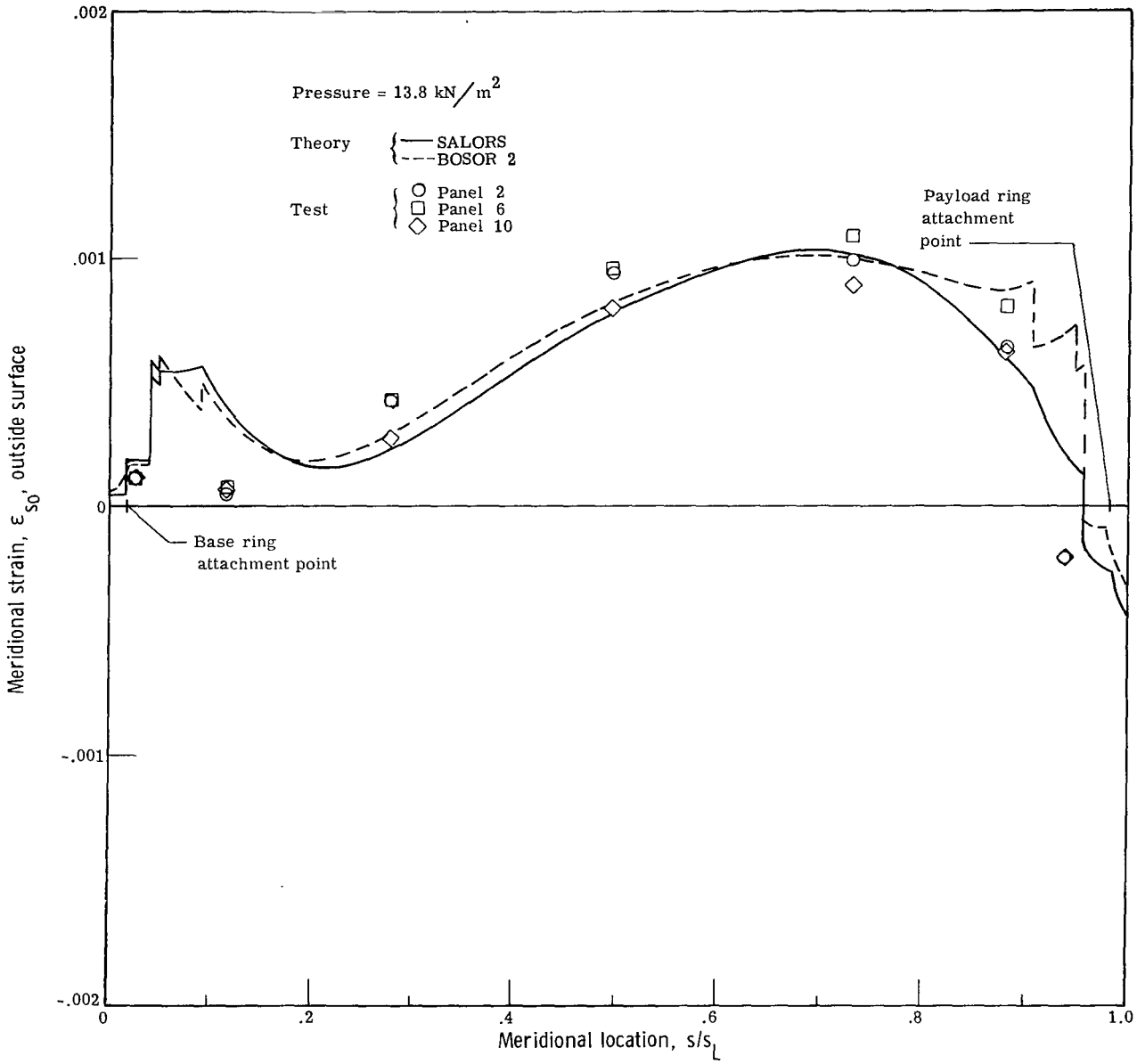

(c) Cone 3.

Figure 8.- Concluded.

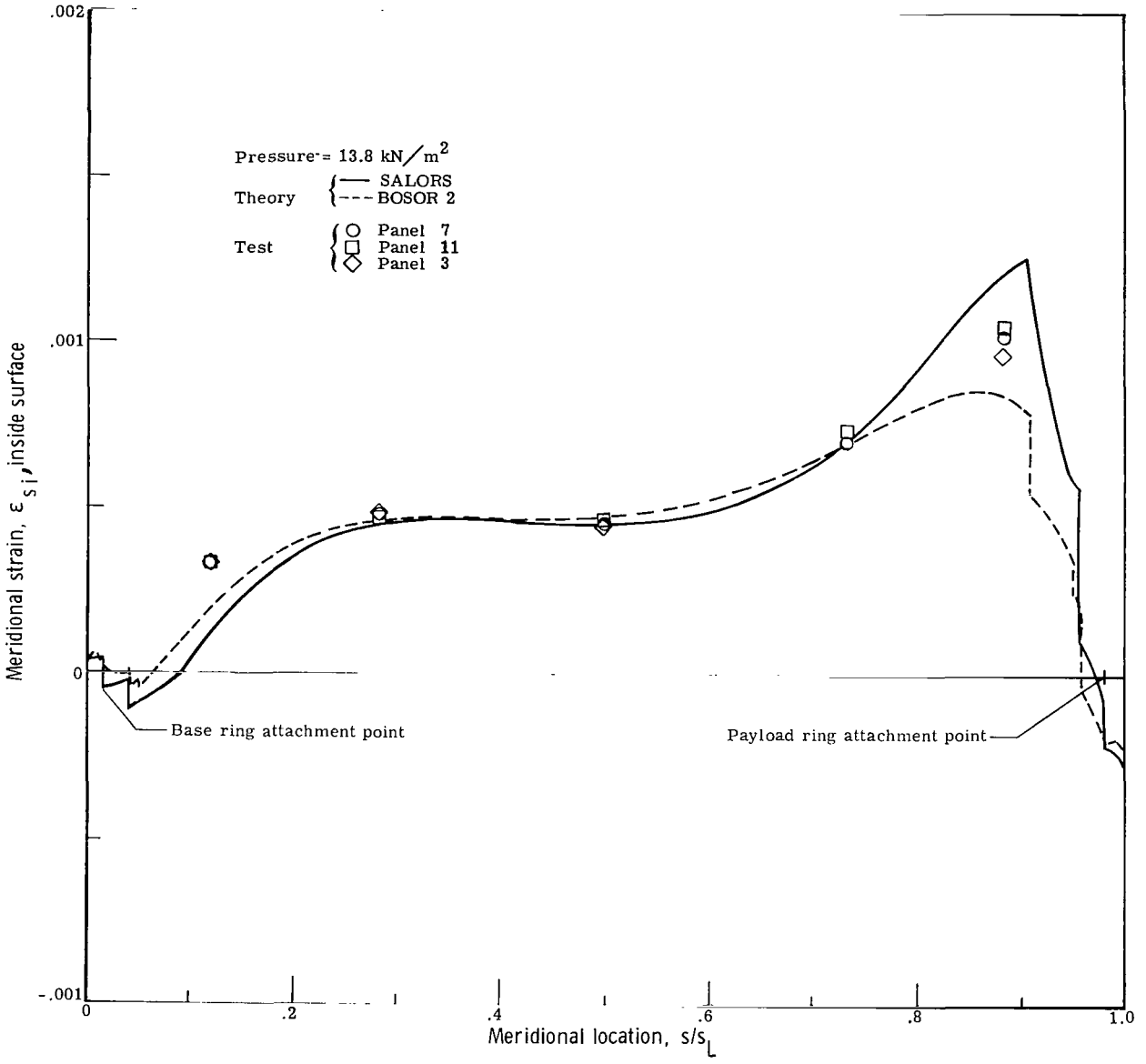

(a) Cone 1.

Figure 9.- Comparison of test and theoretical meridional strains on the inside surface.

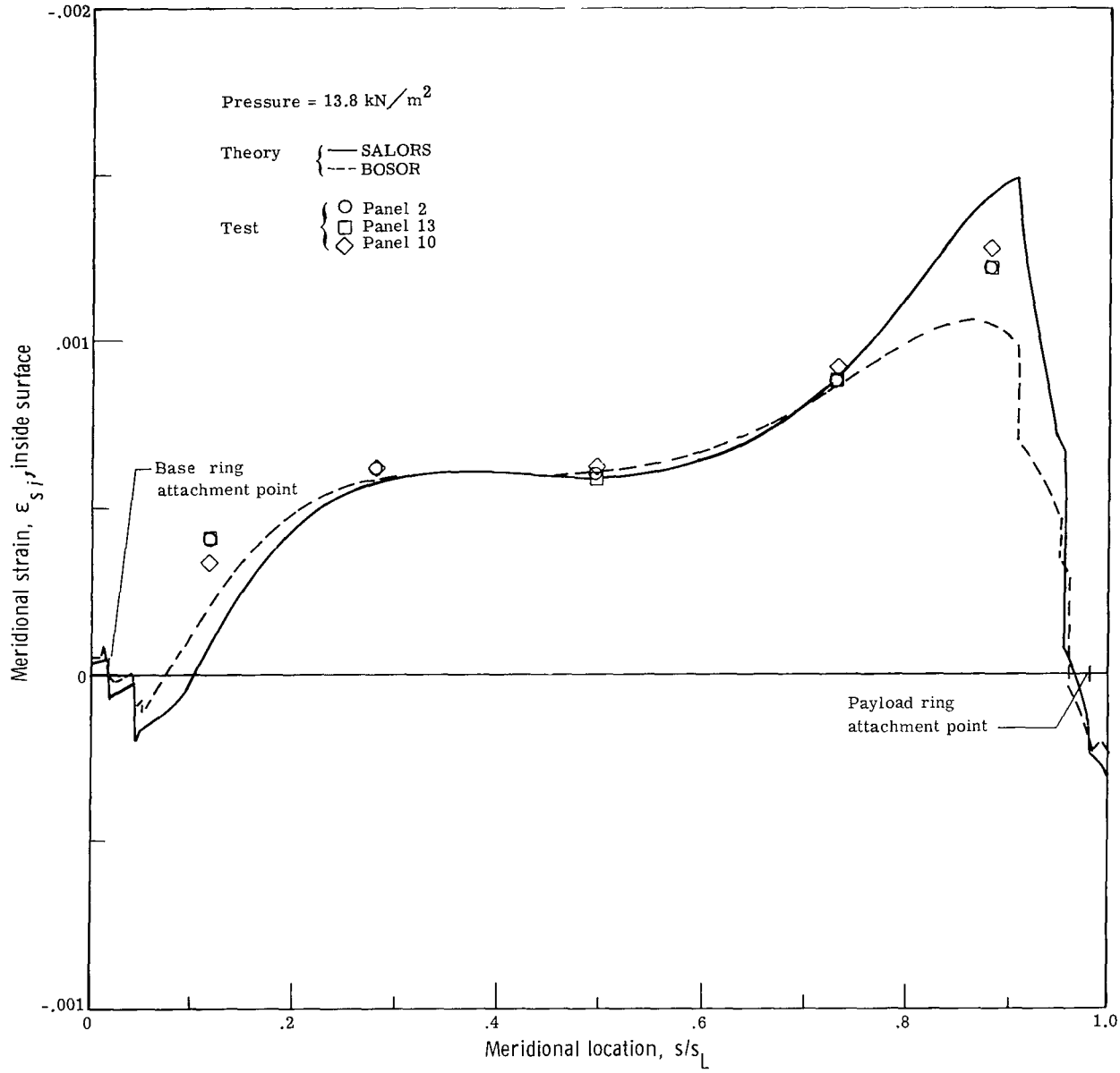

(b) Cone 2.

Figure 9.- Continued.

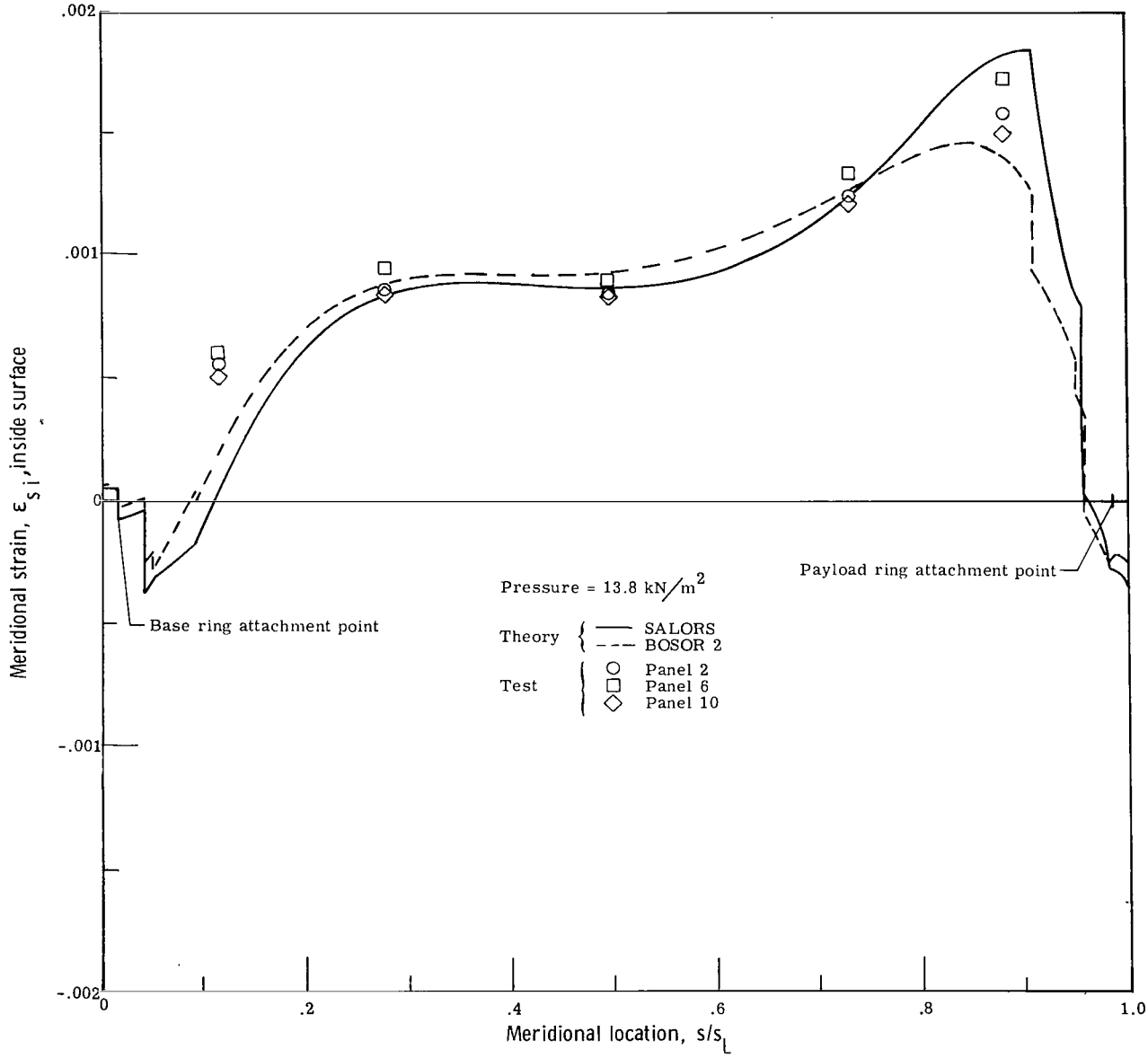

(c) Cone 3.

Figure 9.- Concluded.

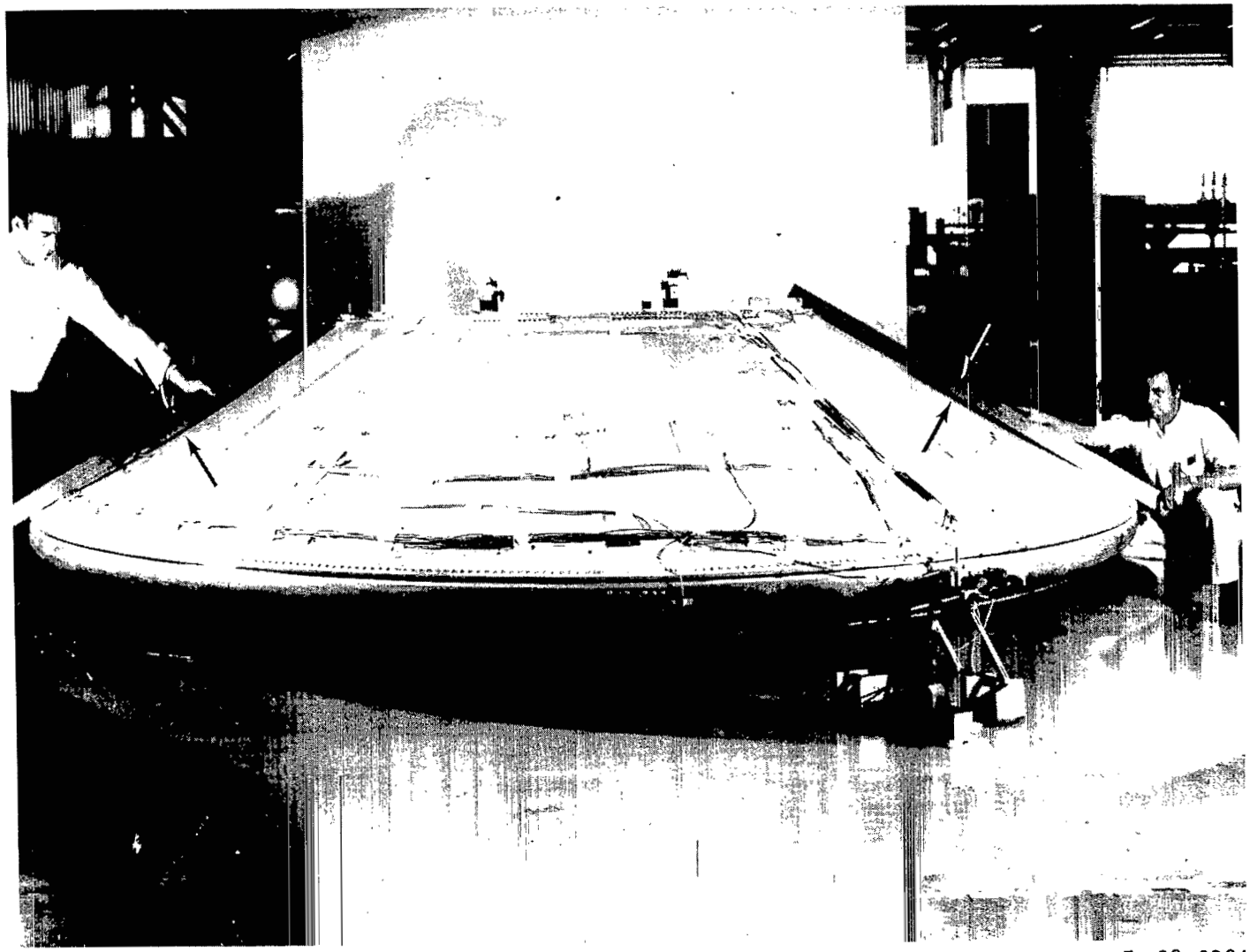

L-69-6094

Figure 10.- Buckled cone 2. (Pressure maintained to hold buckle pattern.)

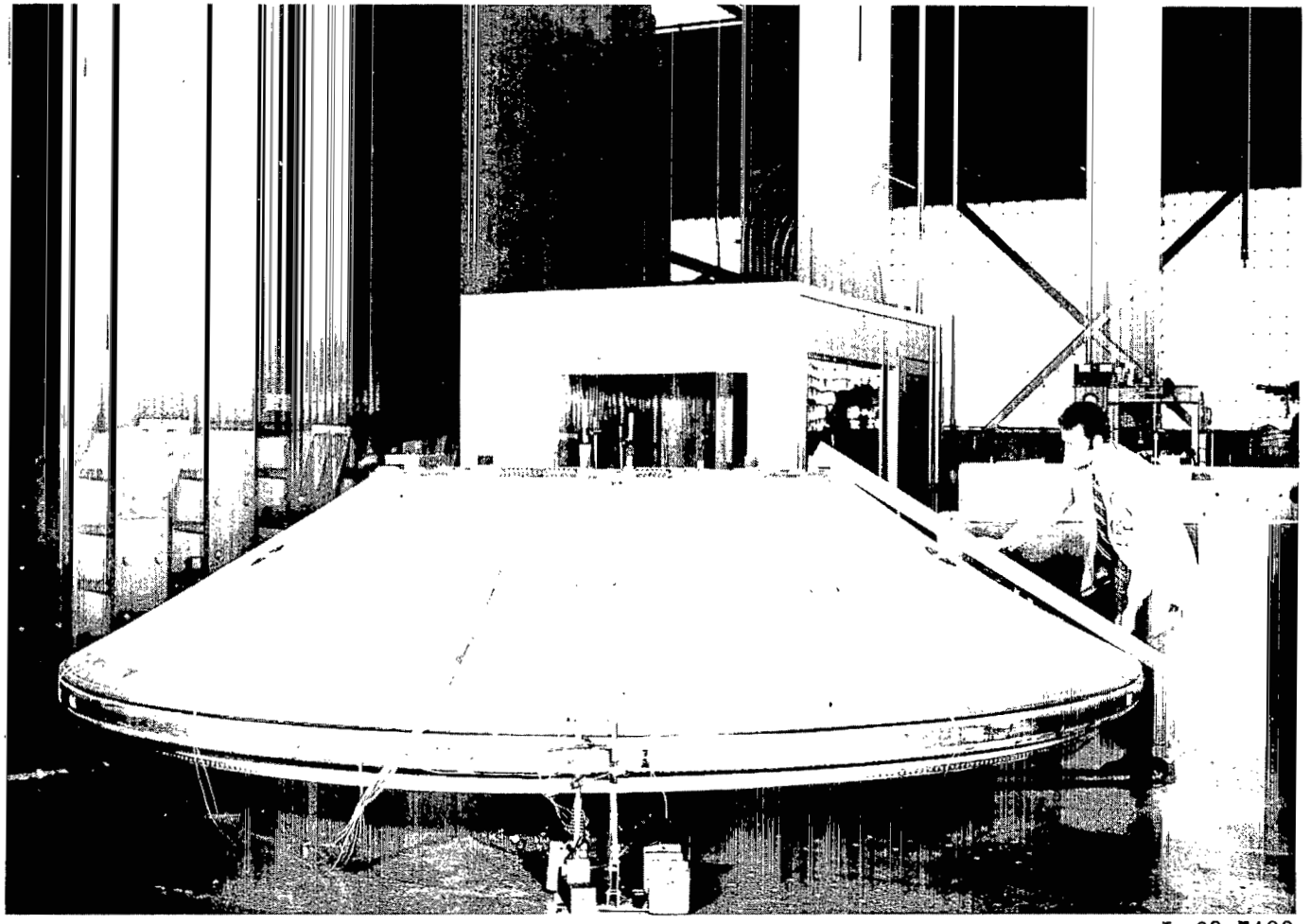

L-69-7489

Figure 11.- Buckled cone 3. (Pressure maintained to hold buckle pattern.)

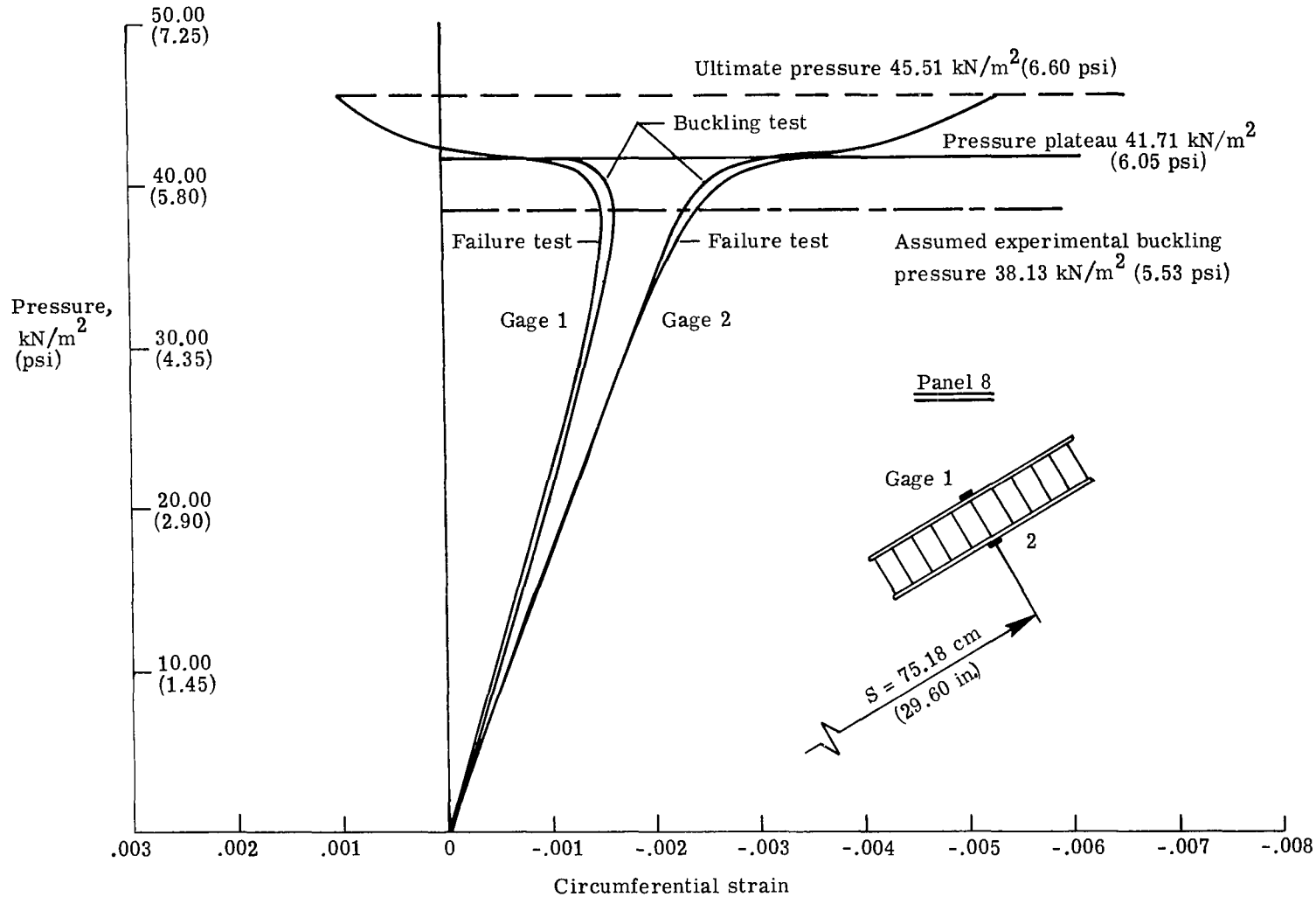

(a) Cone 1.

Figure 12.- Pressure-strain relationship at center of panel exhibiting the most wall bending.

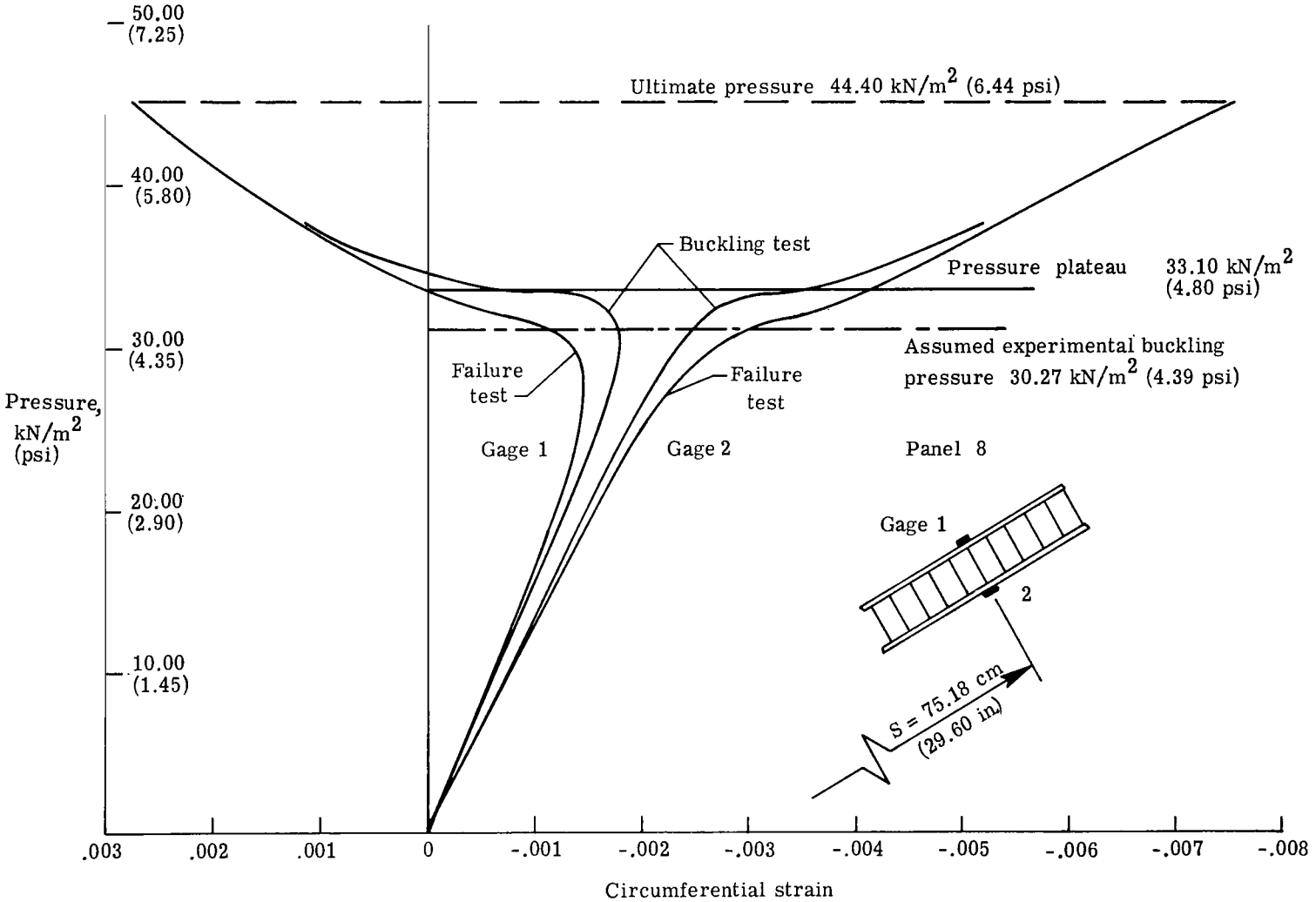

(b) Cone 2.

Figure 12.- Continued.

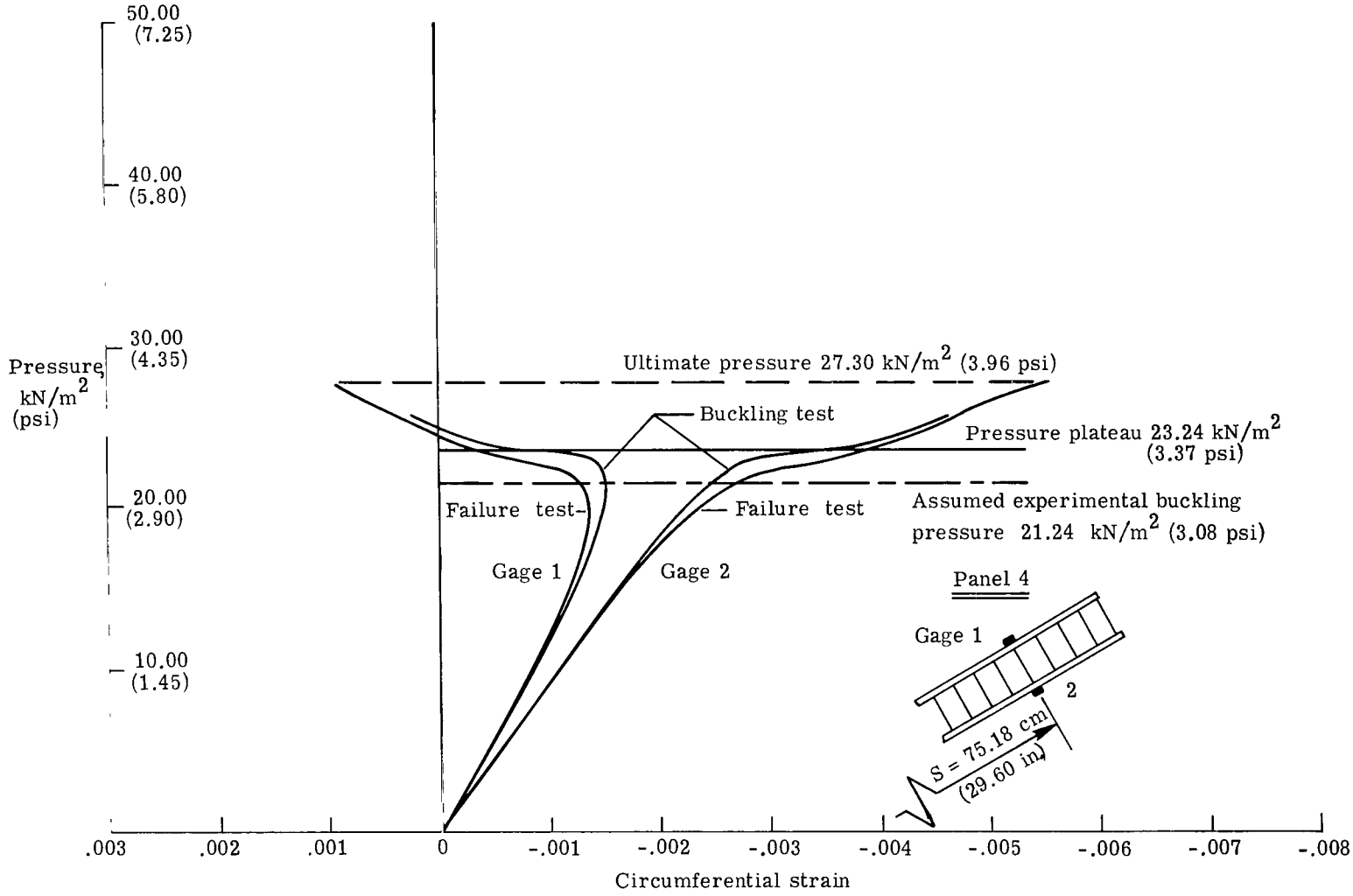

(c) Cone 3.

Figure 12.- Concluded.

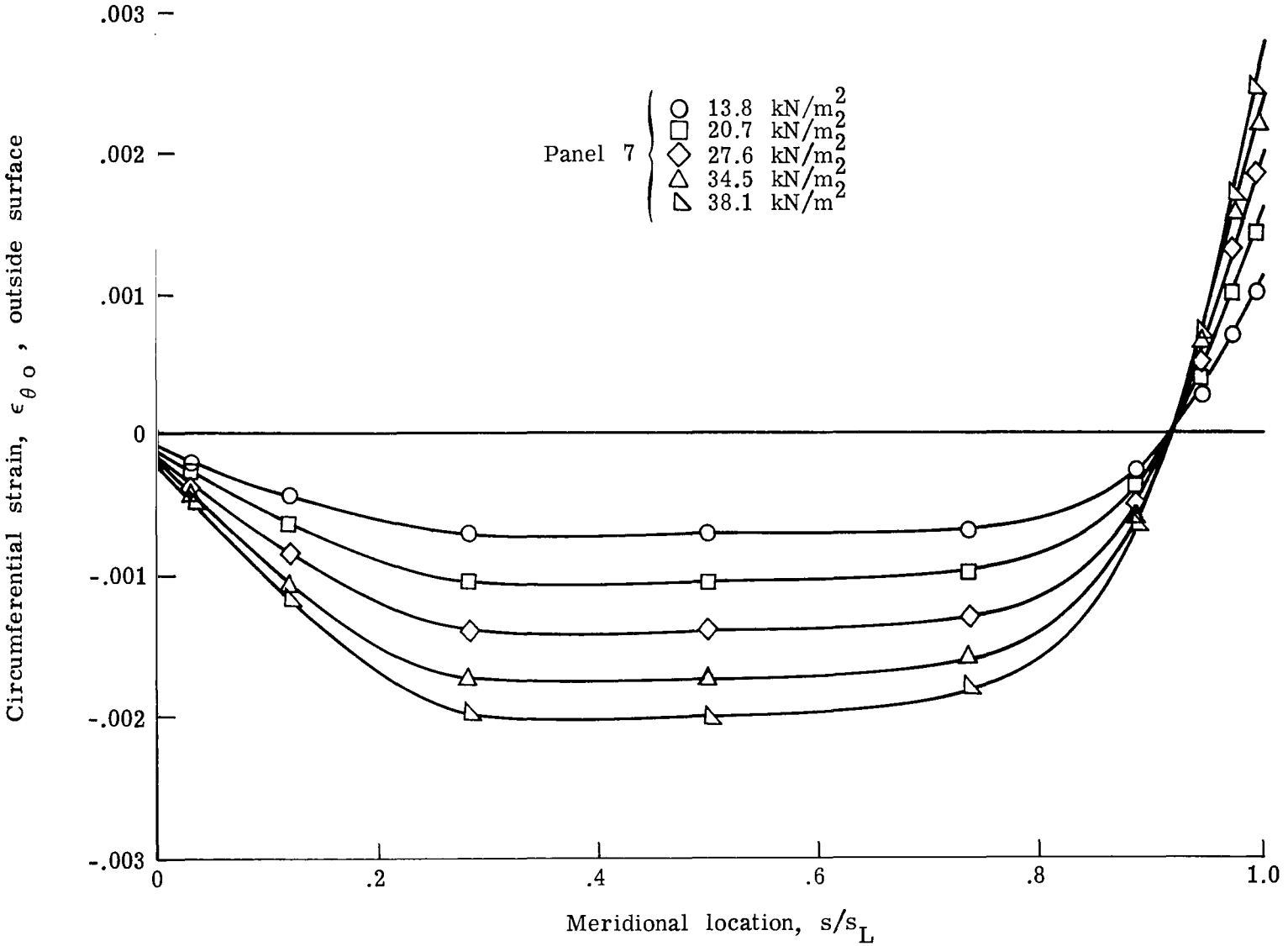

(a) Cone 1.

Figure 13.- Strain profiles during buckling test, outside circumferential strains.

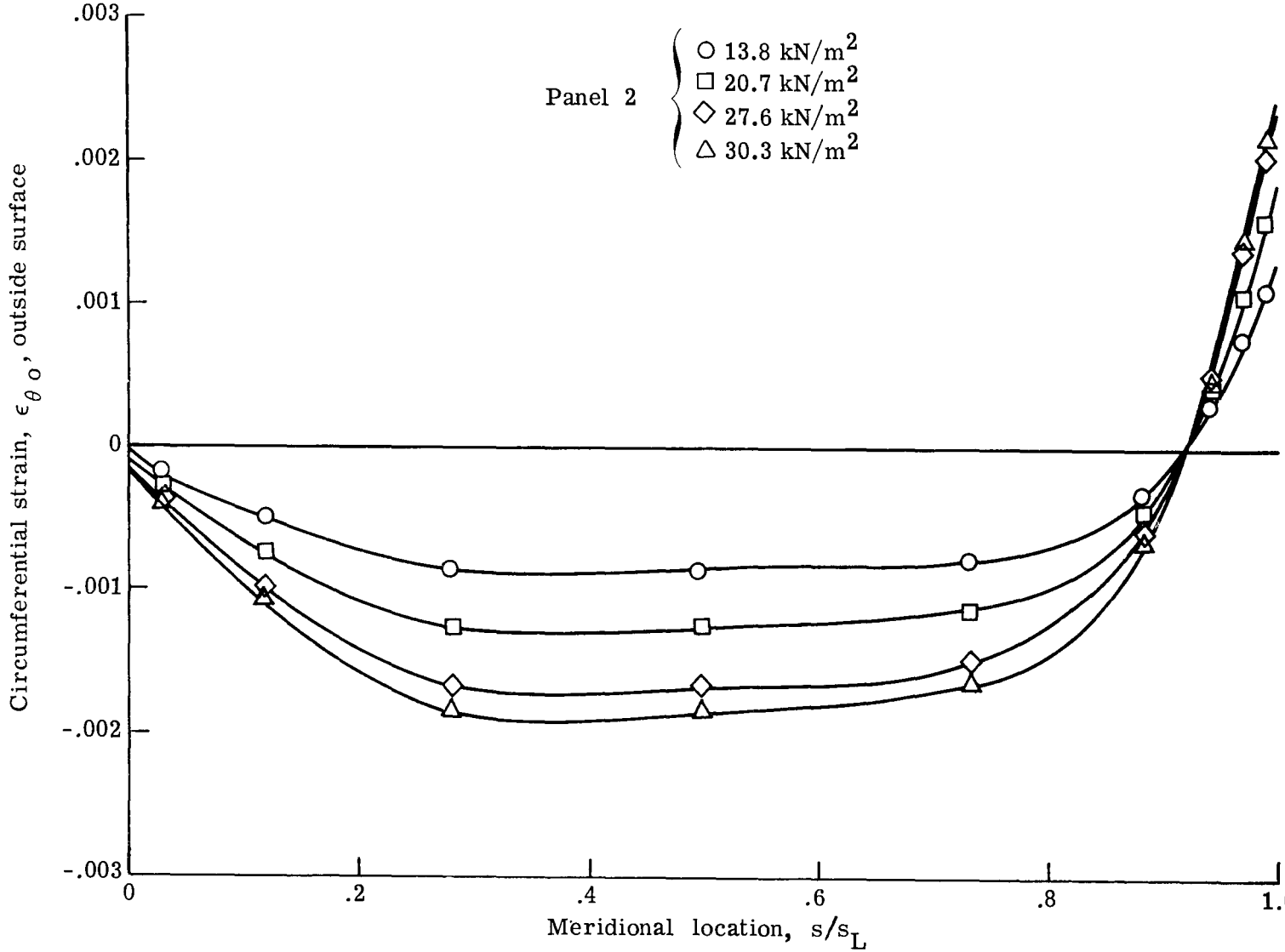

(b) Cone 2.

Figure 13.- Continued.

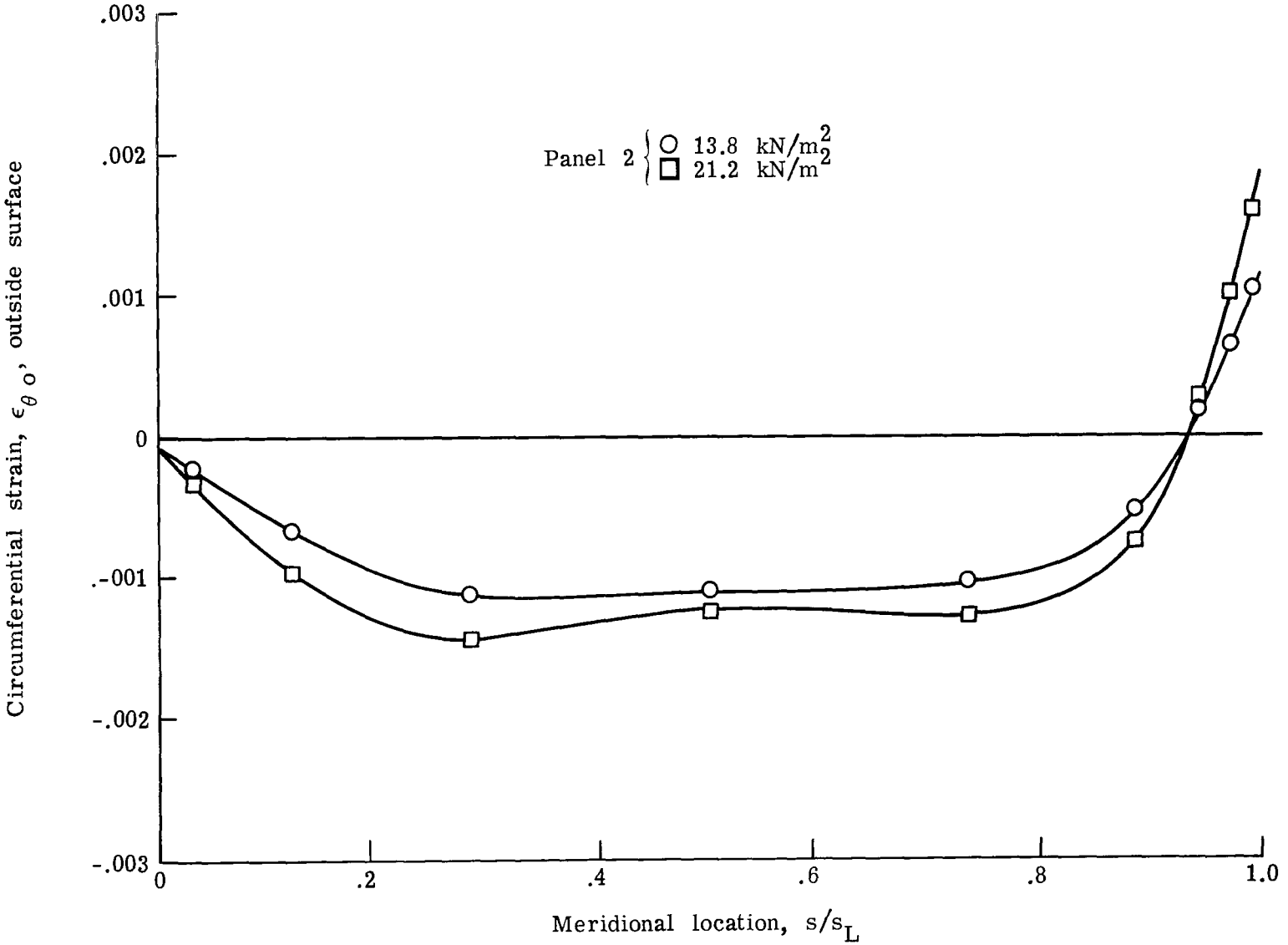

(c) Cone 3.

Figure 13.- Concluded.

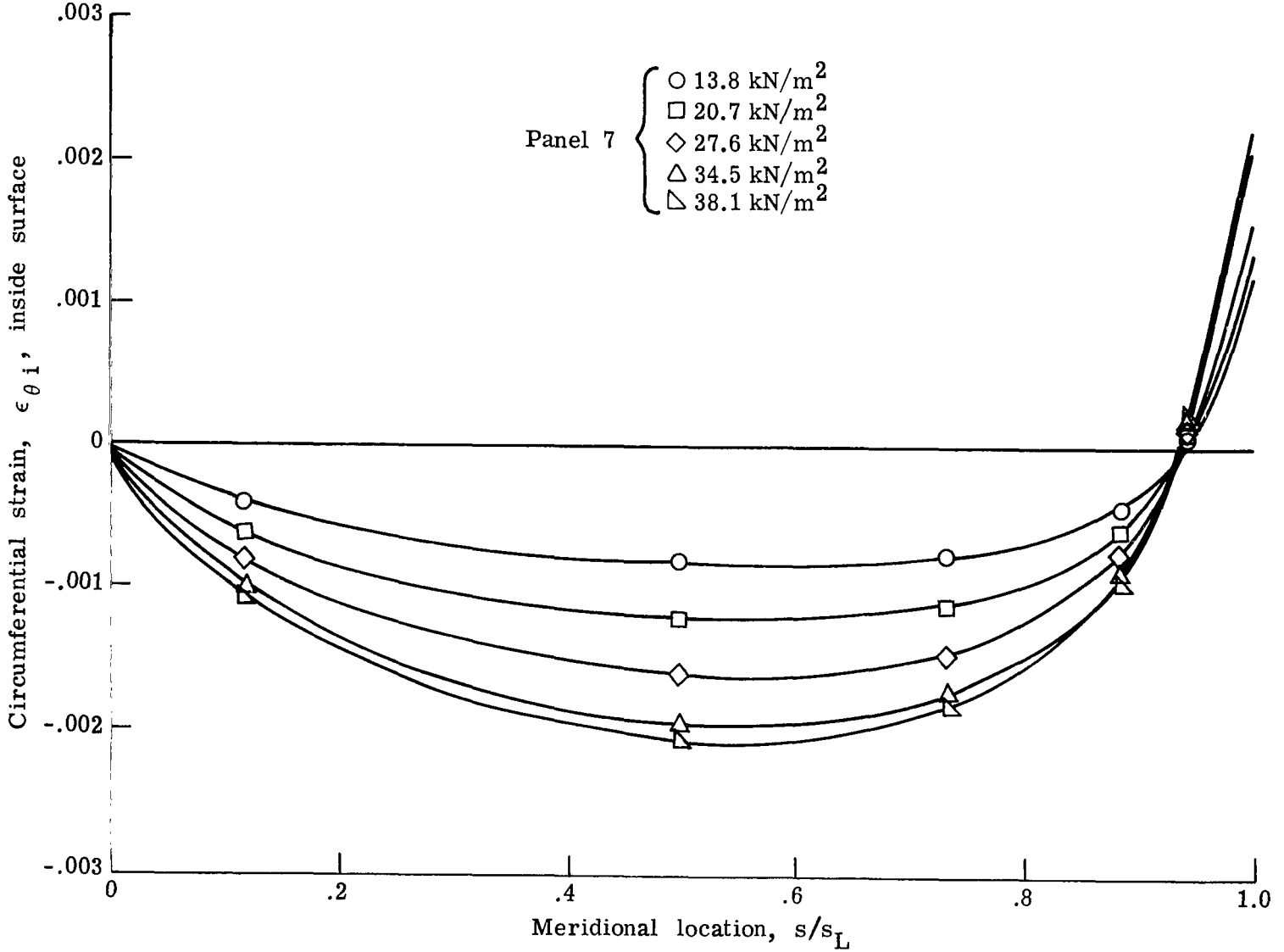

(a) Cone 1.

Figure 14.- Strain profiles during buckling test, inside circumferential strains.

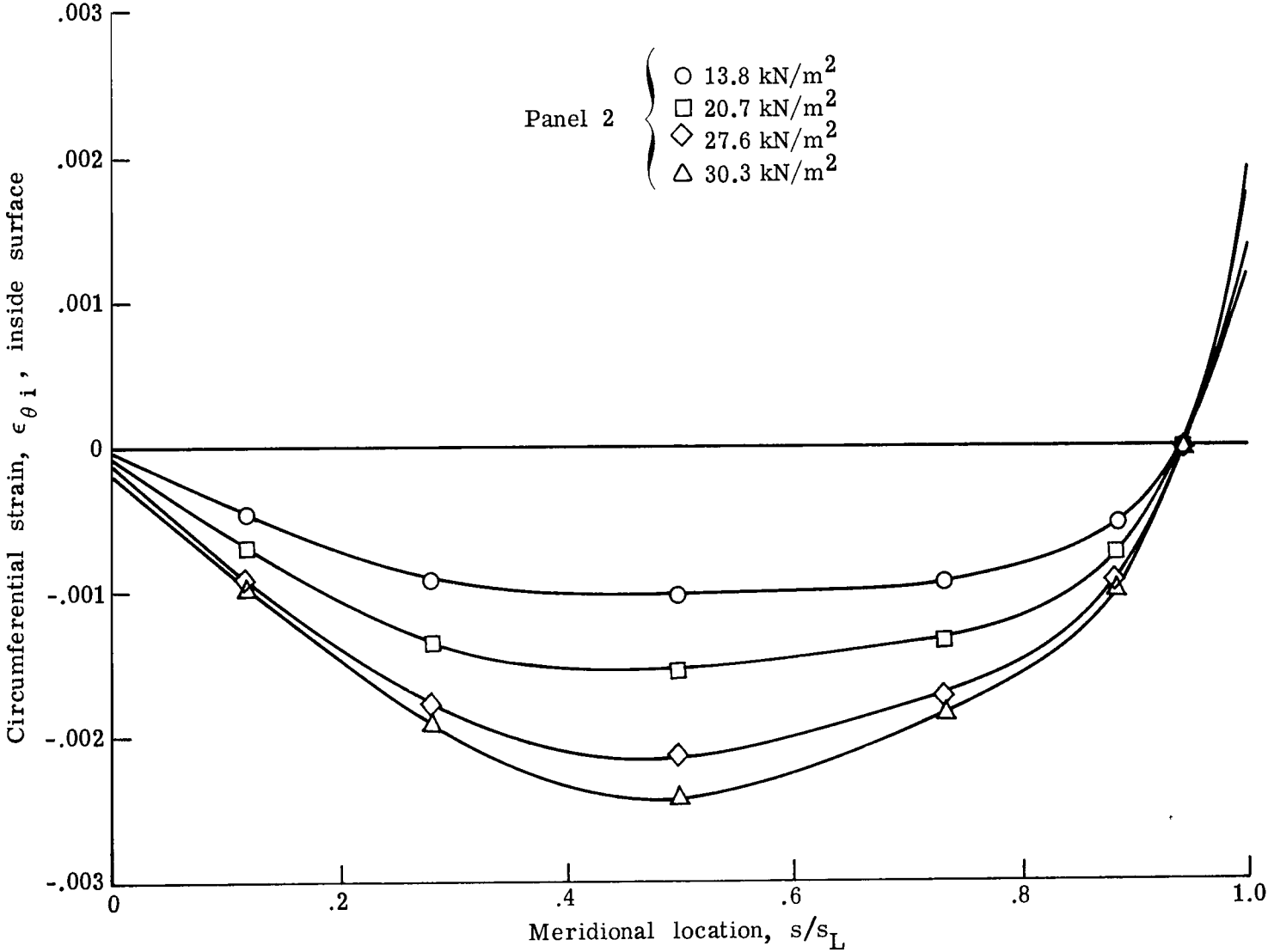

(b) Cone 2.

Figure 14.- Continued.

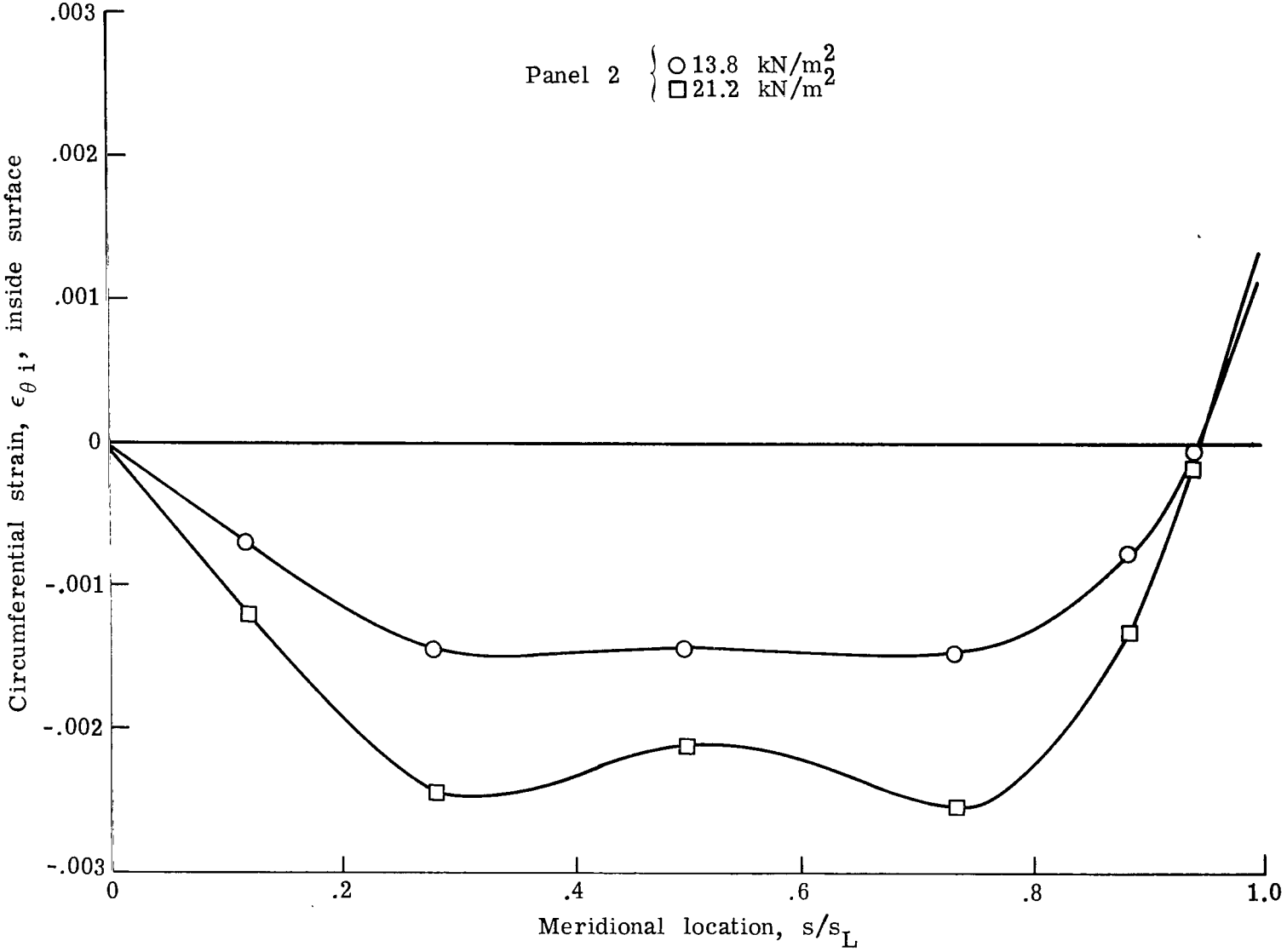

(c) Cone 3.

Figure 14.- Concluded.

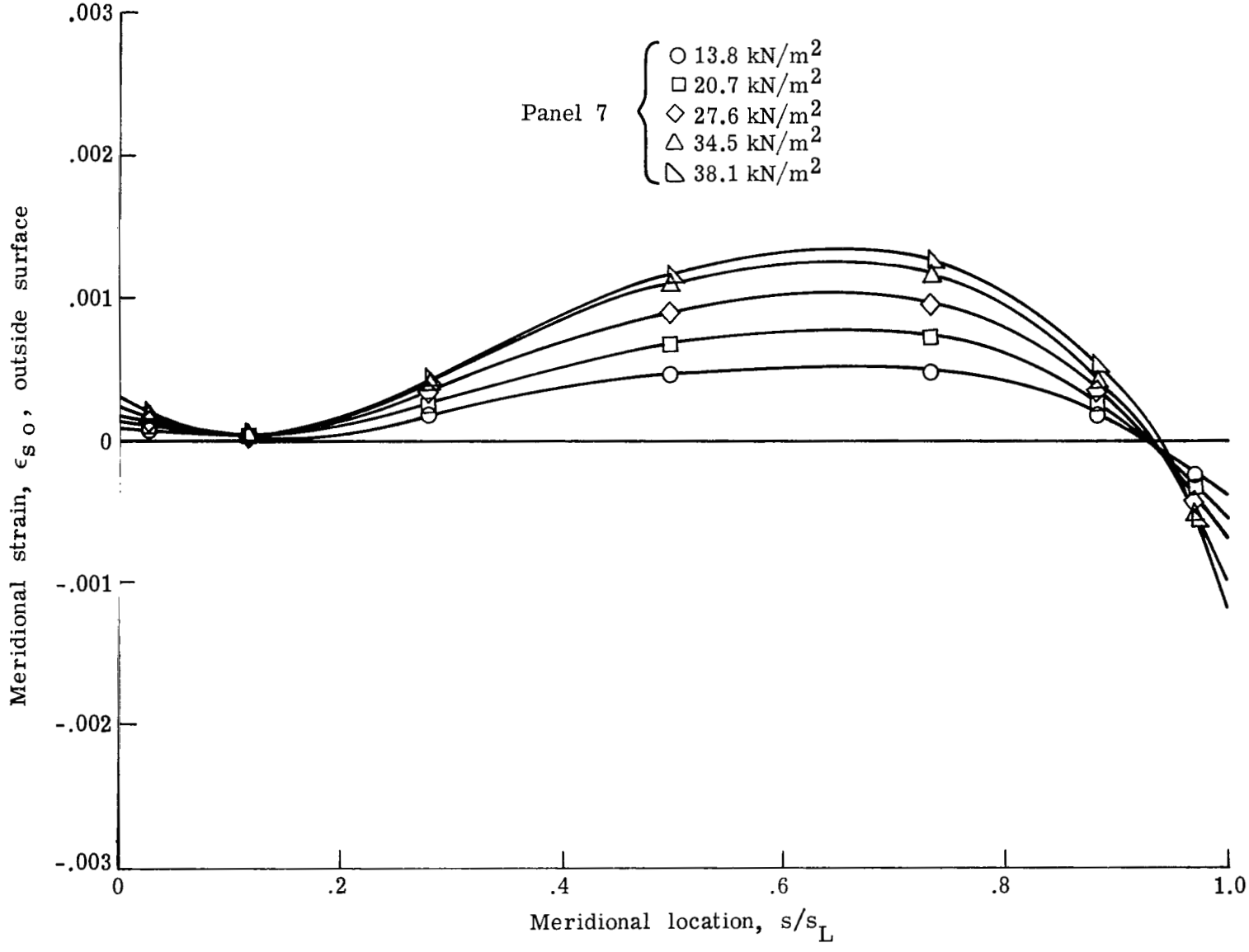

(a) Cone 1.

Figure 15.- Strain profiles during buckling test, outside meridional strains.

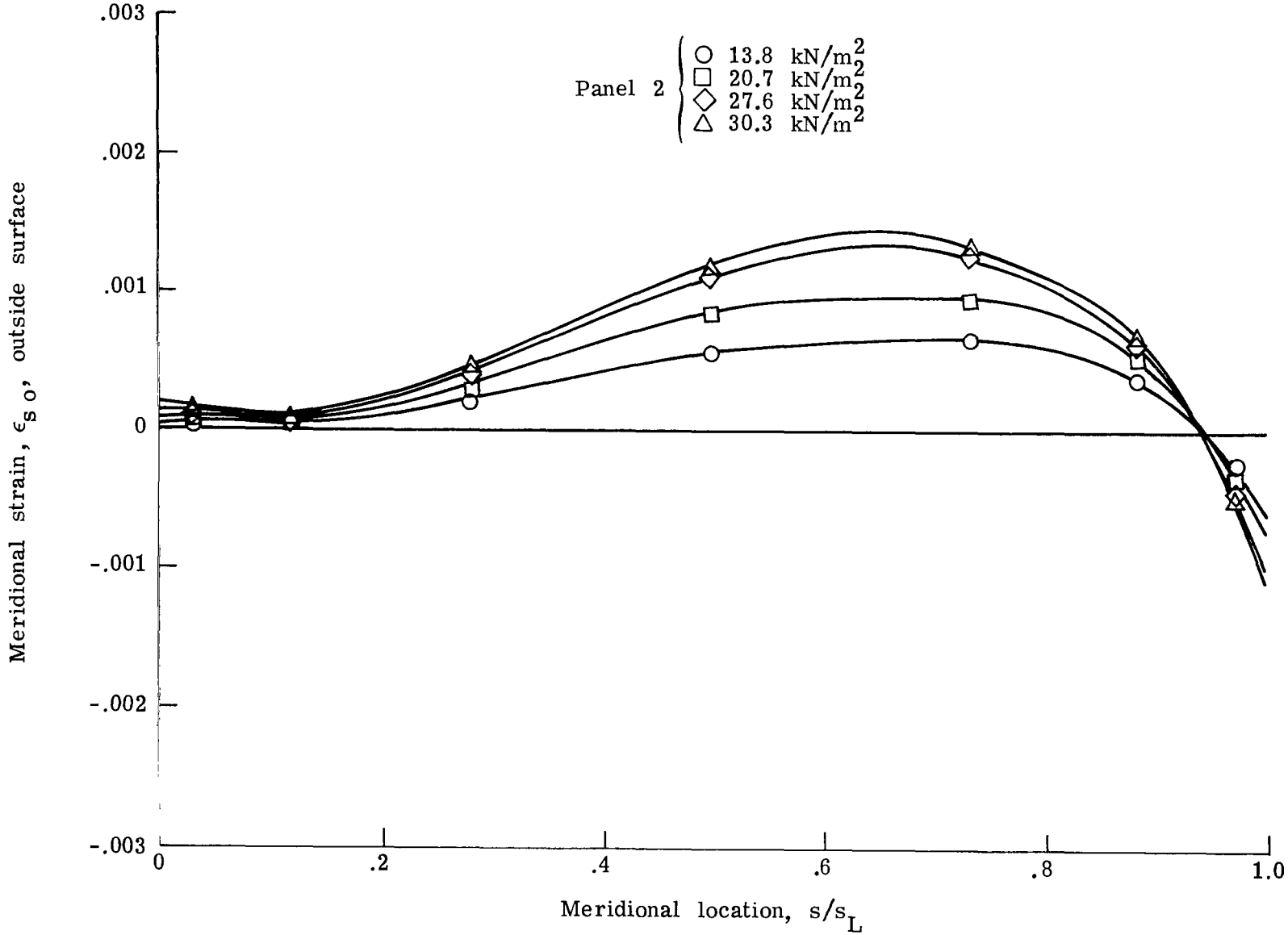

(b) Cone 2.

Figure 15.- Continued.

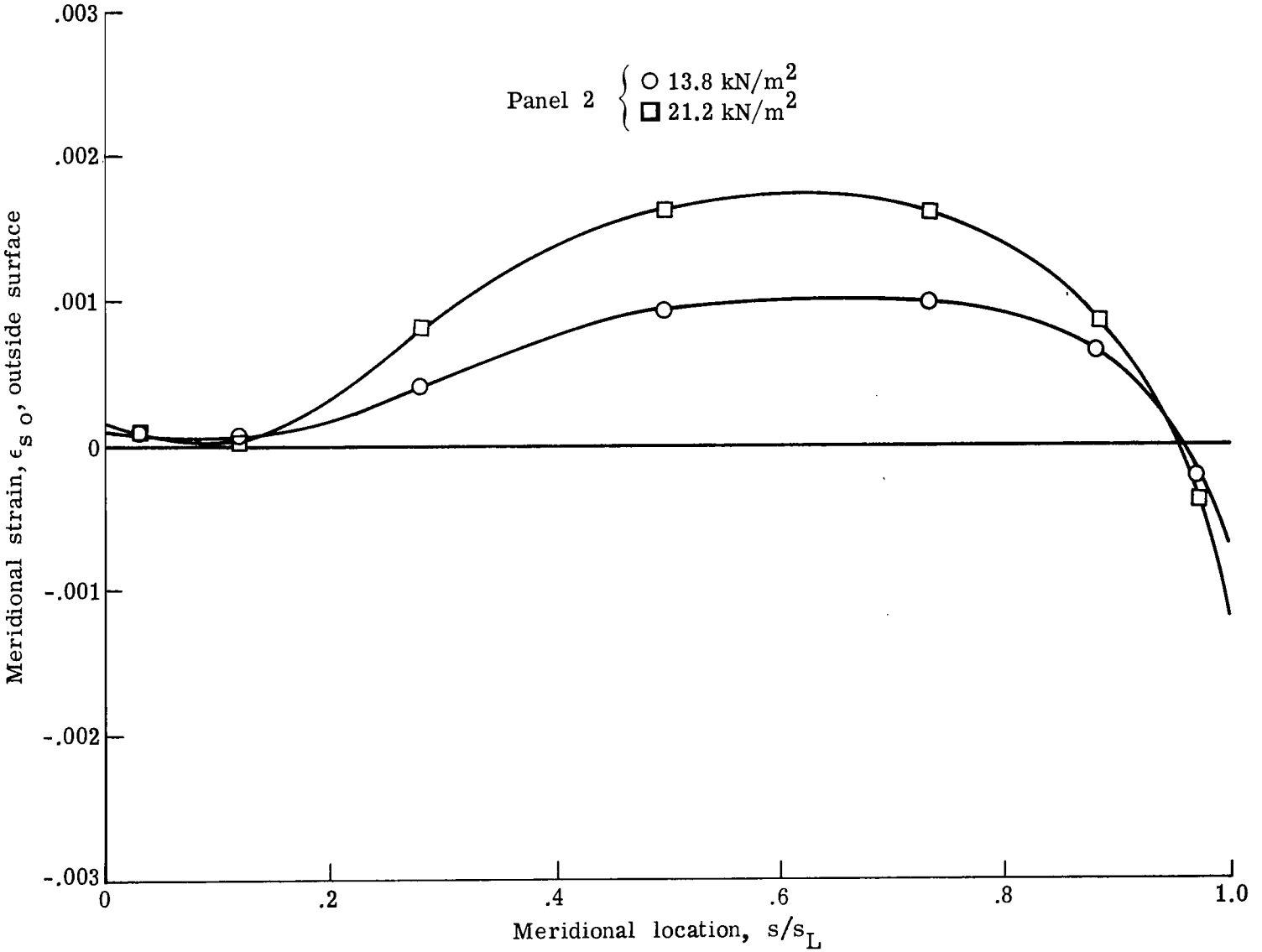

(c) Cone 3.

Figure 15.- Concluded.

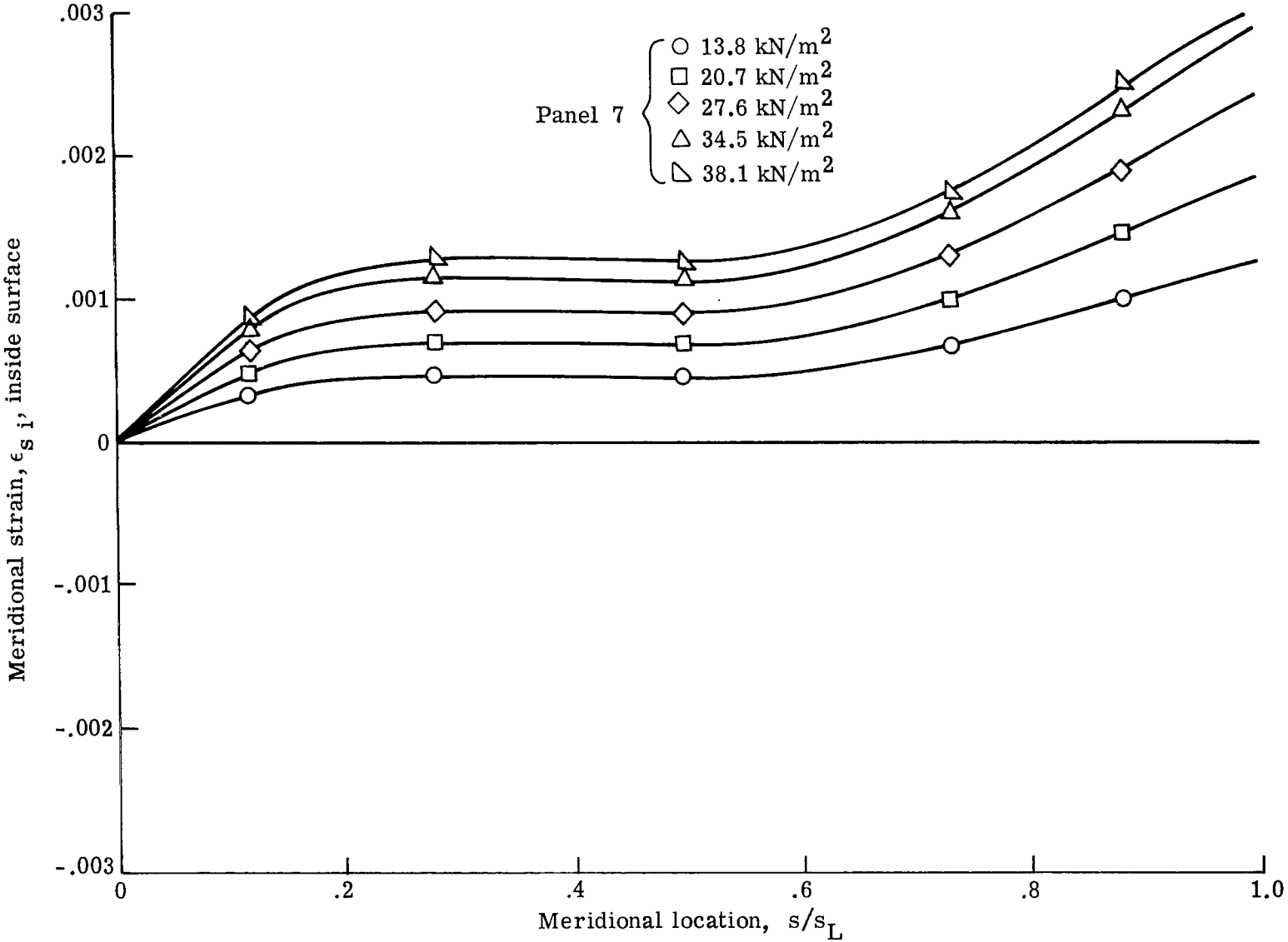

(a) Cone 1.

Figure 16.- Strain profiles during buckling test, inside meridional strains.

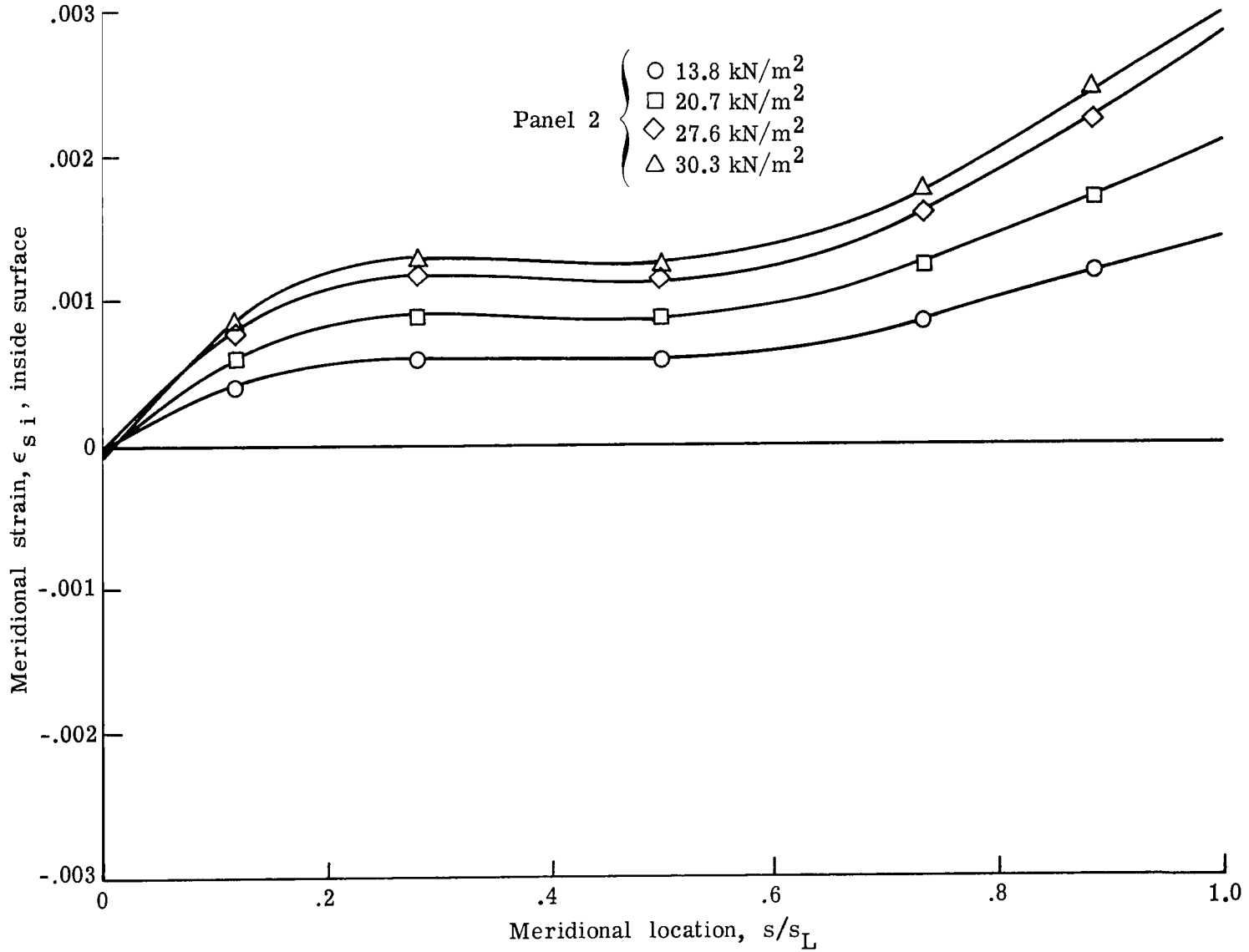

(b) Cone 2

Figure 16.- Continued.

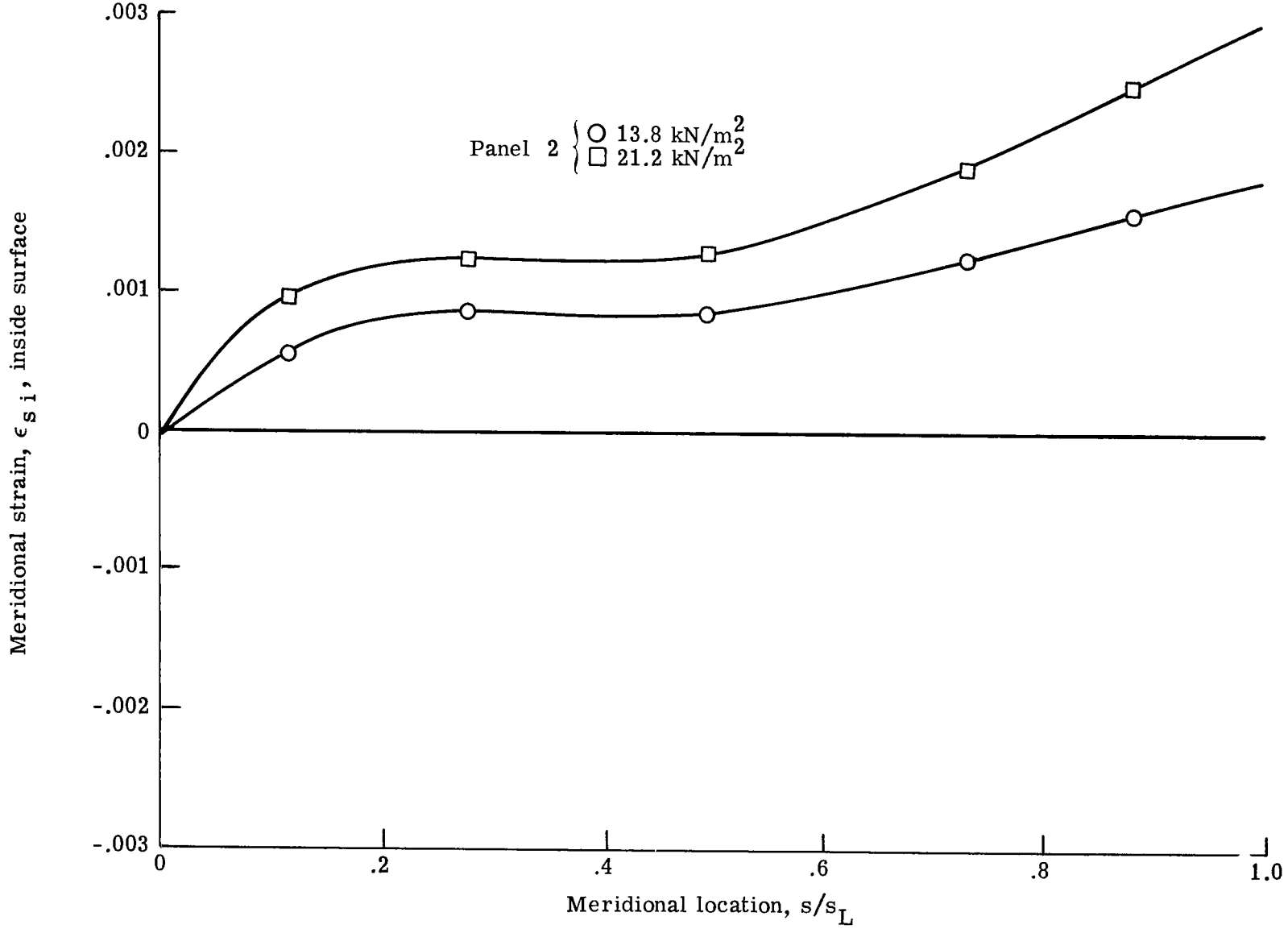

(c) Cone 3.

Figure 16.- Concluded.

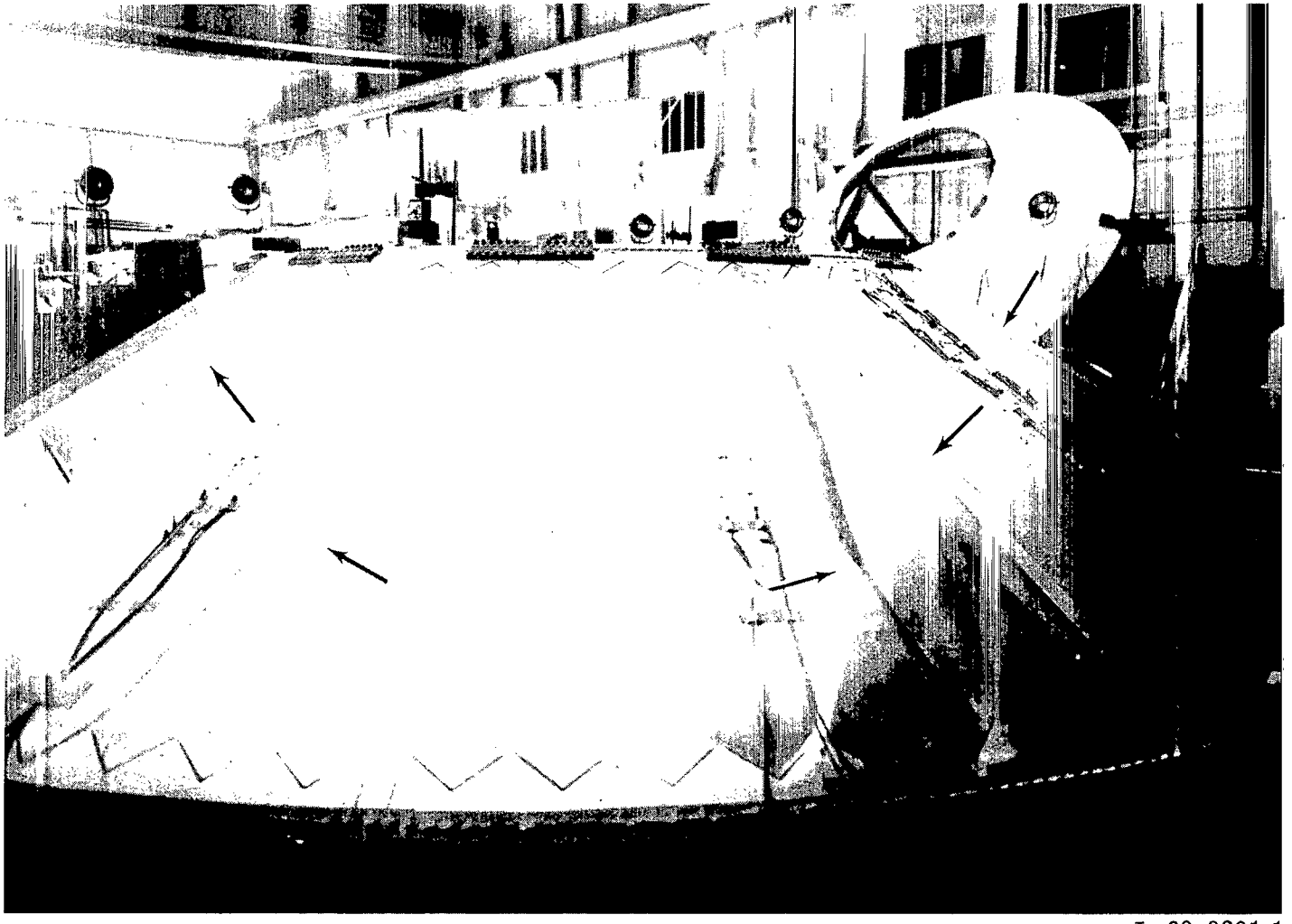

L-69-8201.1

Figure 17.- Failure of cone 1. p_{ult} = 45.51 kN/m^2 (6.60 psi).

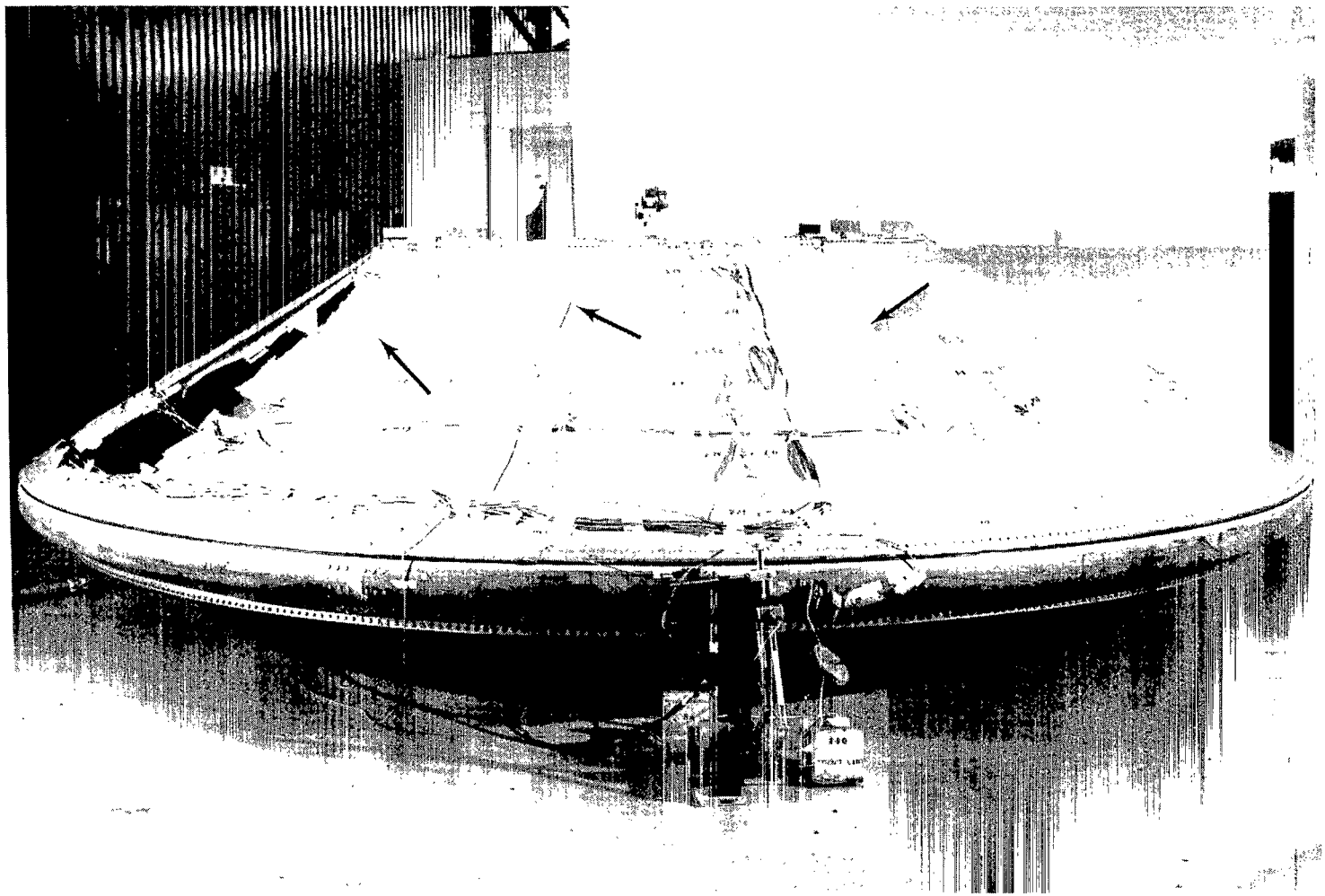

L-69-6096.1

(a) Overall view.

Figure 18.- Failure of cone 2. p_{ult} = 44.40 kN/m^2 (6.44 psi).

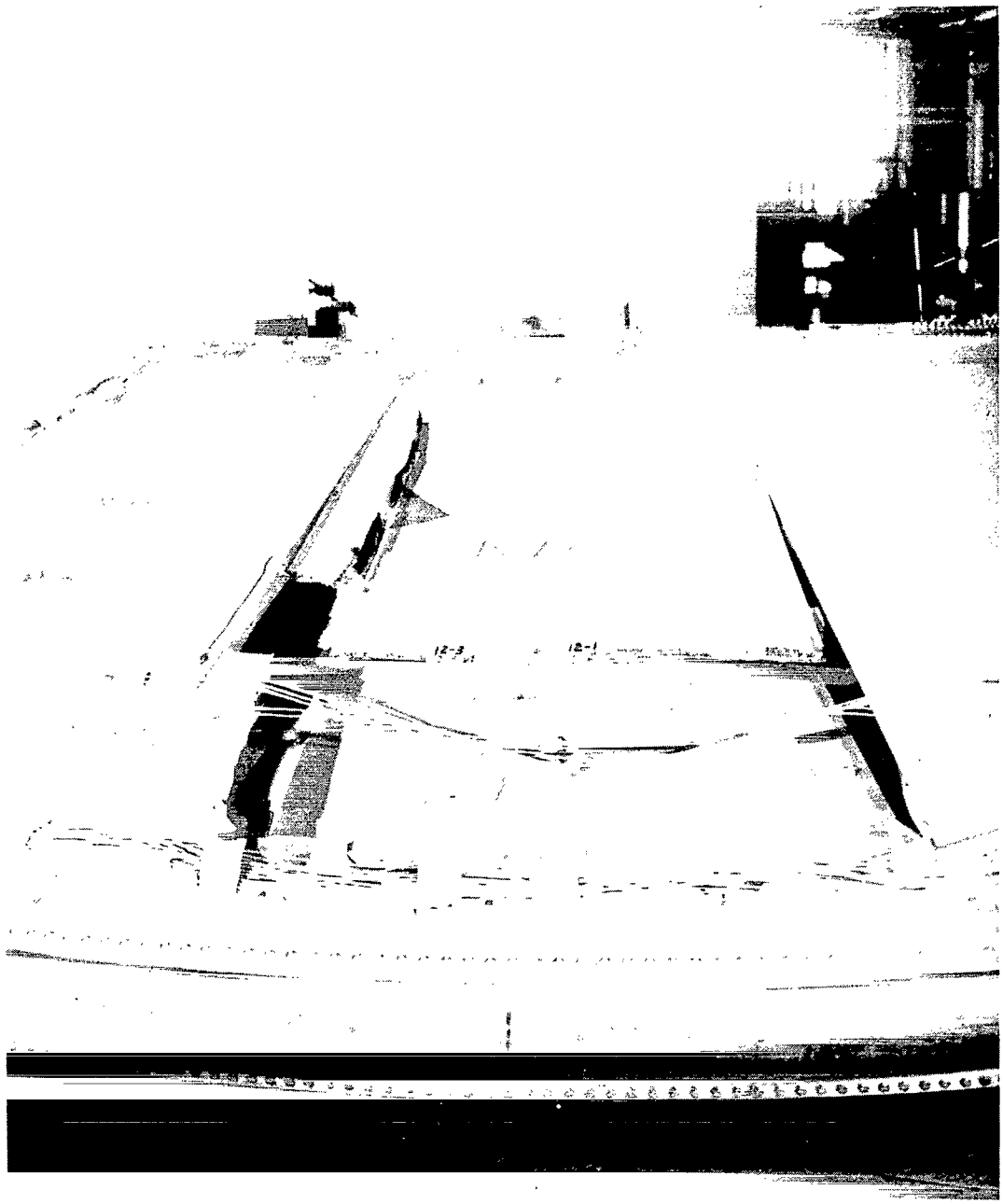

L-69-6089

(b) Close-up view of ruptured area.

Figure 18.- Concluded.

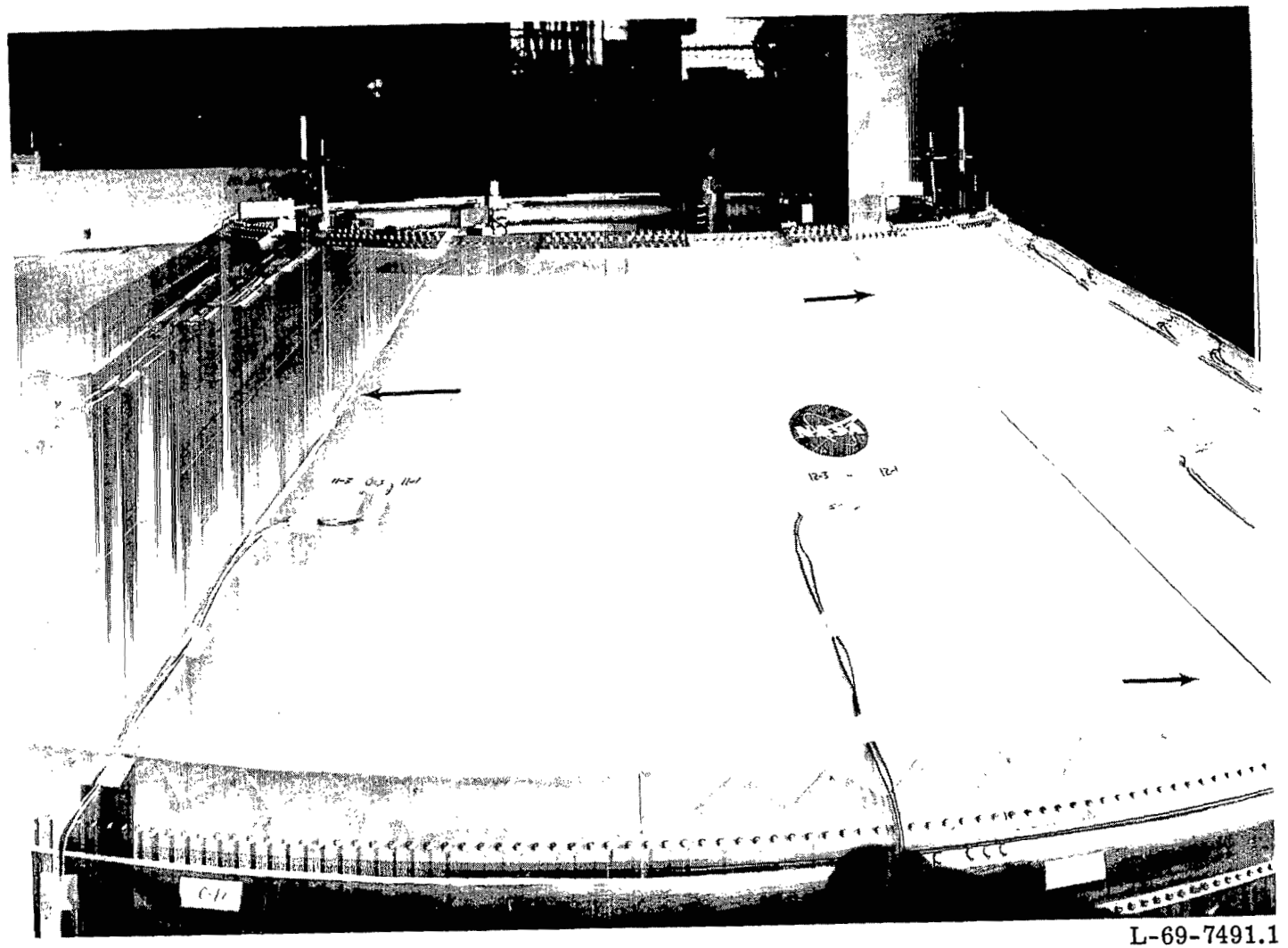

L-69-7491.1

(a) Outside overall view.

Figure 19.- Failure of cone 3. p_{ult} = 27.30 kN/m^2 (3.96 psi).

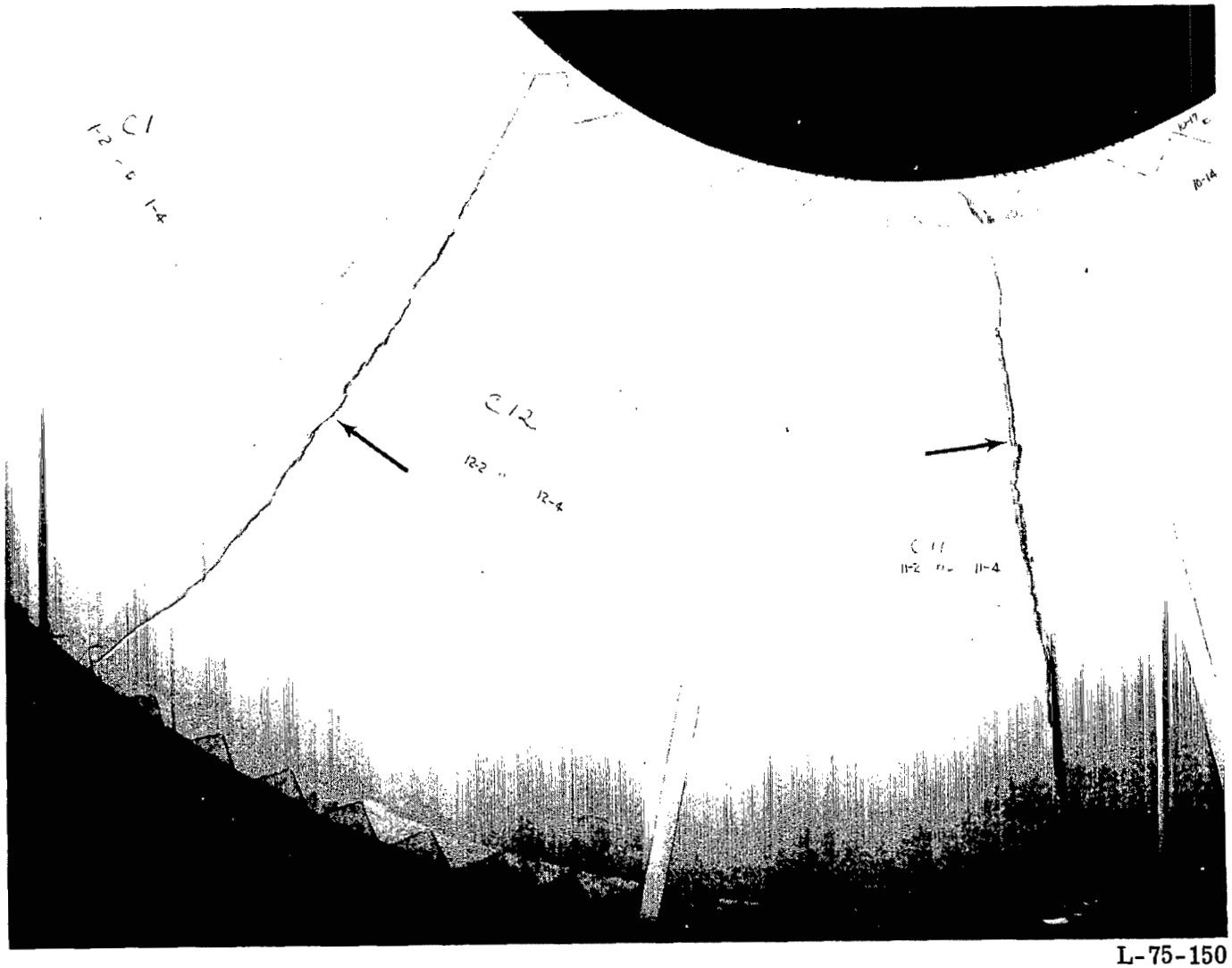

L-75-150

(b) Inside close-up view.

Figure 19.- Concluded.

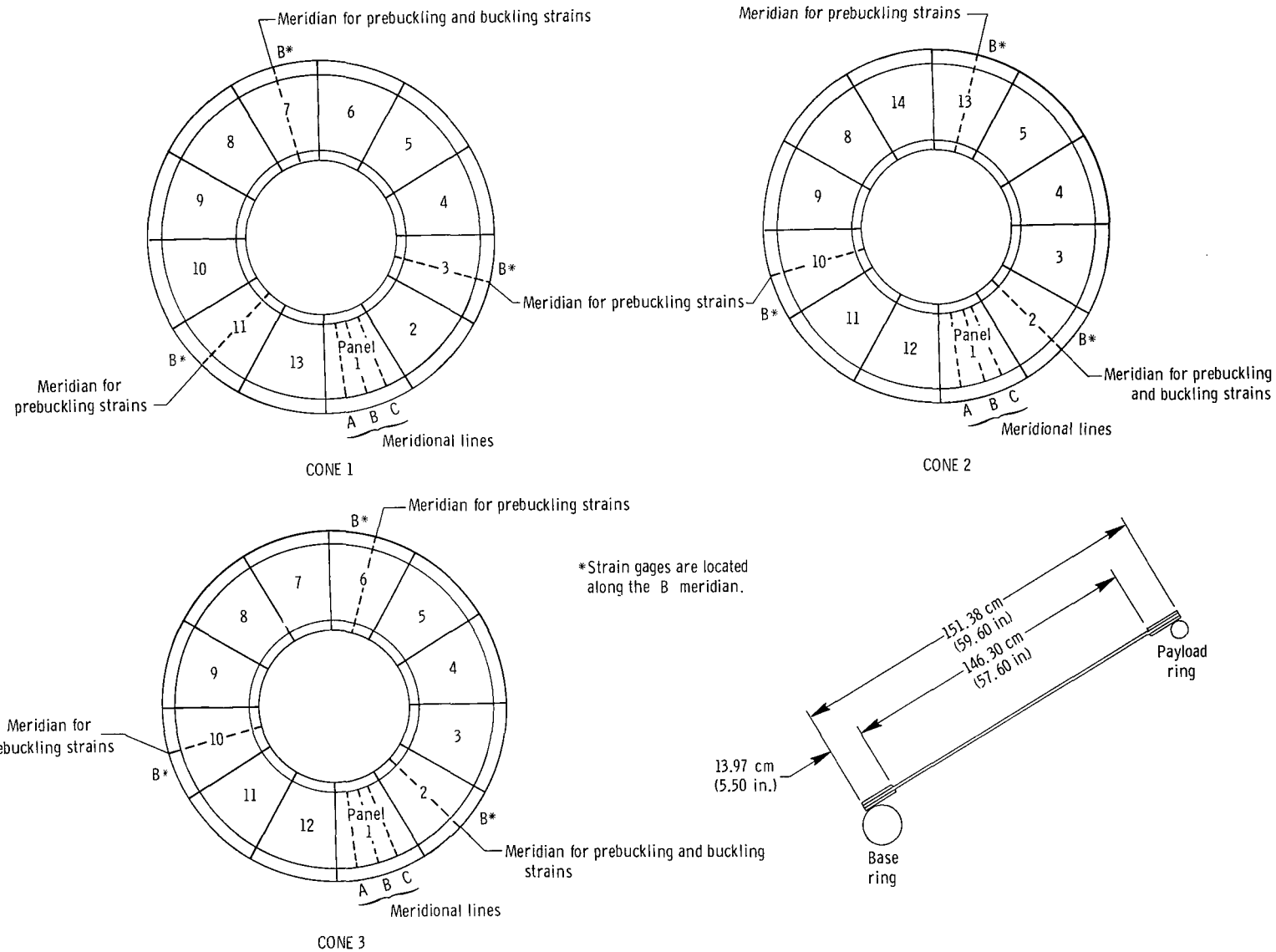

Figure 20.- Panel orientation and imperfection measuring details for cones 1, 2, and 3.

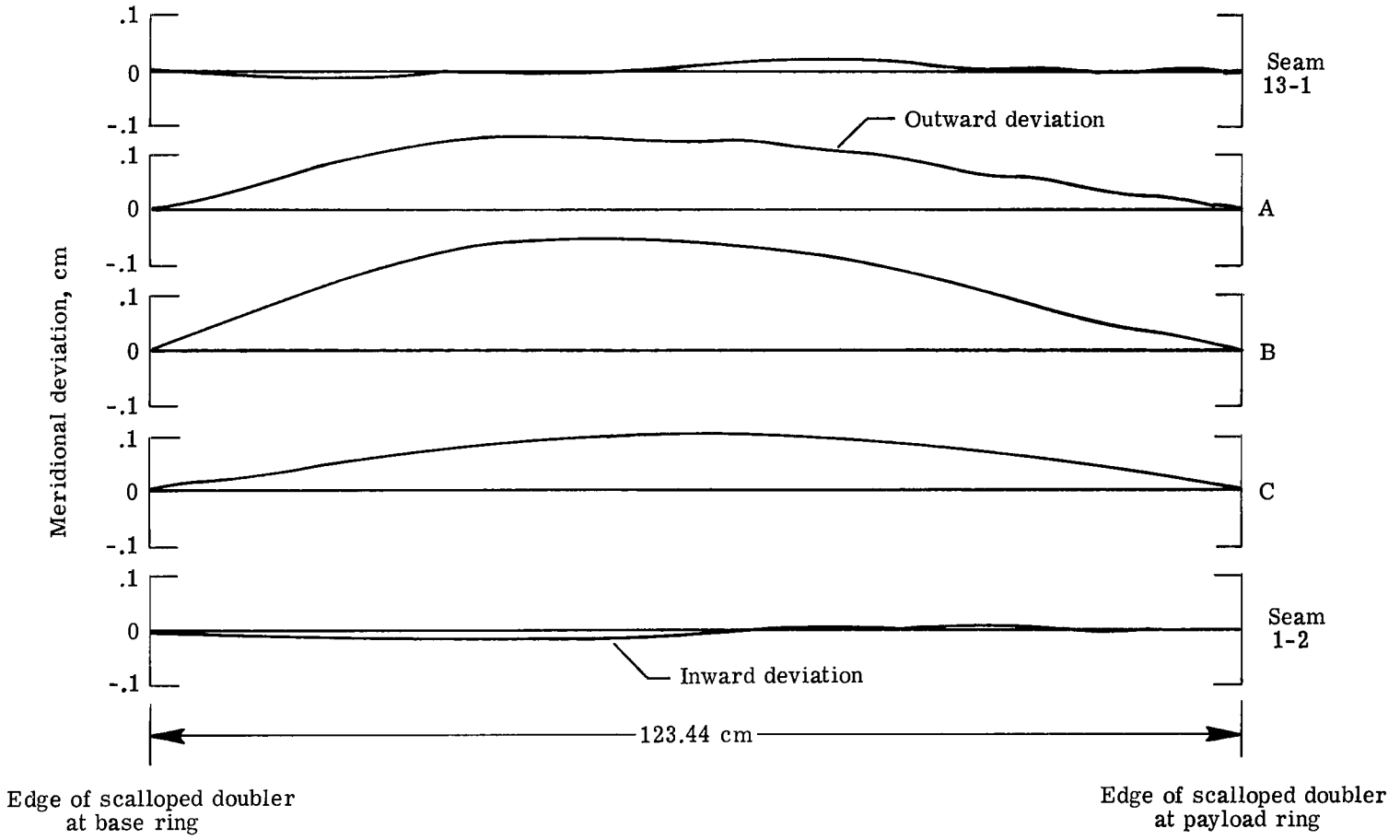

(a) Panel 1.

Figure 21.- Imperfection measurements of cone 1.

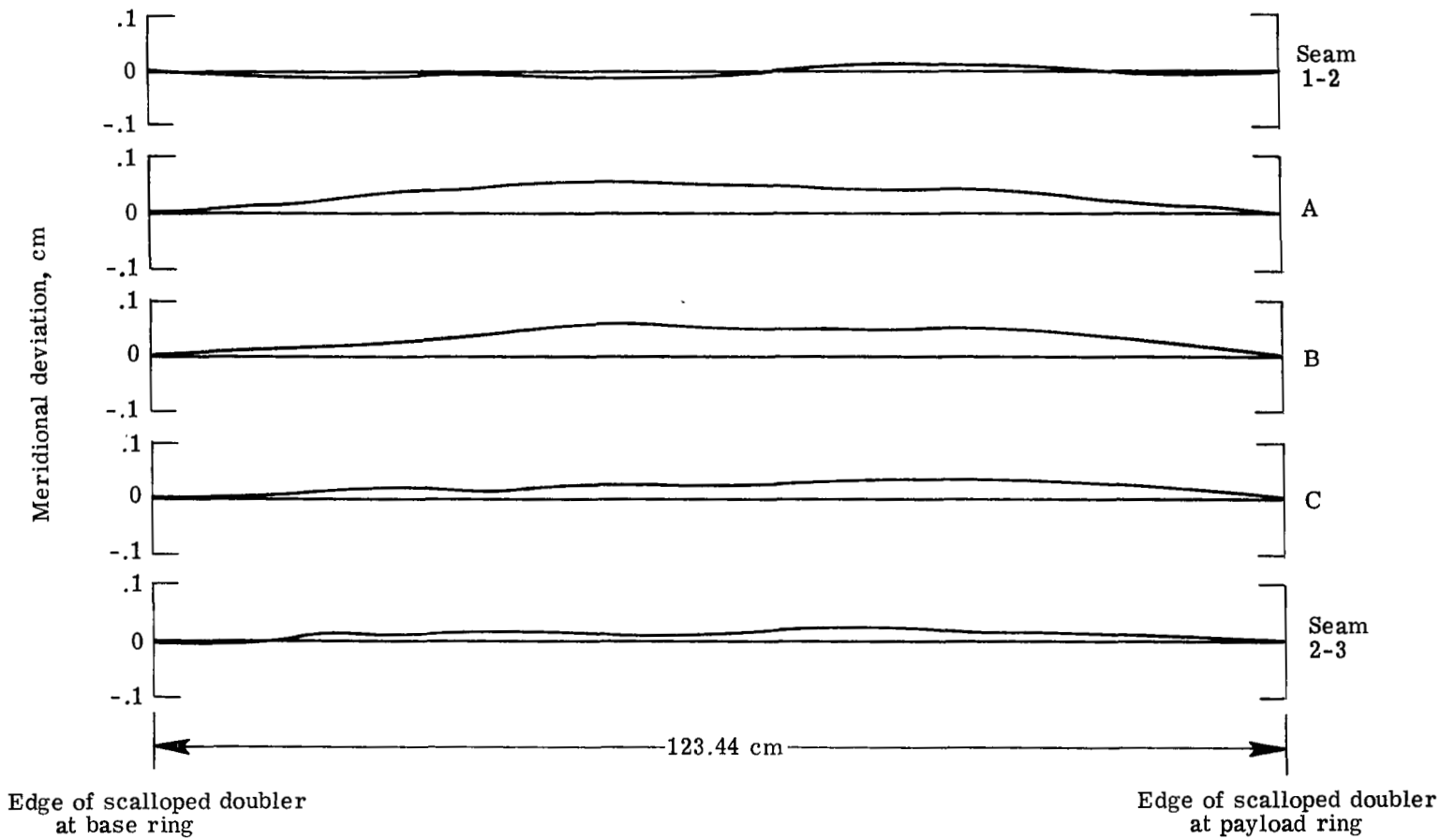

(b) Panel 2.

Figure 21.- Continued.

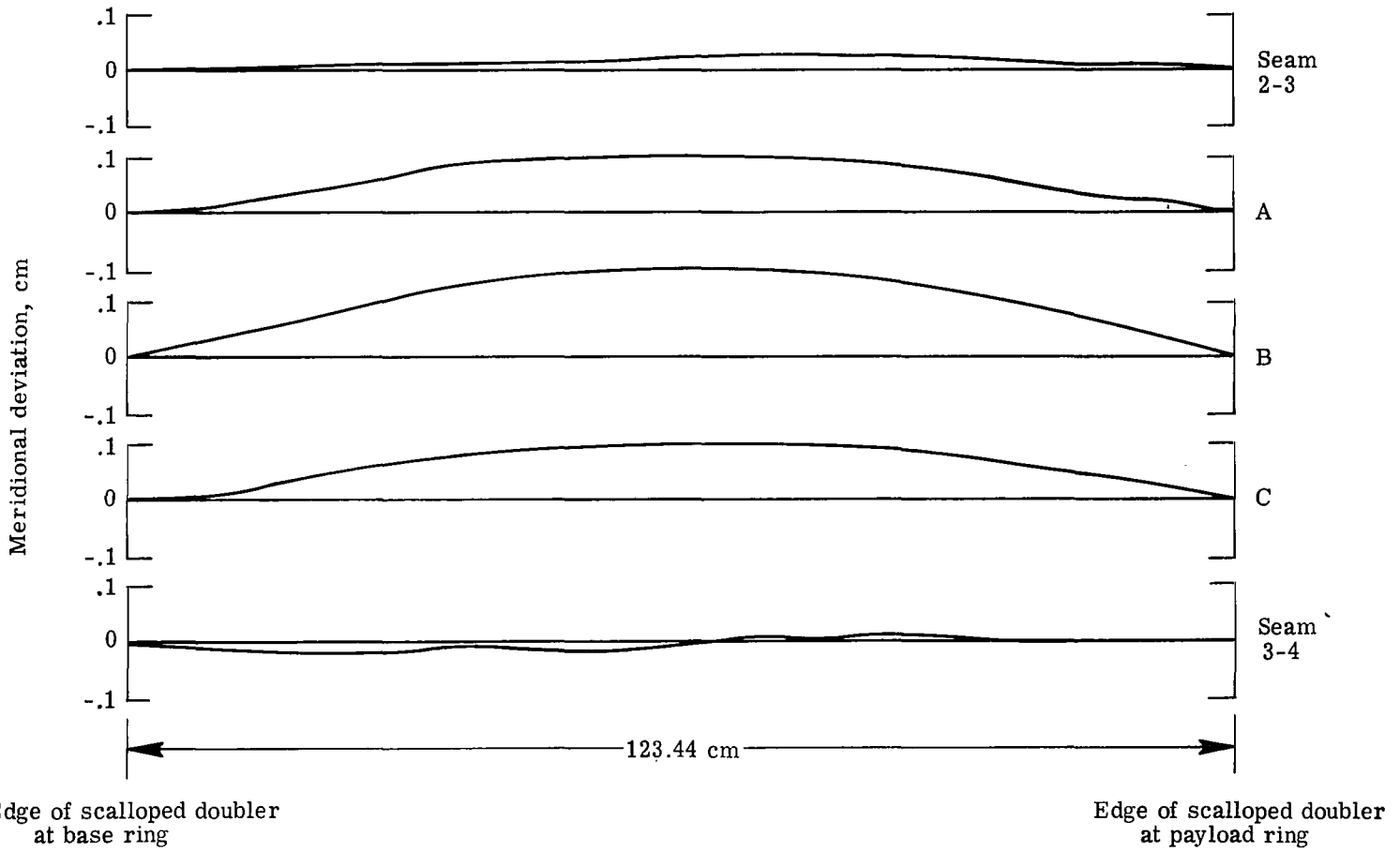

(c) Panel 3.

Figure 21.- Continued.

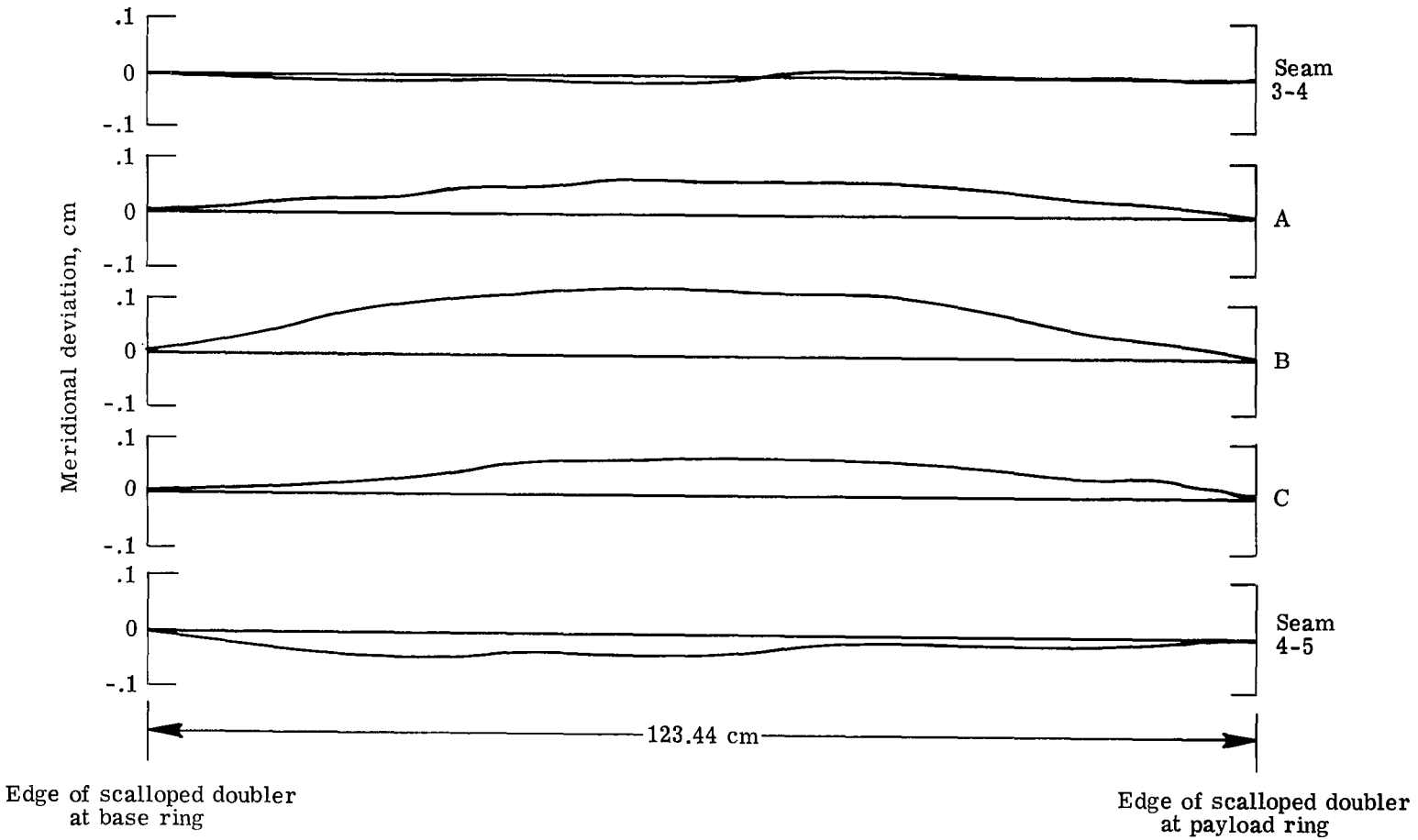

(d) Panel 4.

Figure 21.- Continued.

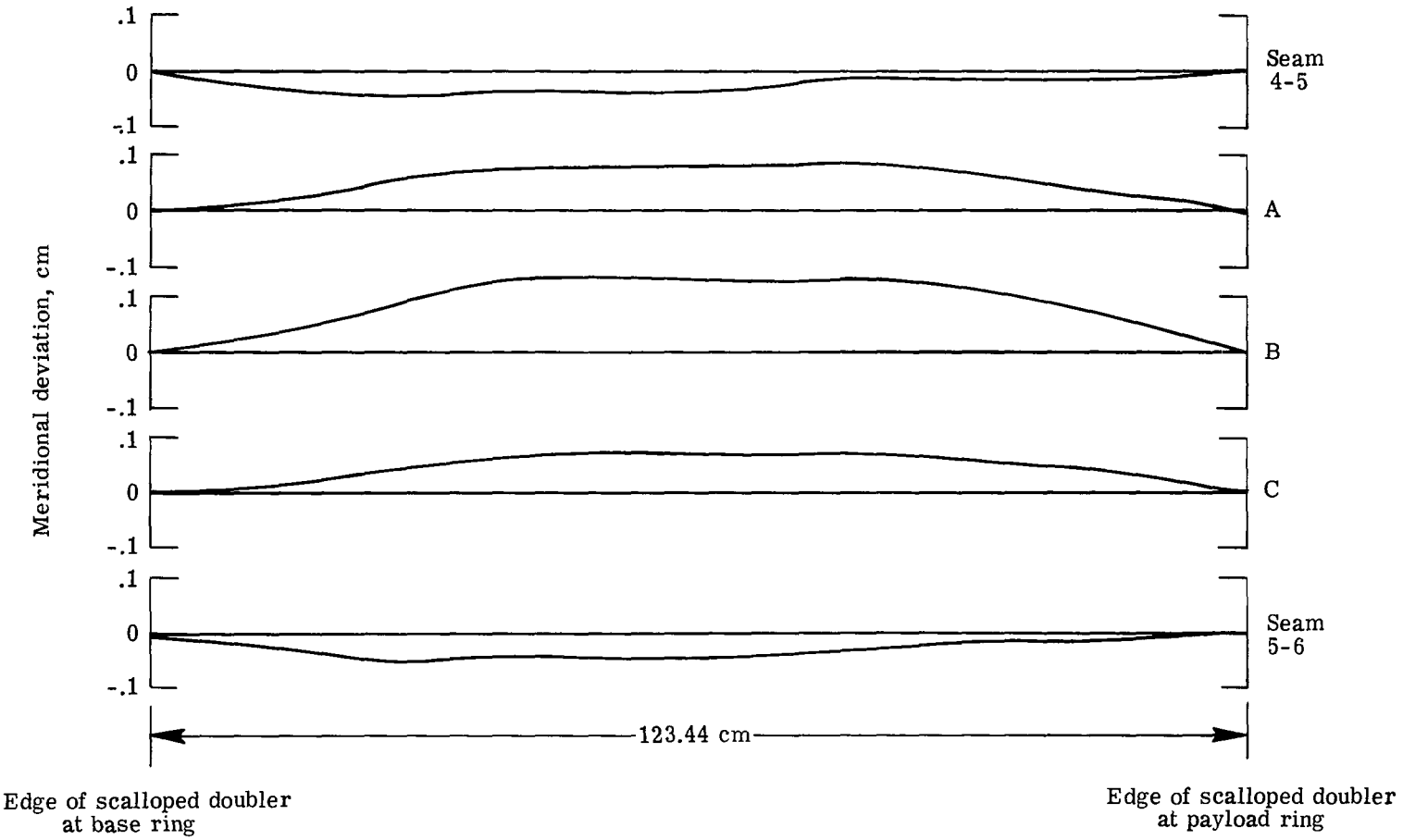

(e) Panel 5.

Figure 21.- Continued.

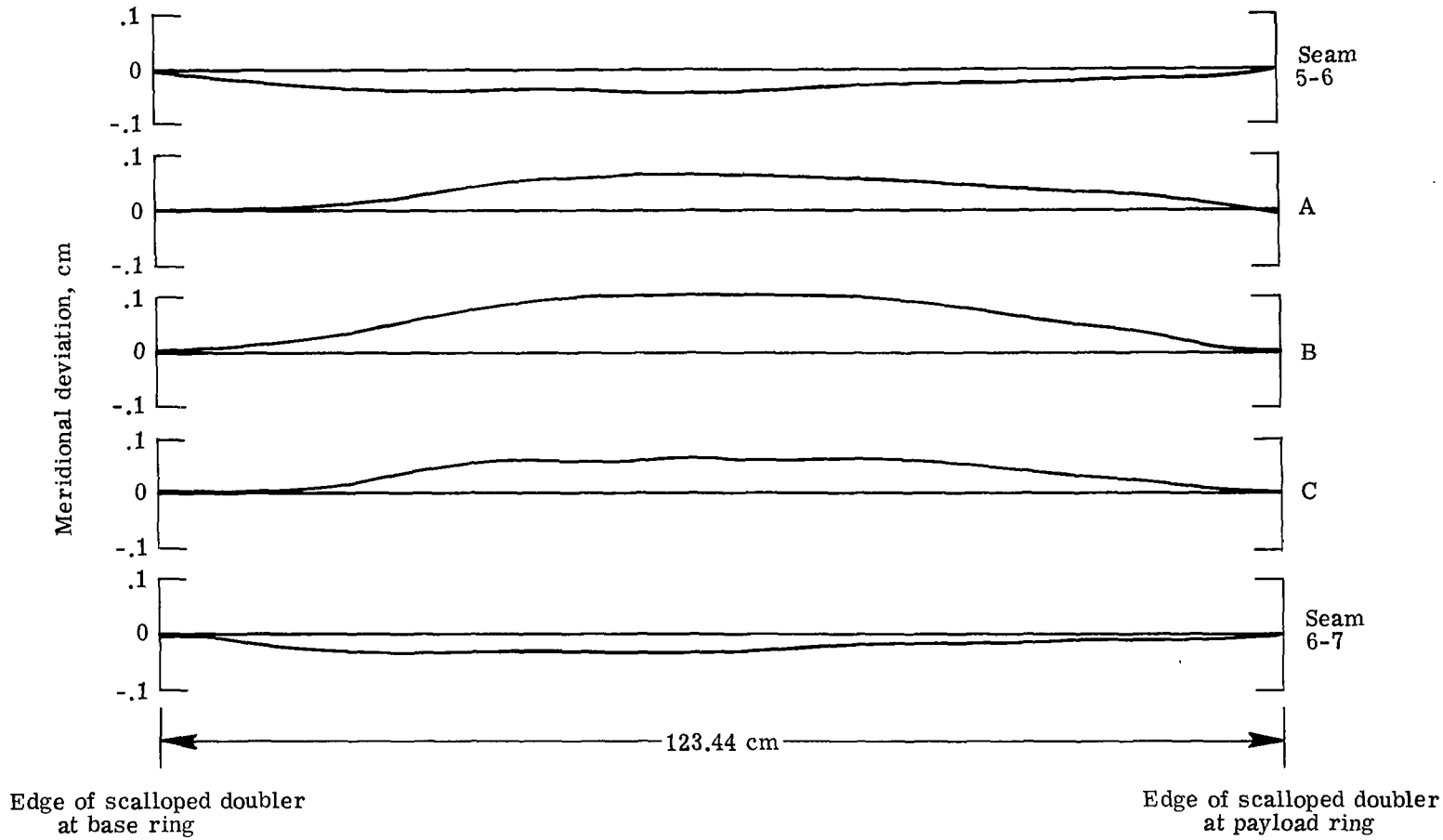

(f) Panel 6.

Figure 21.- Continued.

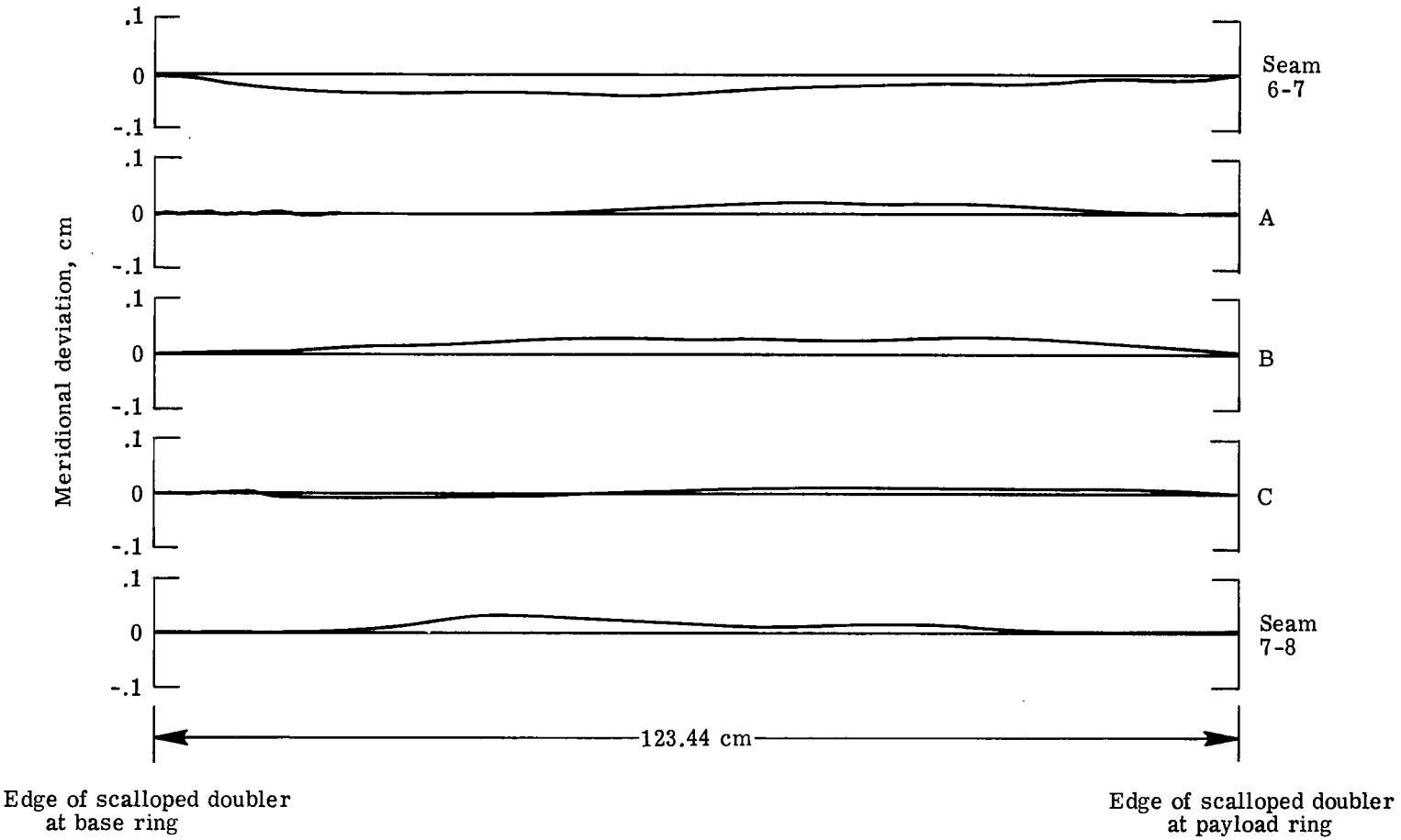

(g) Panel 7.

Figure 21.- Continued.

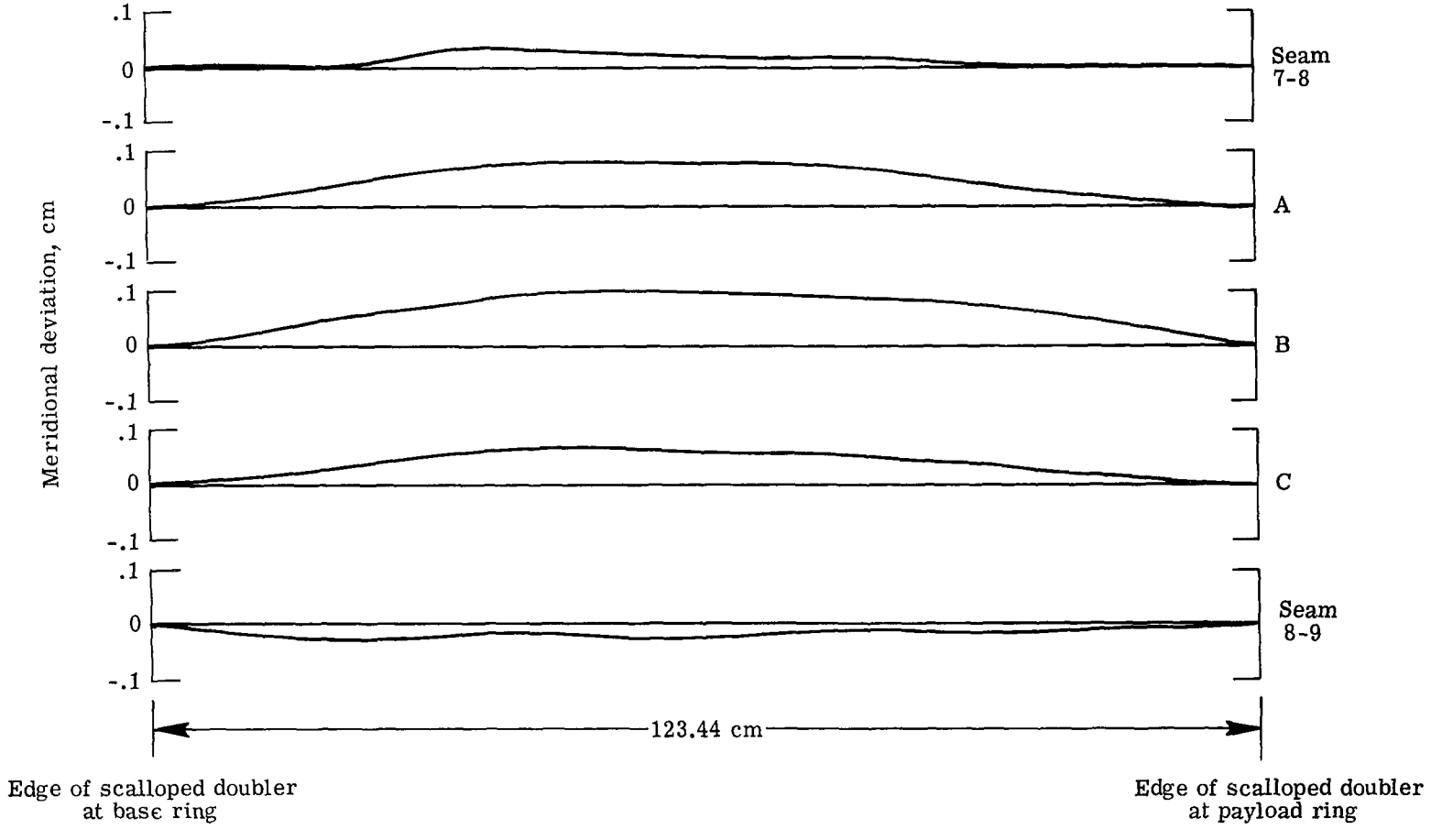

(h) Panel 8.

Figure 21.- Continued.

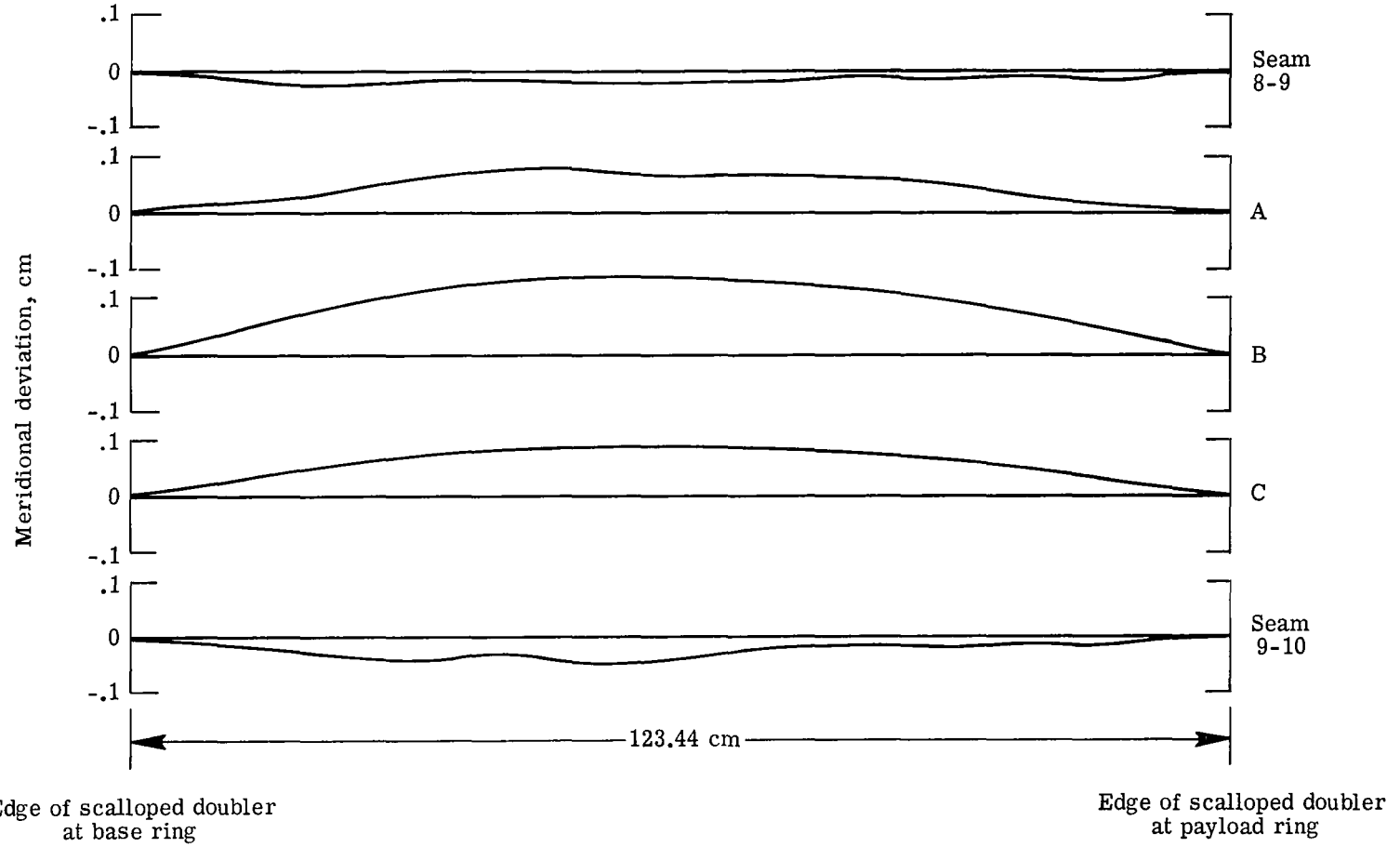

(i) Panel 9.

Figure 21.- Continued.

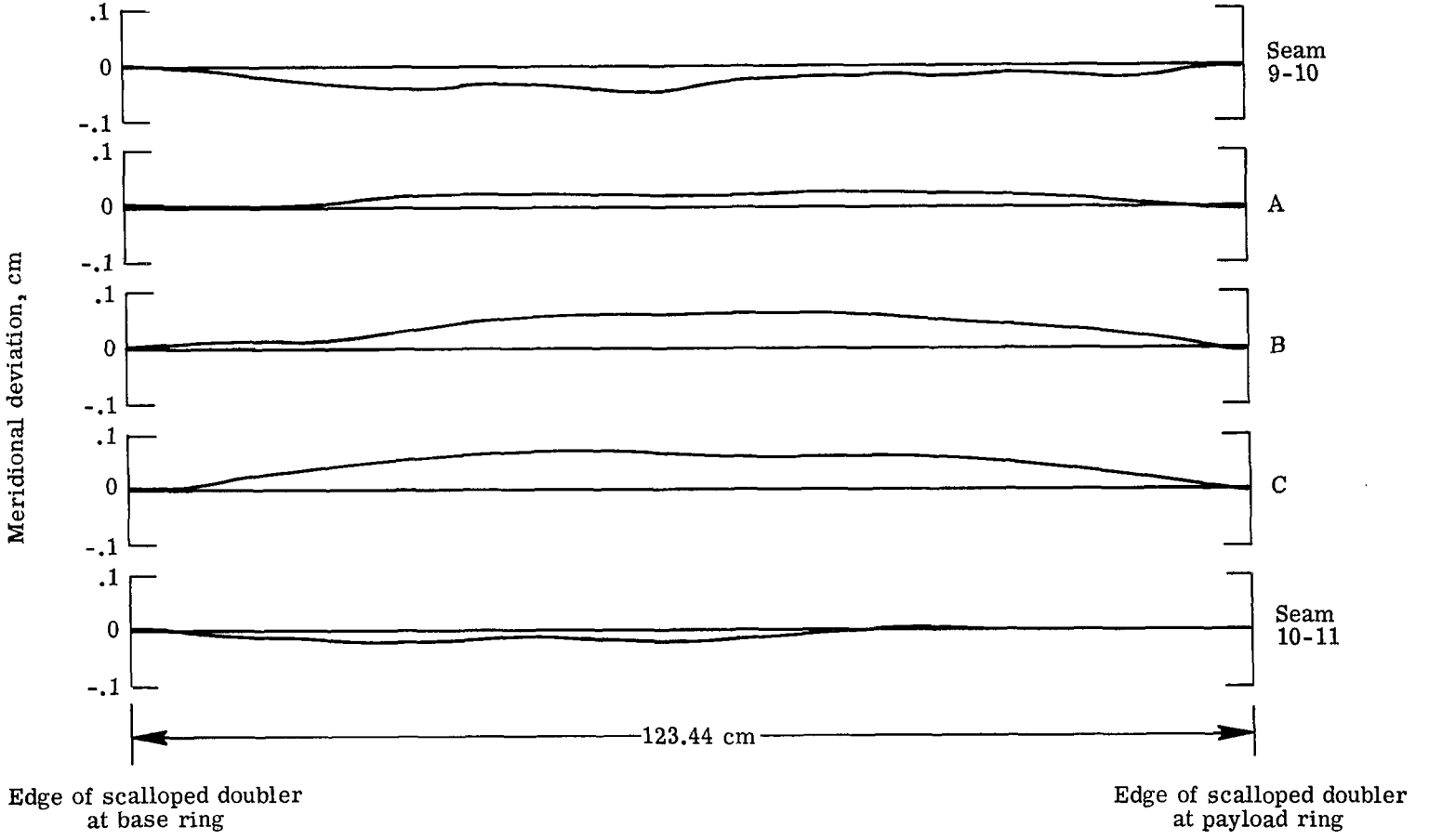

(j) Panel 10.

Figure 21.- Continued.

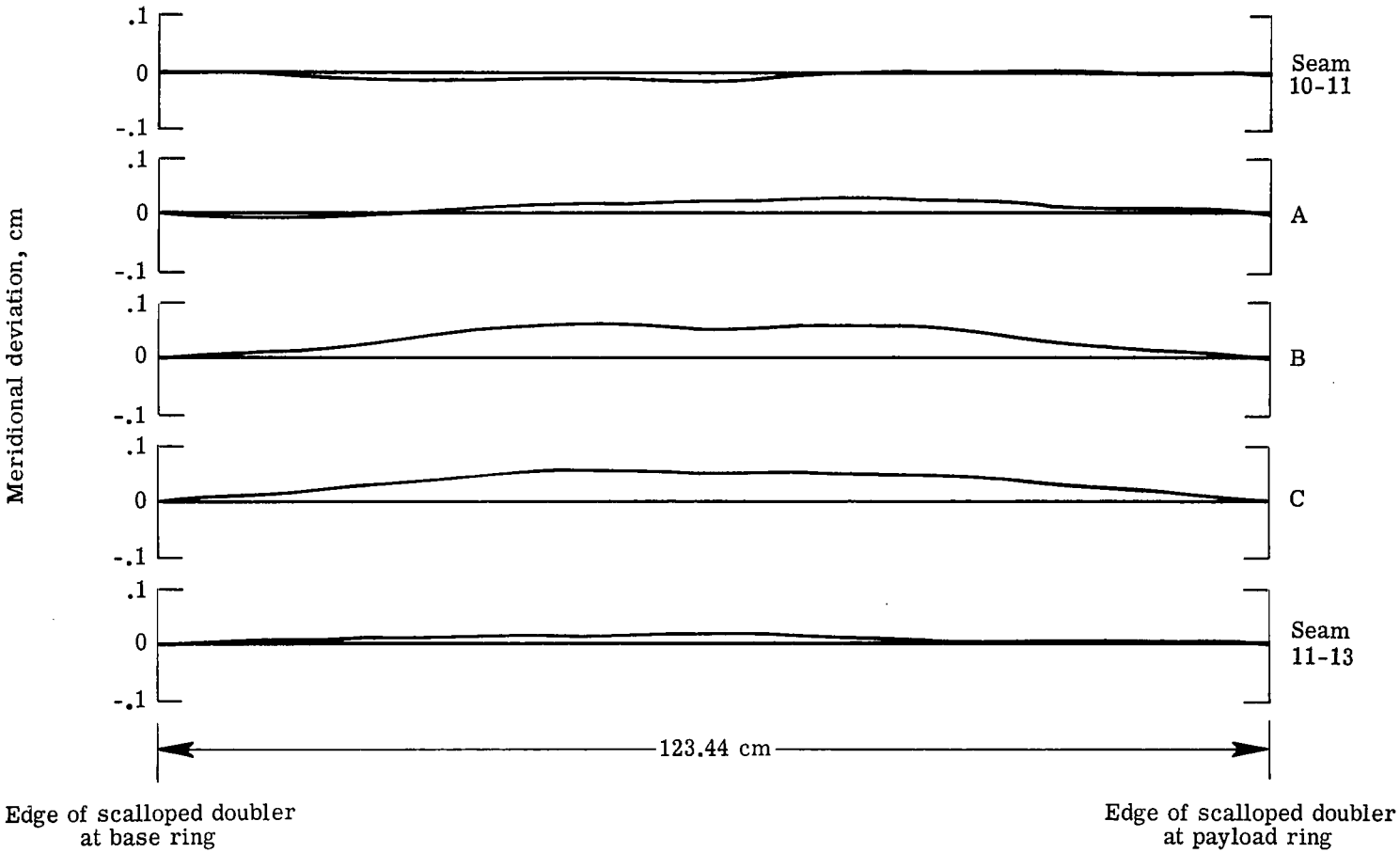

(k) Panel 11.

Figure 21.- Continued.

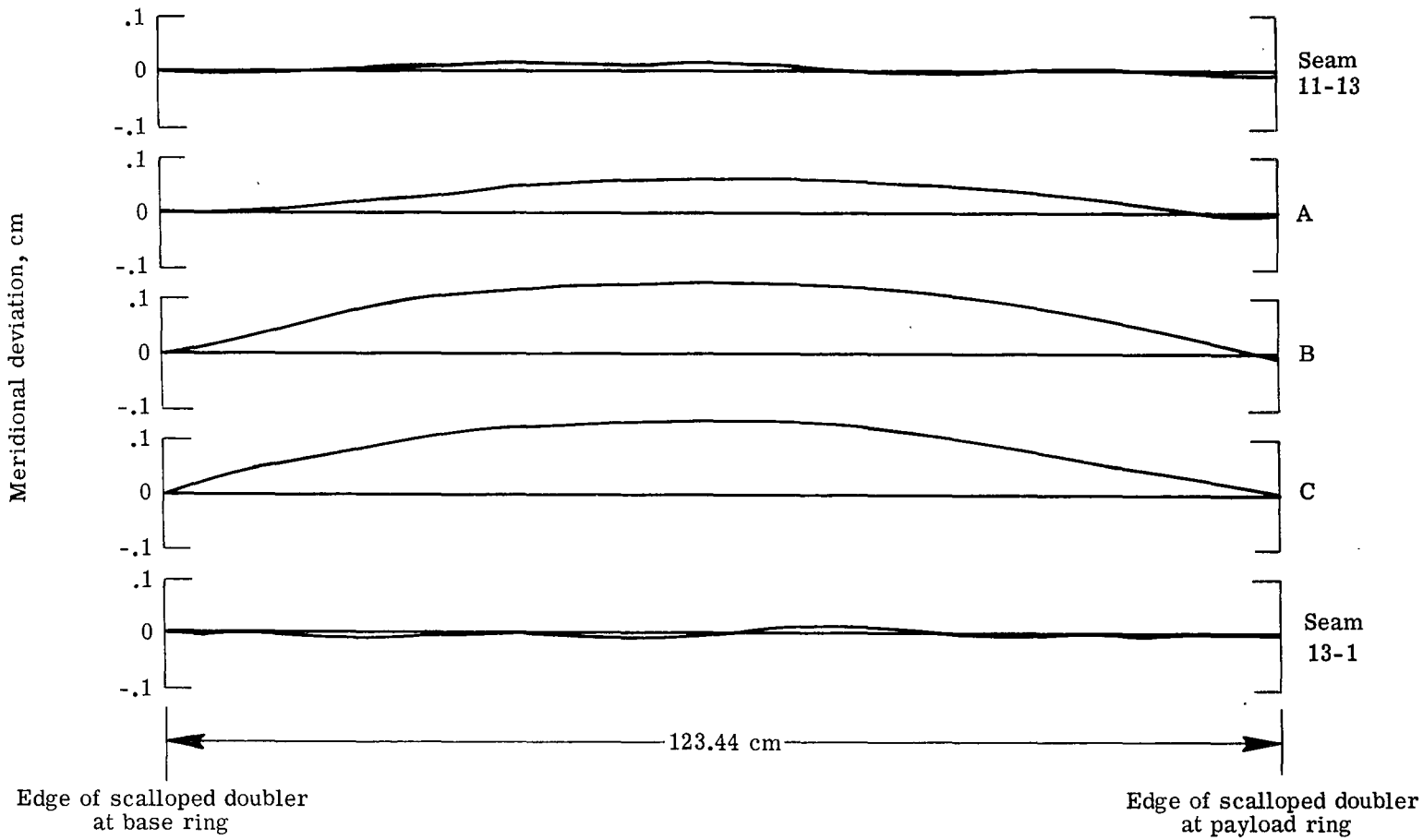

(l) Panel 13.

Figure 21.- Concluded.

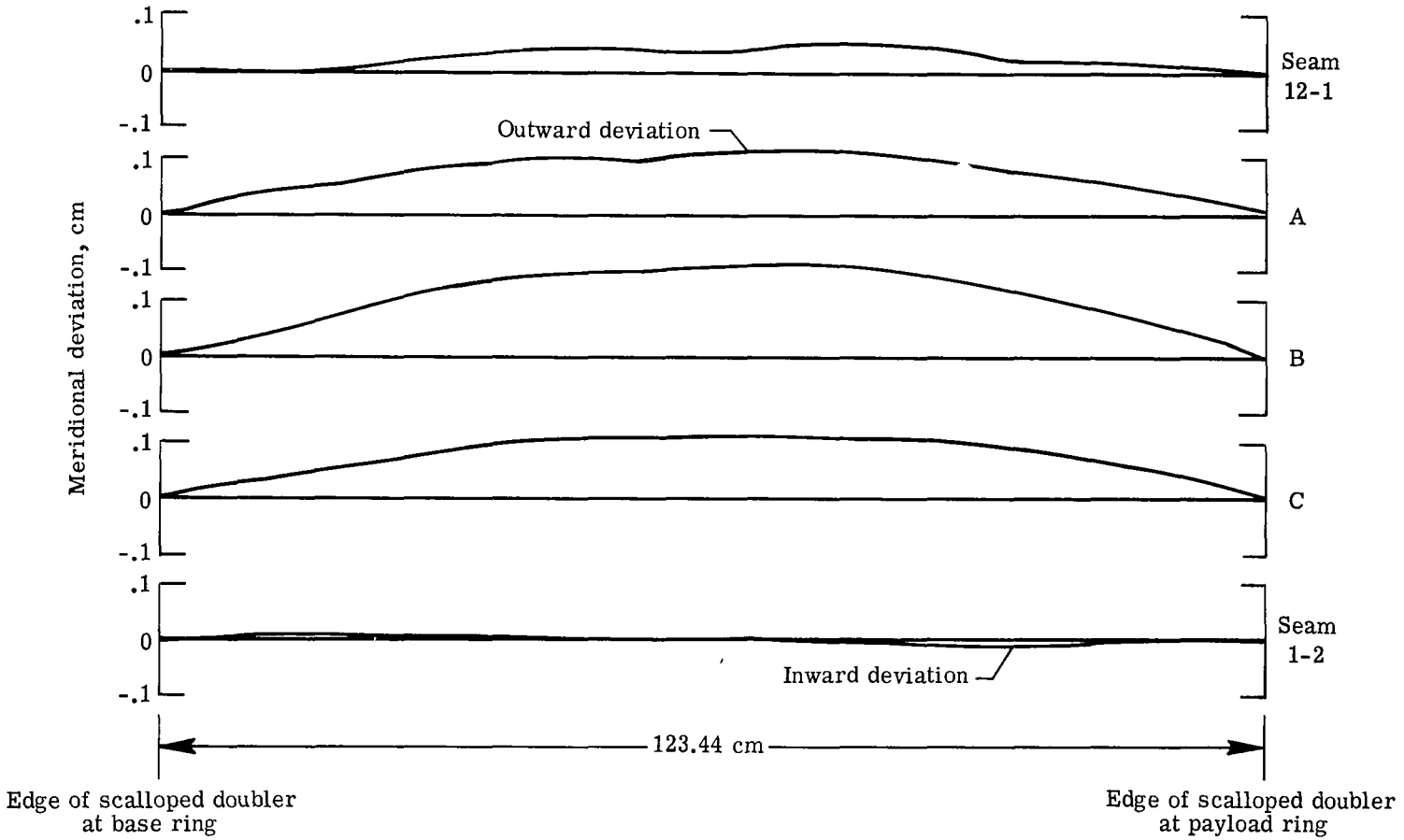

(a) Panel 1.

Figure 22.- Imperfection measurements of cone 2.

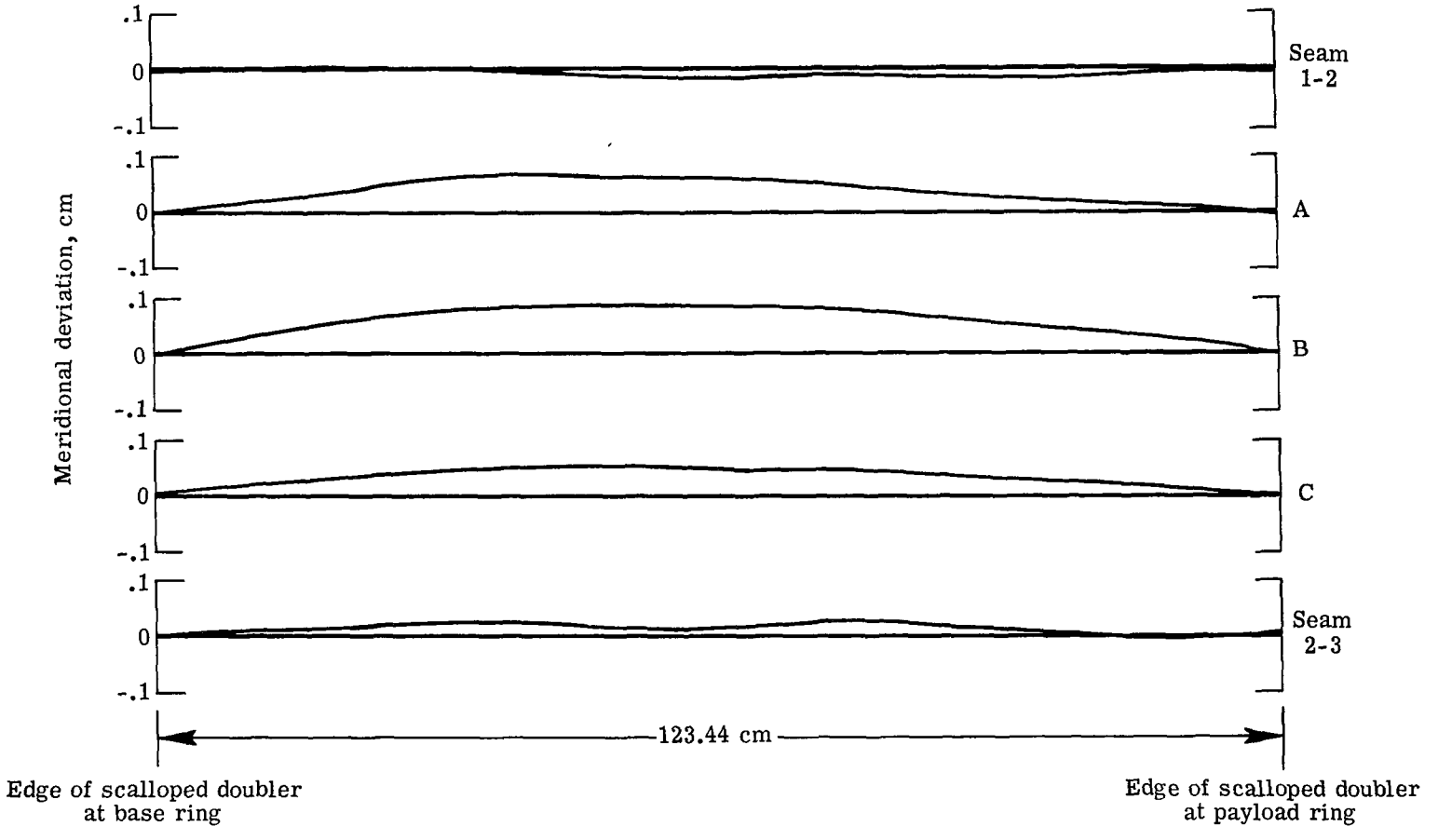

(b) Panel 2.

Figure 22.- Continued.

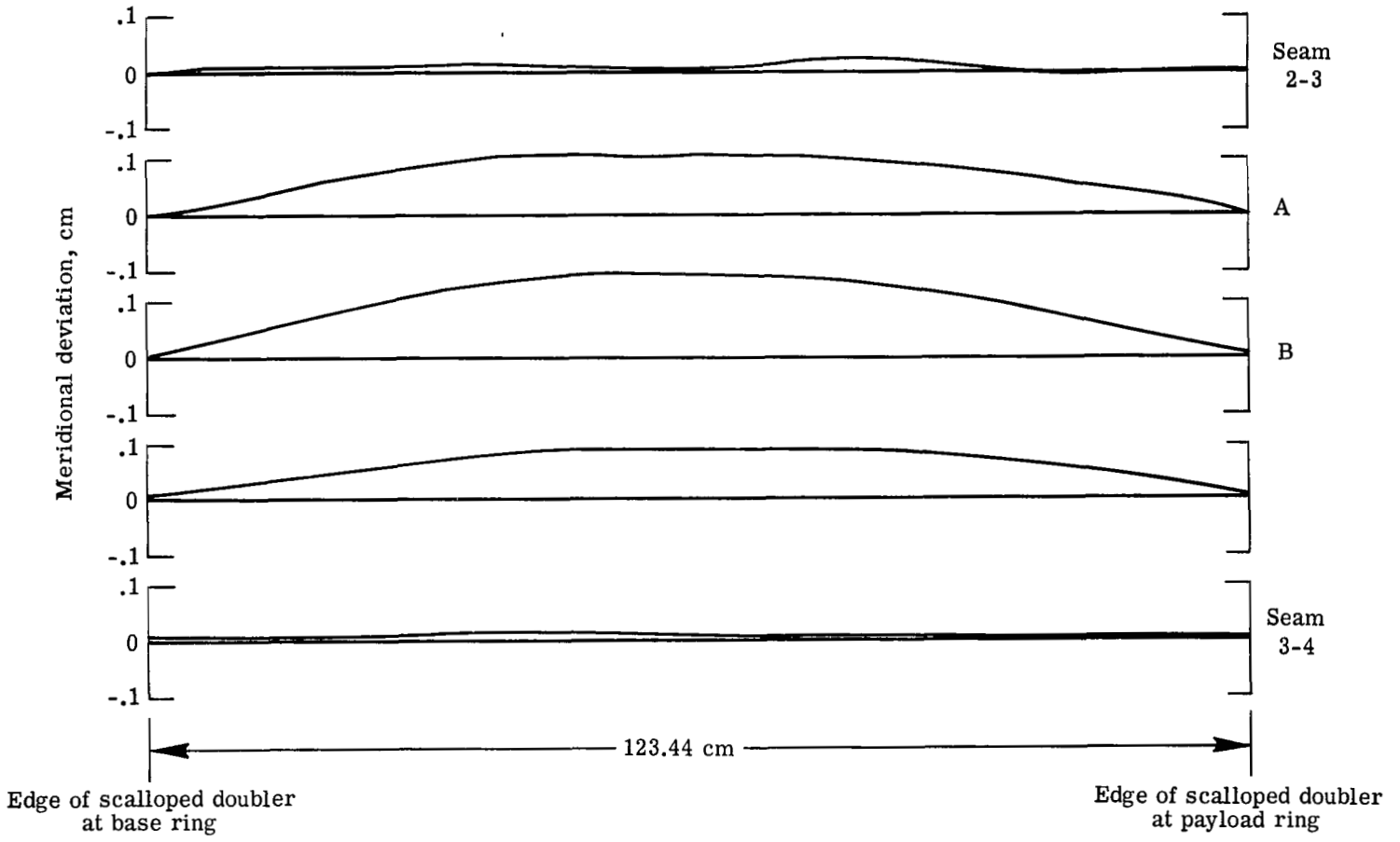

(c) Panel 3.

Figure 22.- Continued.

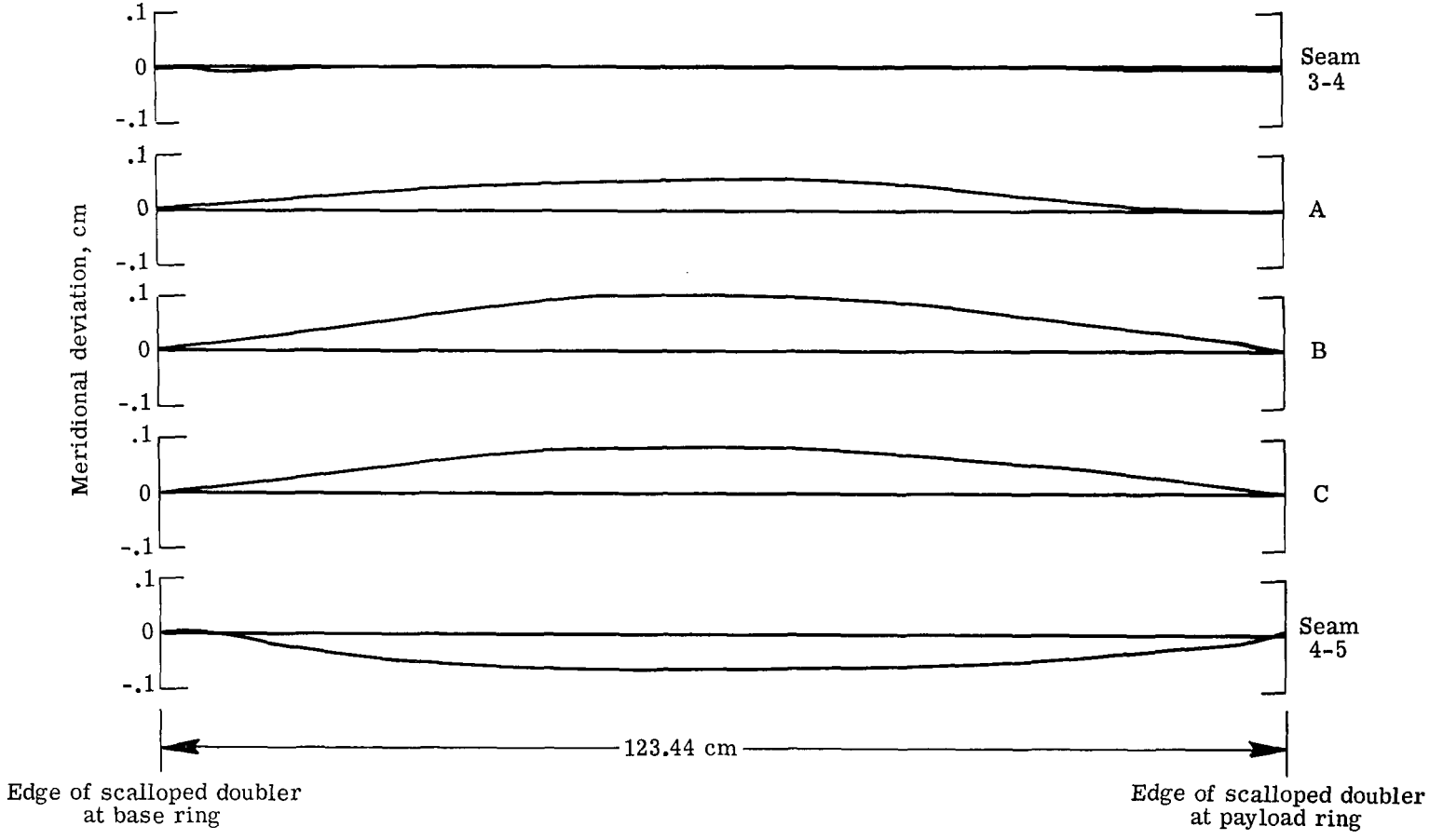

(d) Panel 4.

Figure 22.- Continued.

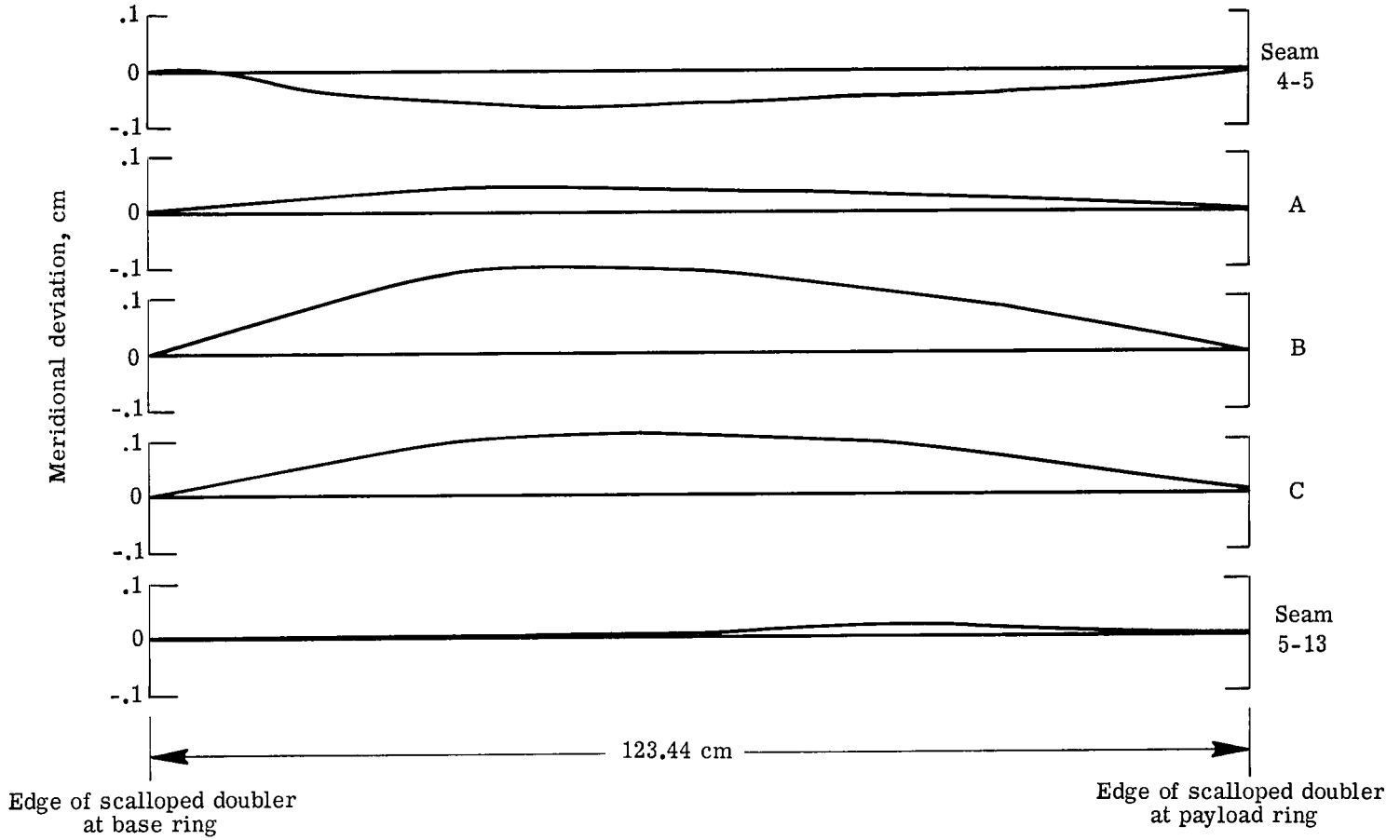

(e) Panel 5.

Figure 22.- Continued.

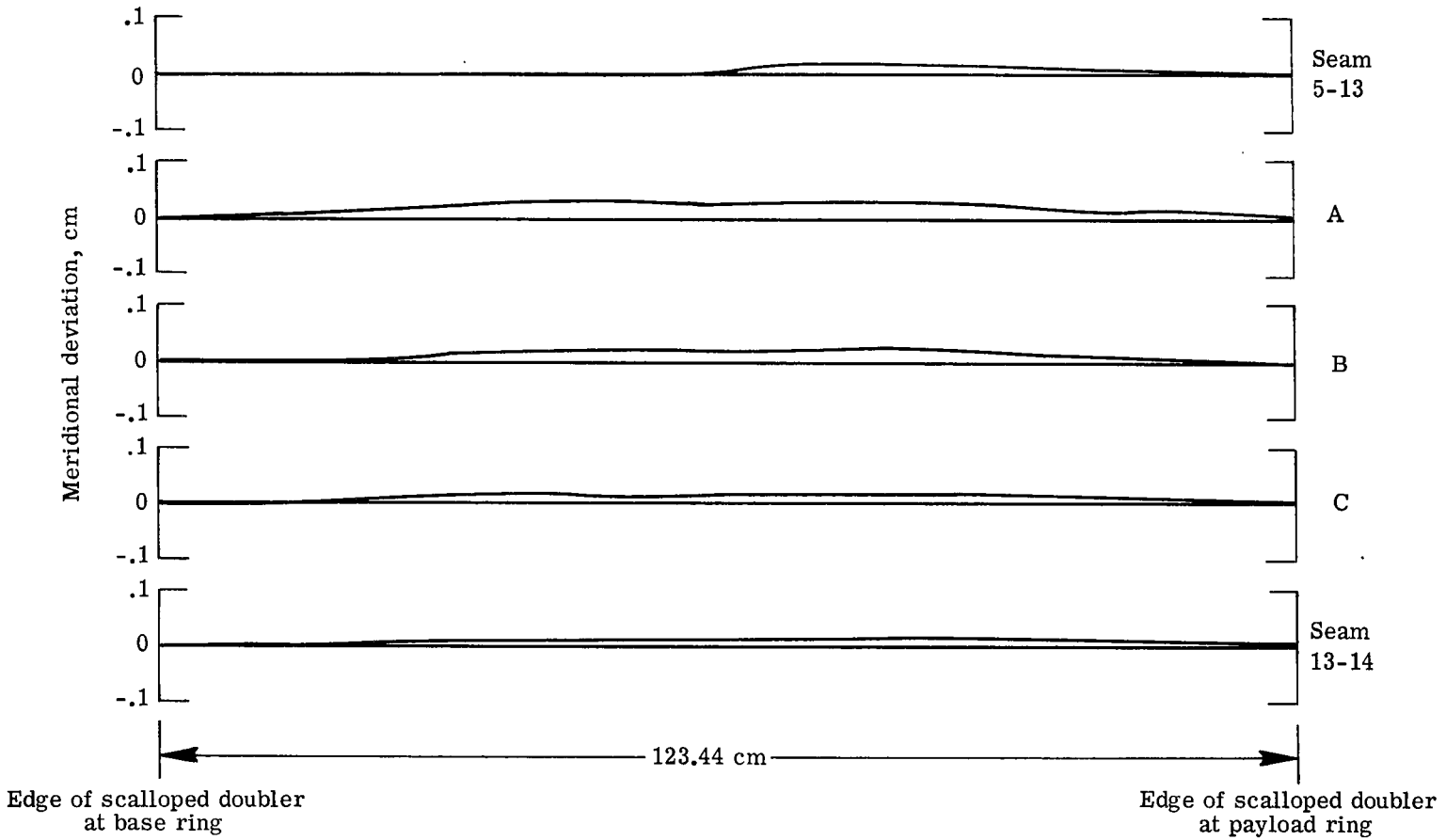

(f) Panel 13.

Figure 22.- Continued.

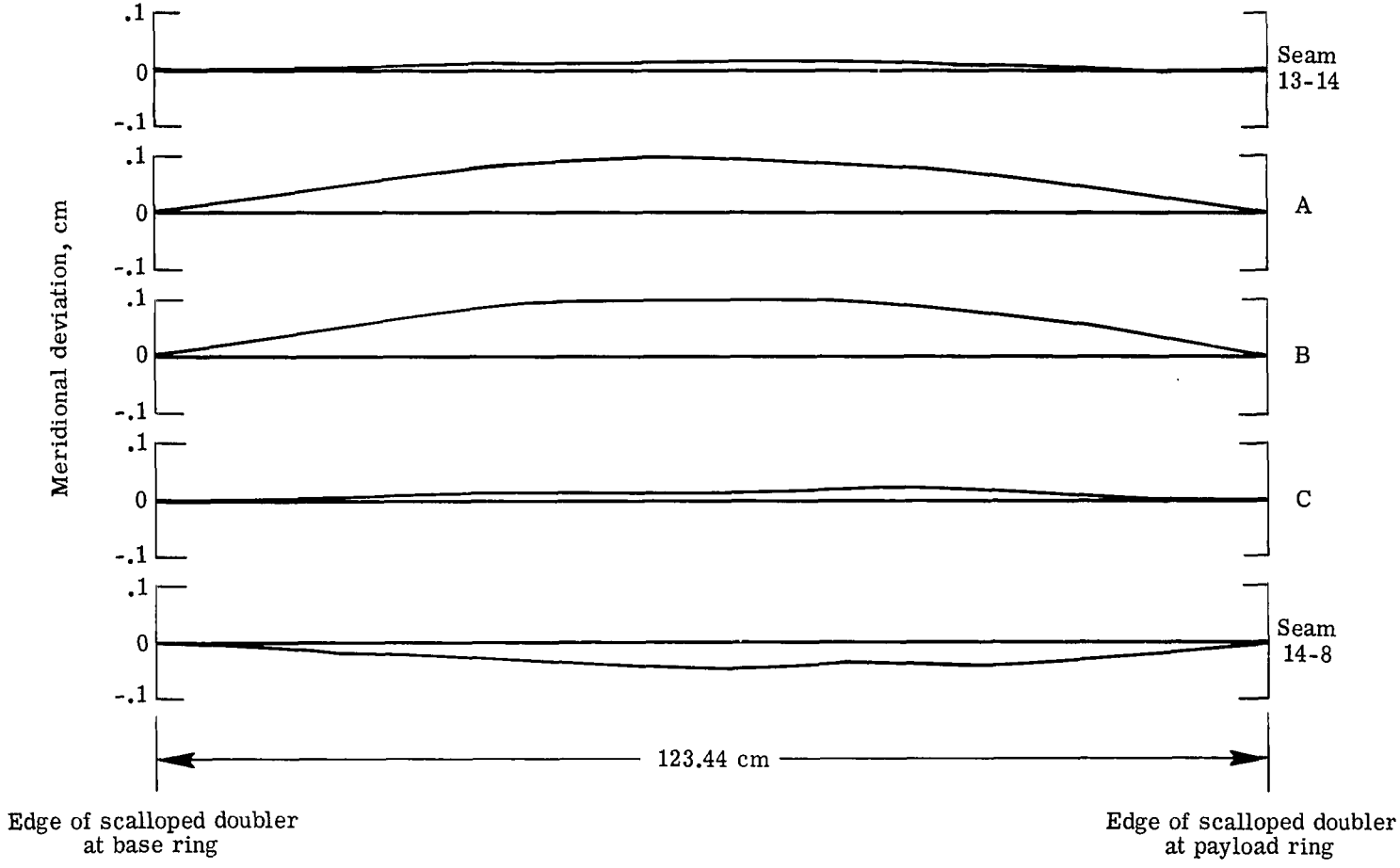

(g) Panel 14.

Figure 22.- Continued.

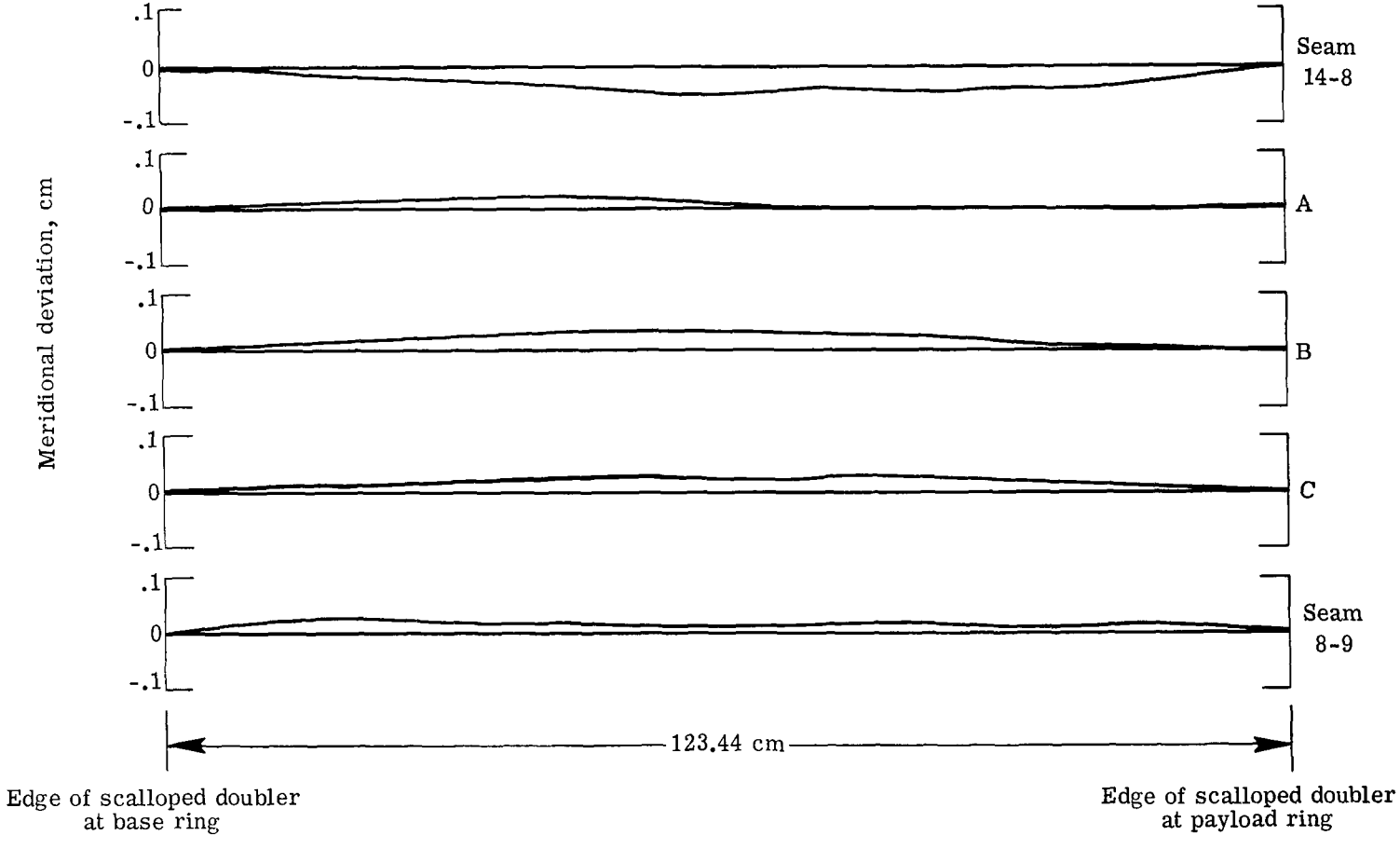

(h) Panel 8.

Figure 22.- Continued.

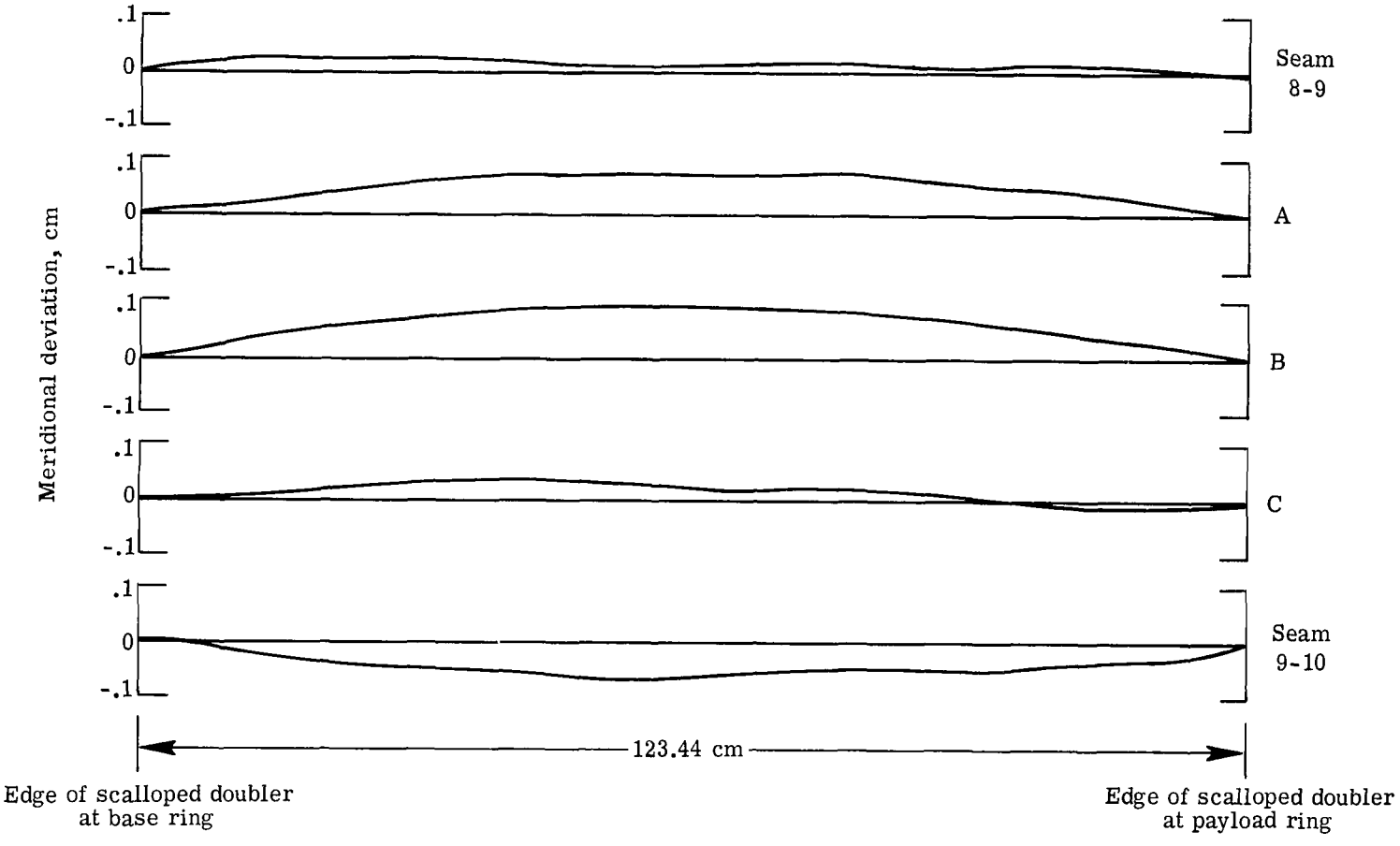

(i) Panel 9.

Figure 22.- Continued.

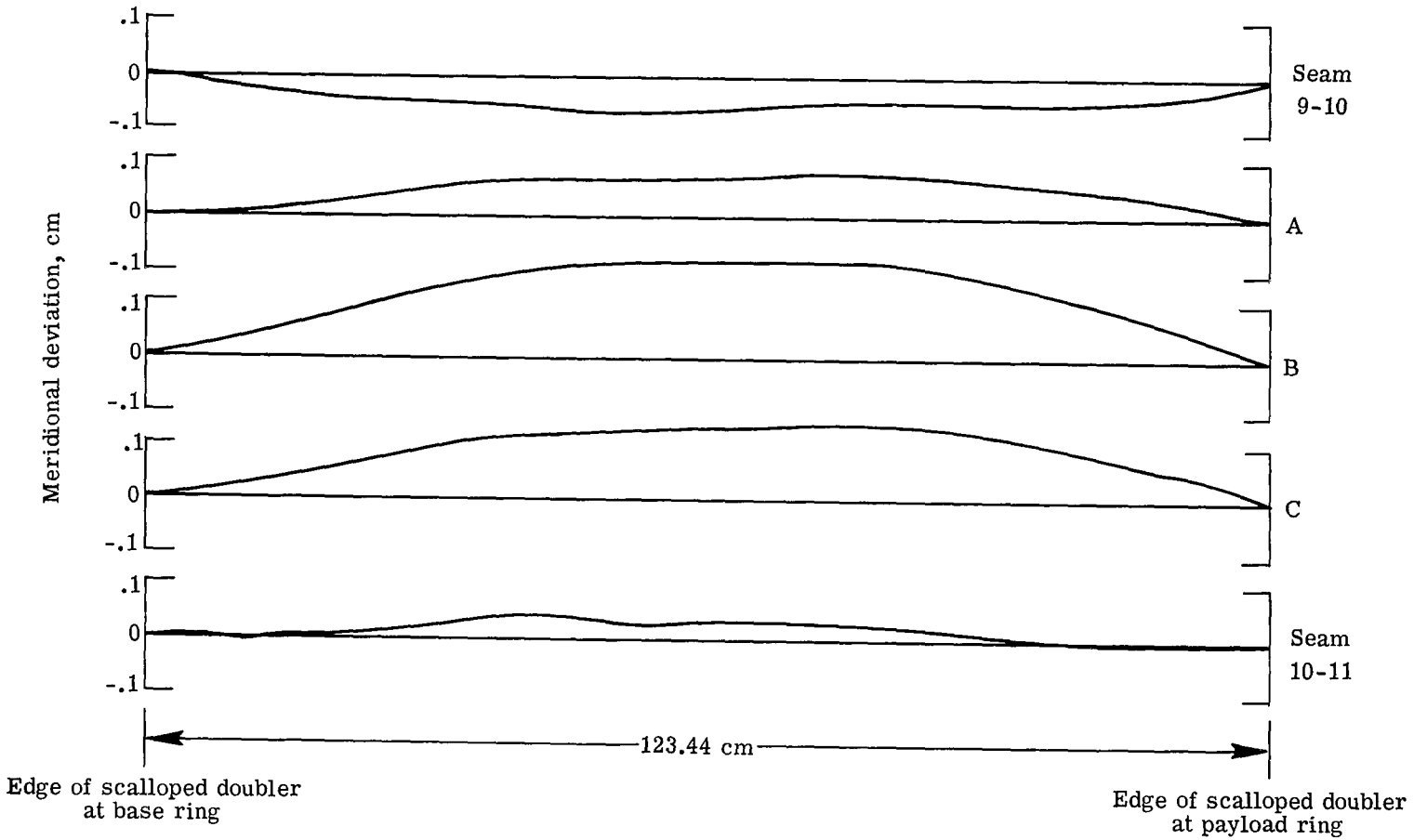

(j) Panel 10.

Figure 22.- Continued.

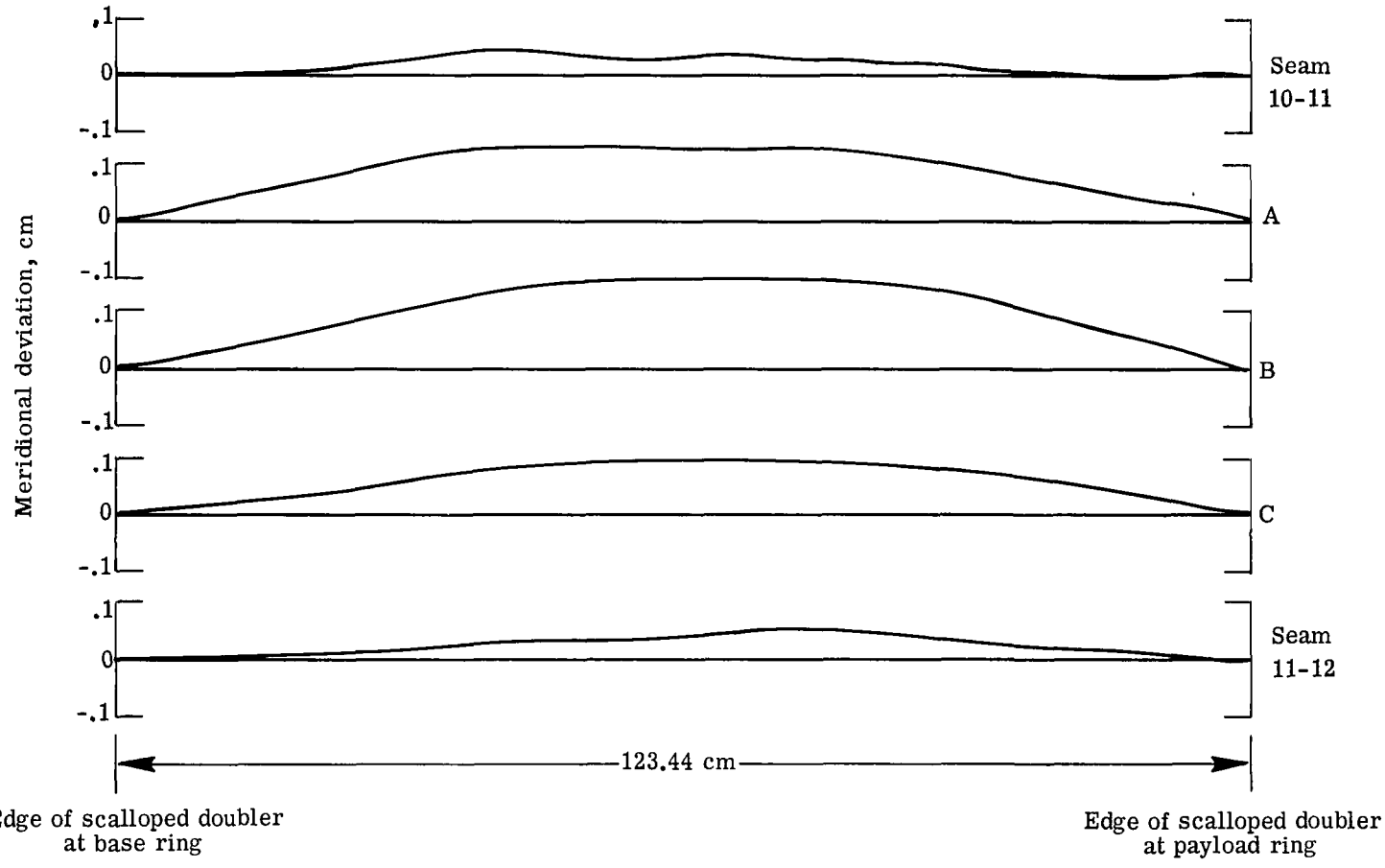

(k) Panel 11.

Figure 22.- Continued.

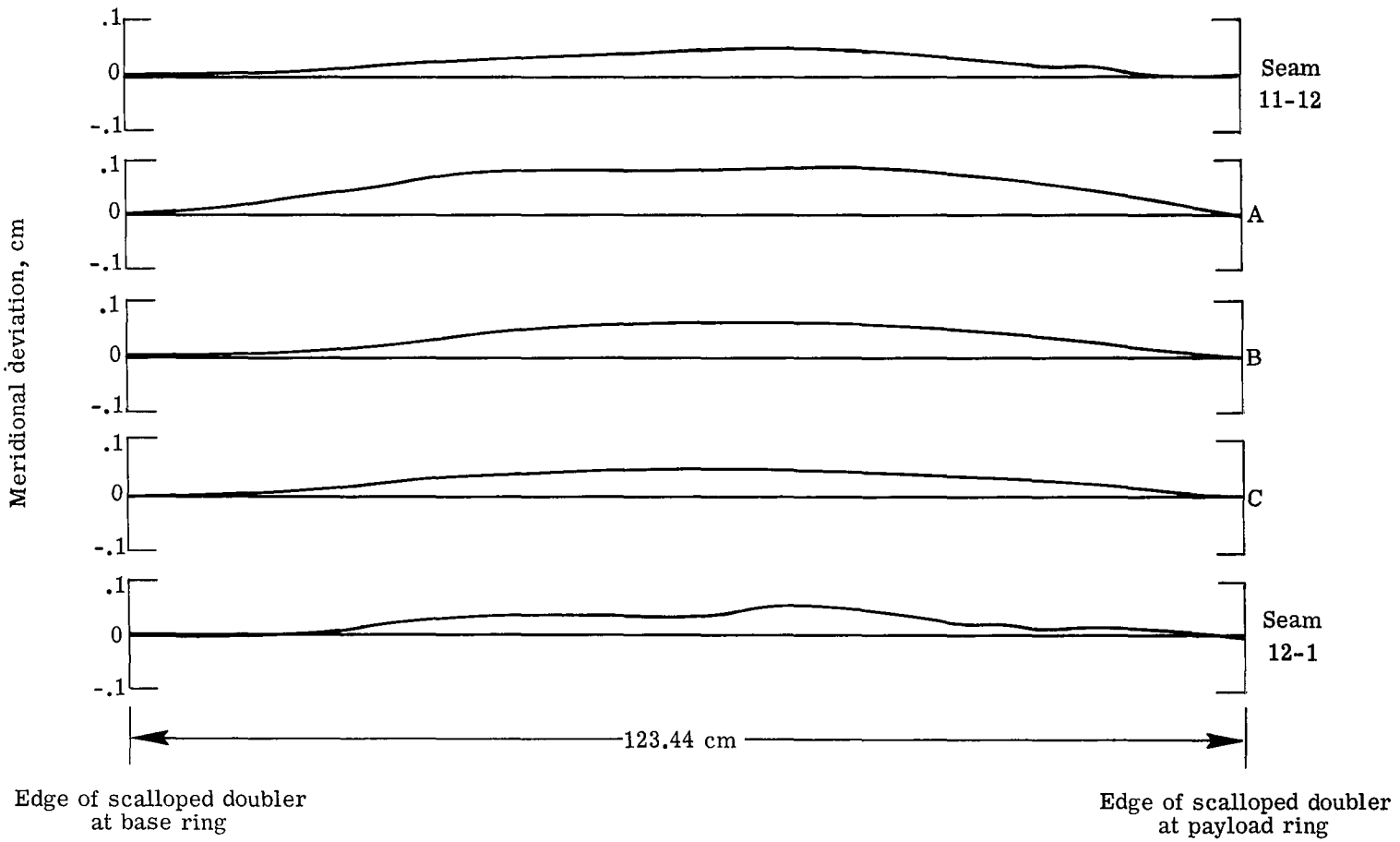

(l) Panel 12.

Figure 22.- Concluded.

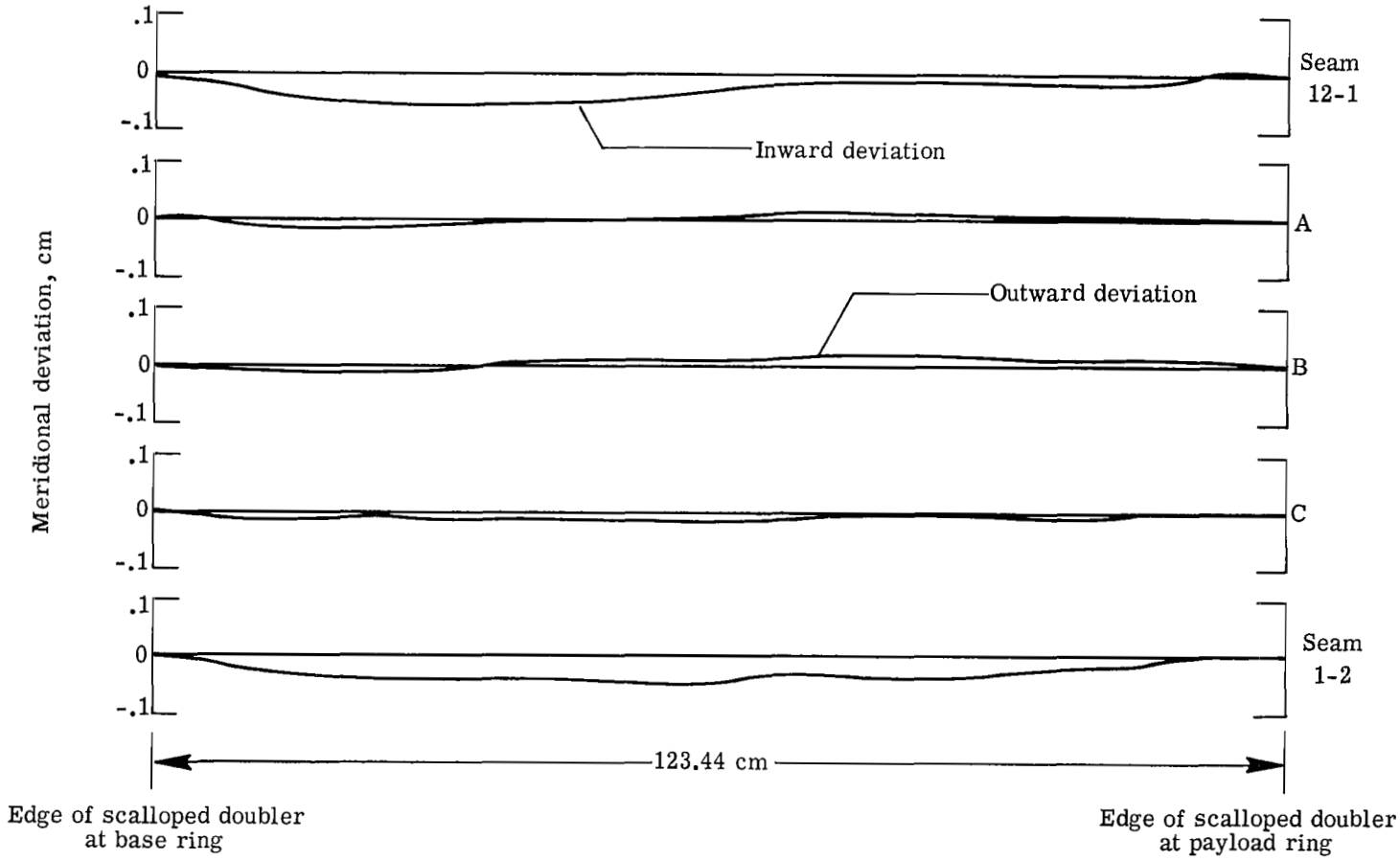

(a) Panel 1.

Figure 23.- Imperfection measurements of cone 3.

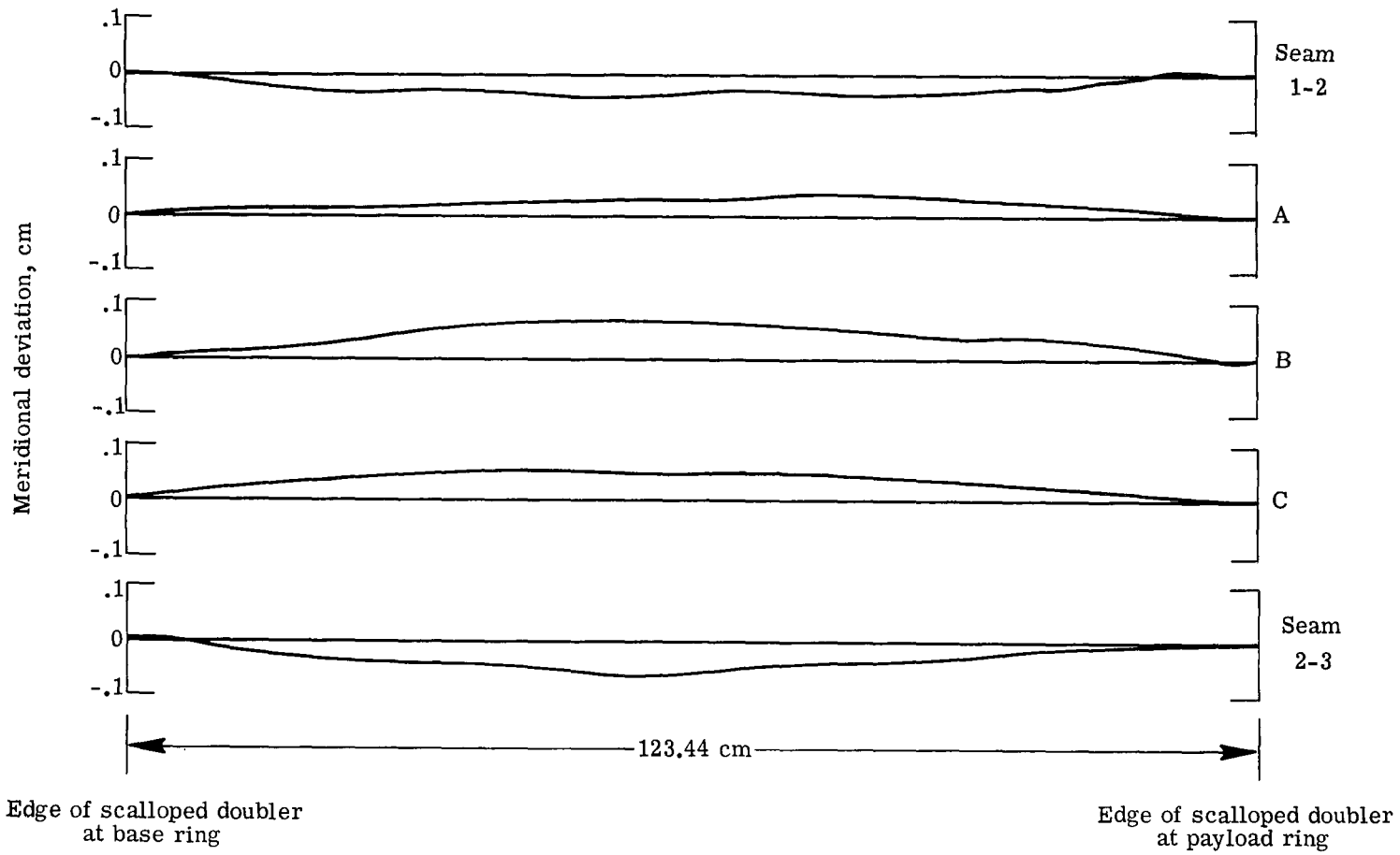

(b) Panel 2.

Figure 23.- Continued.

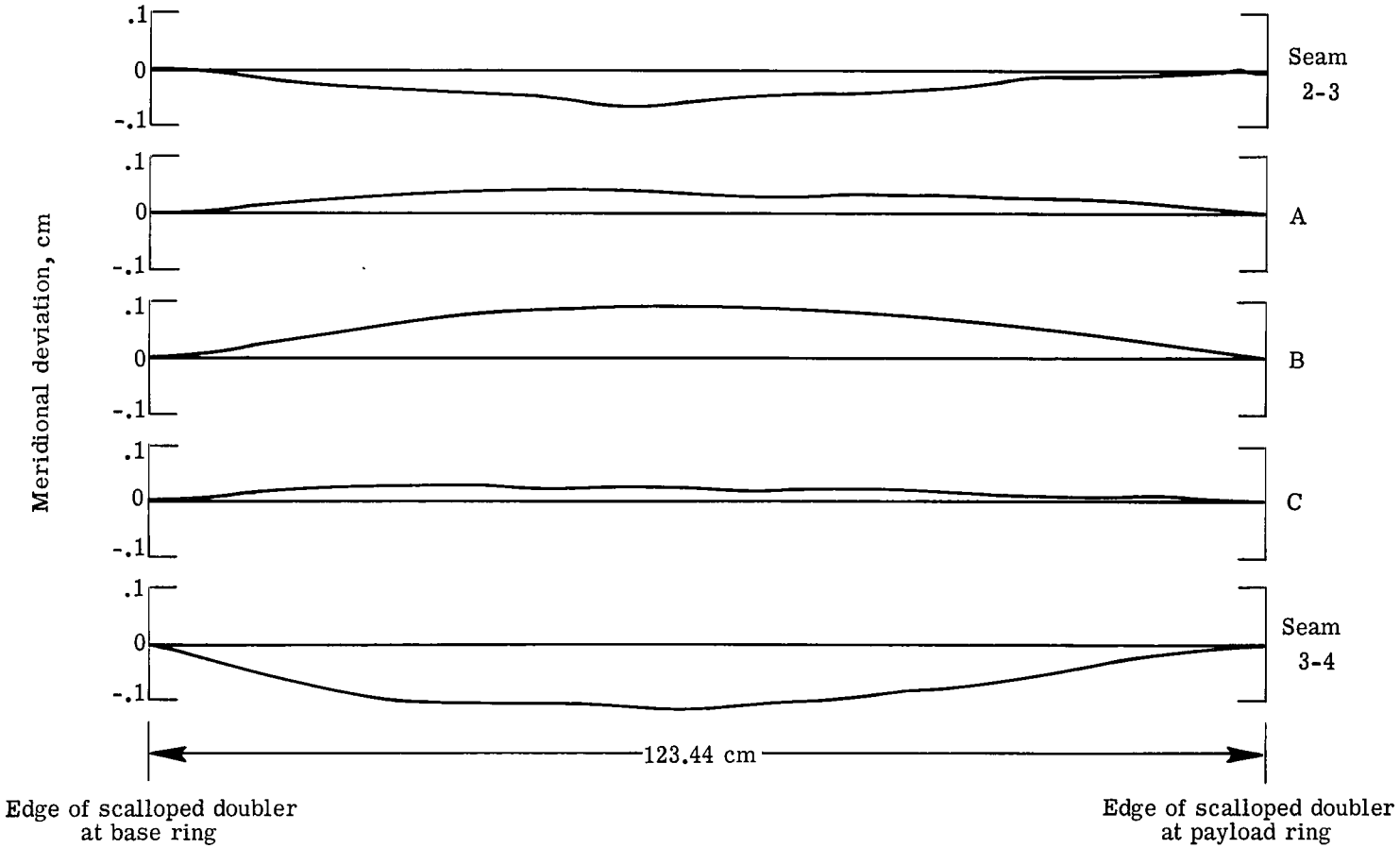

(c) Panel 3.

Figure 23.- Continued.

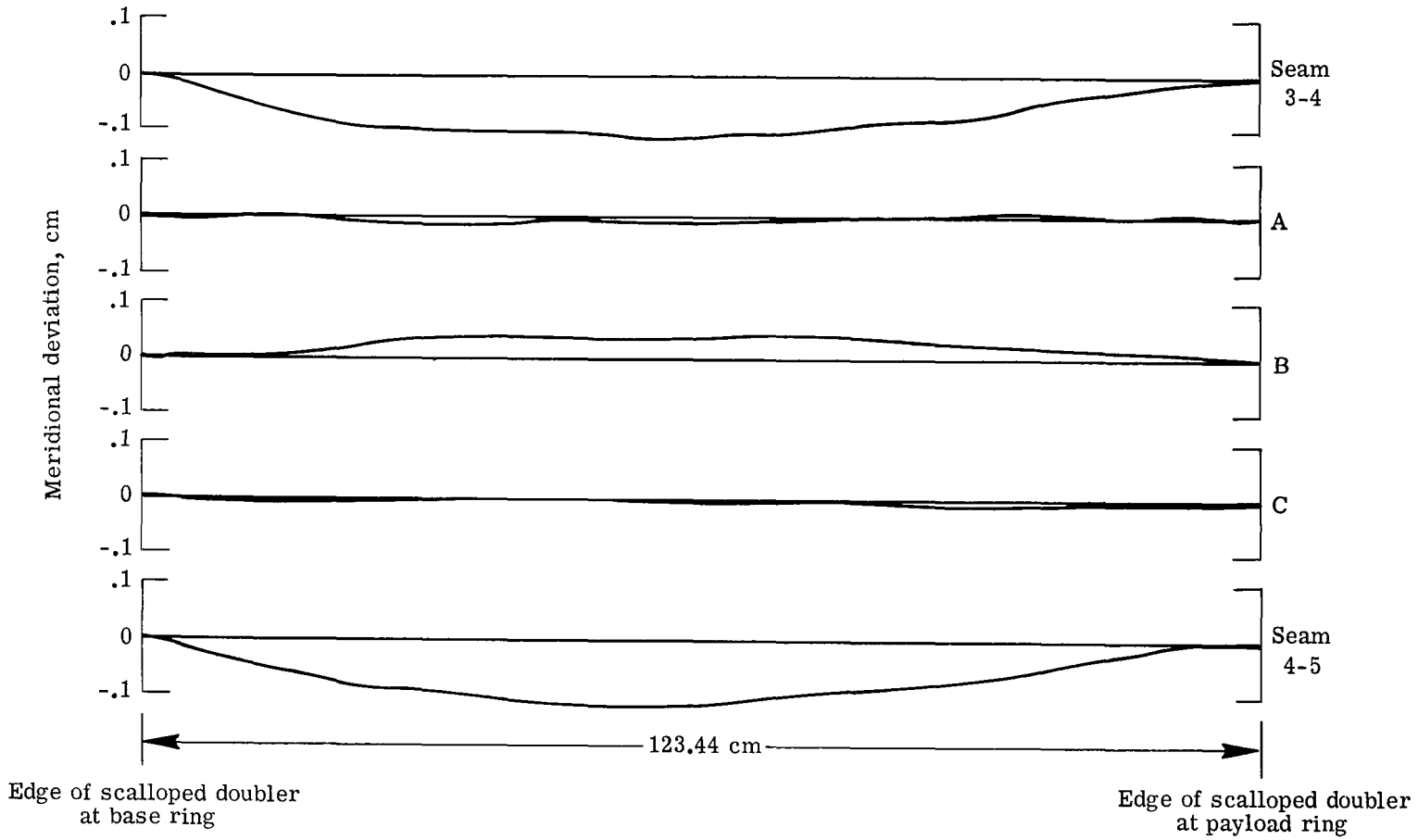

(d) Panel 4.

Figure 23.- Continued.

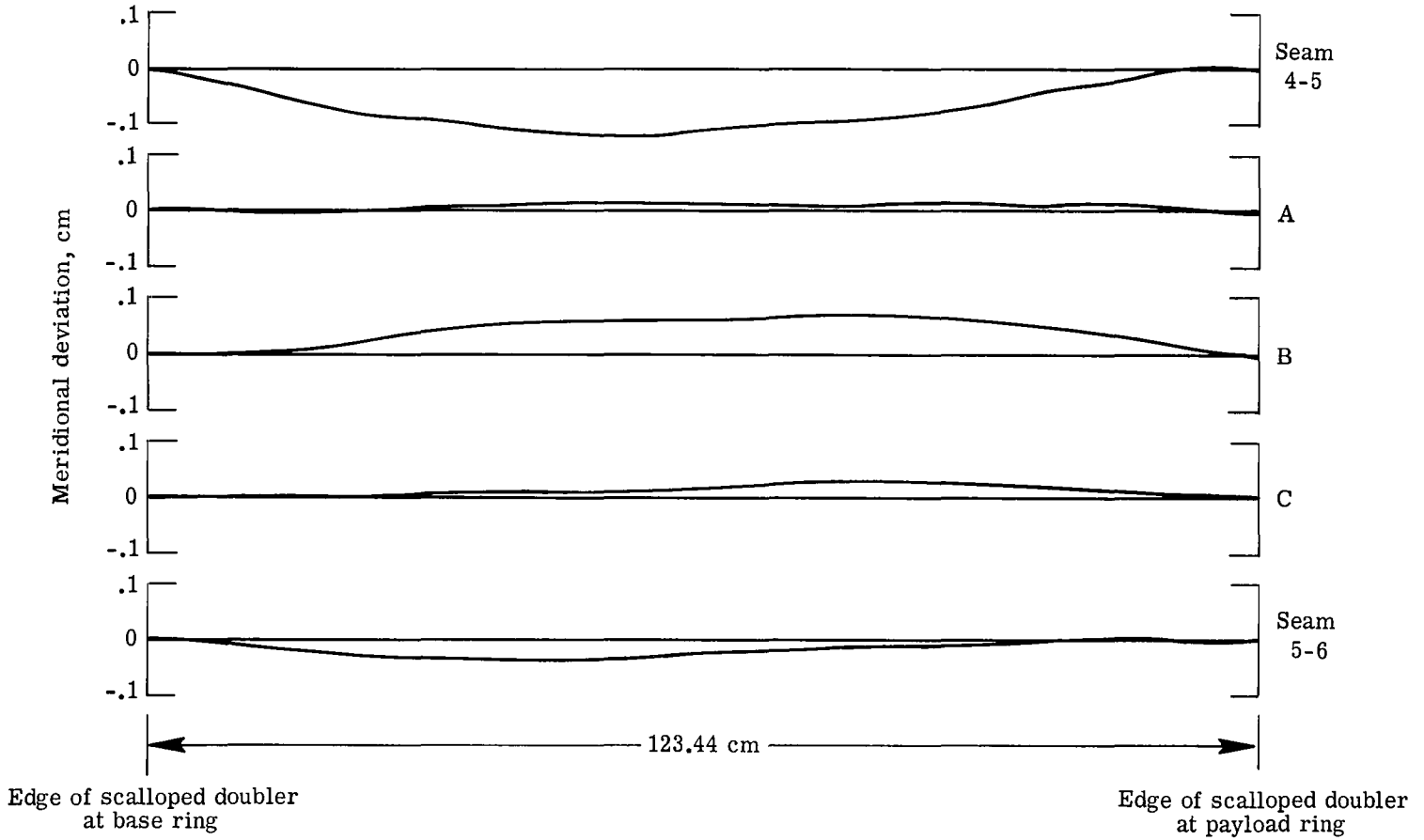

(e) Panel 5.

Figure 23.- Continued.

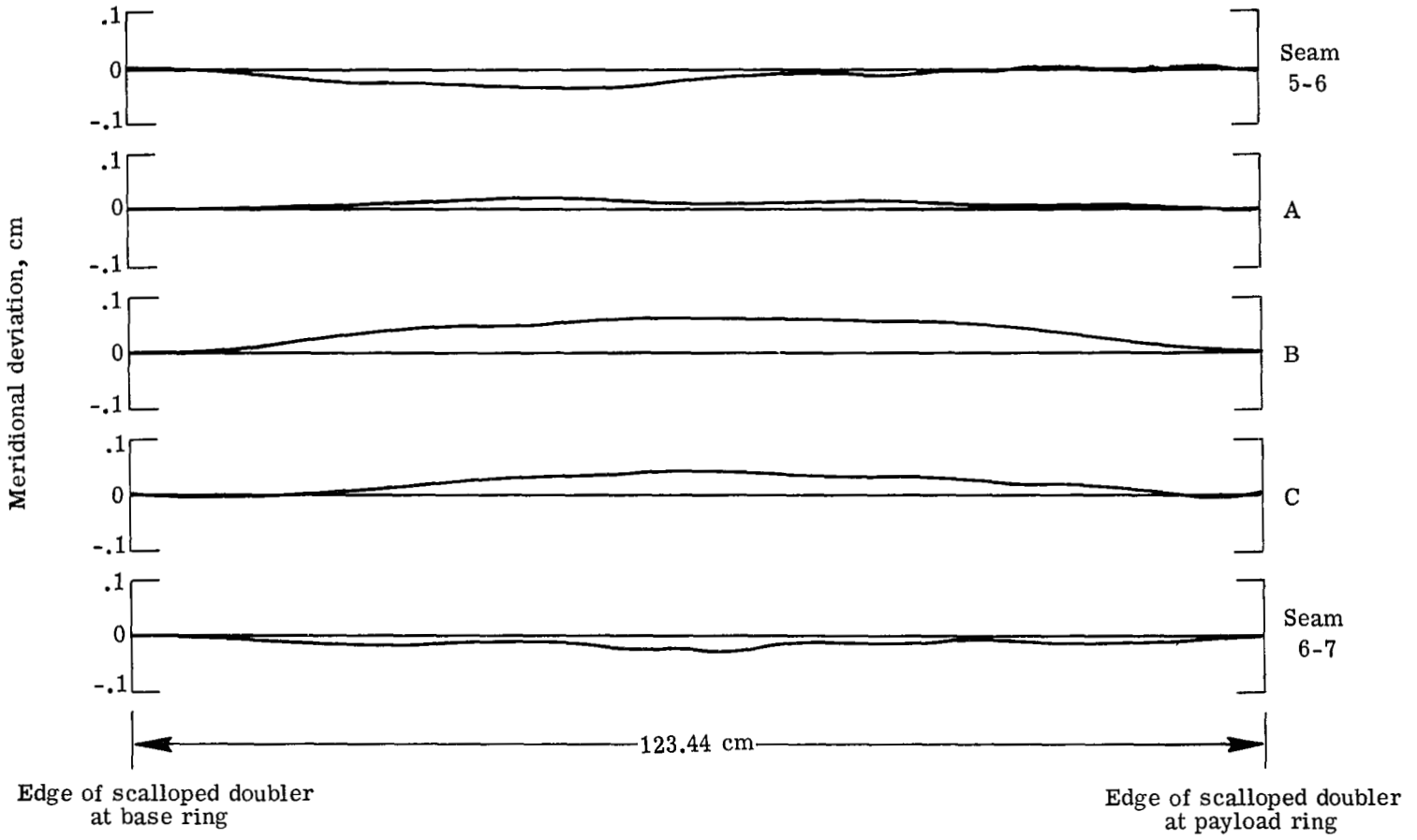

(f) Panel 6.

Figure 23.- Continued.

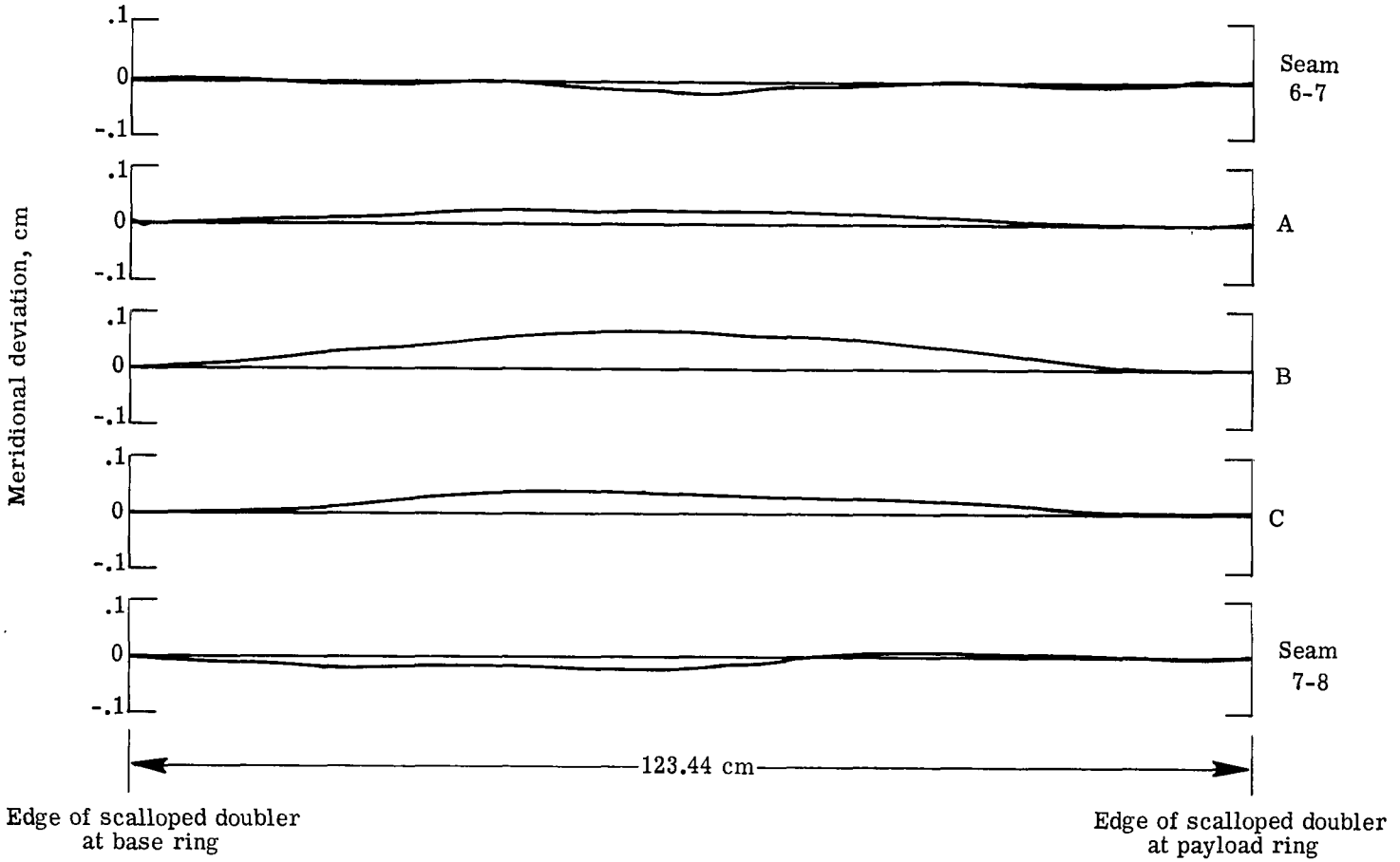

(g) Panel 7.

Figure 23.- Continued.

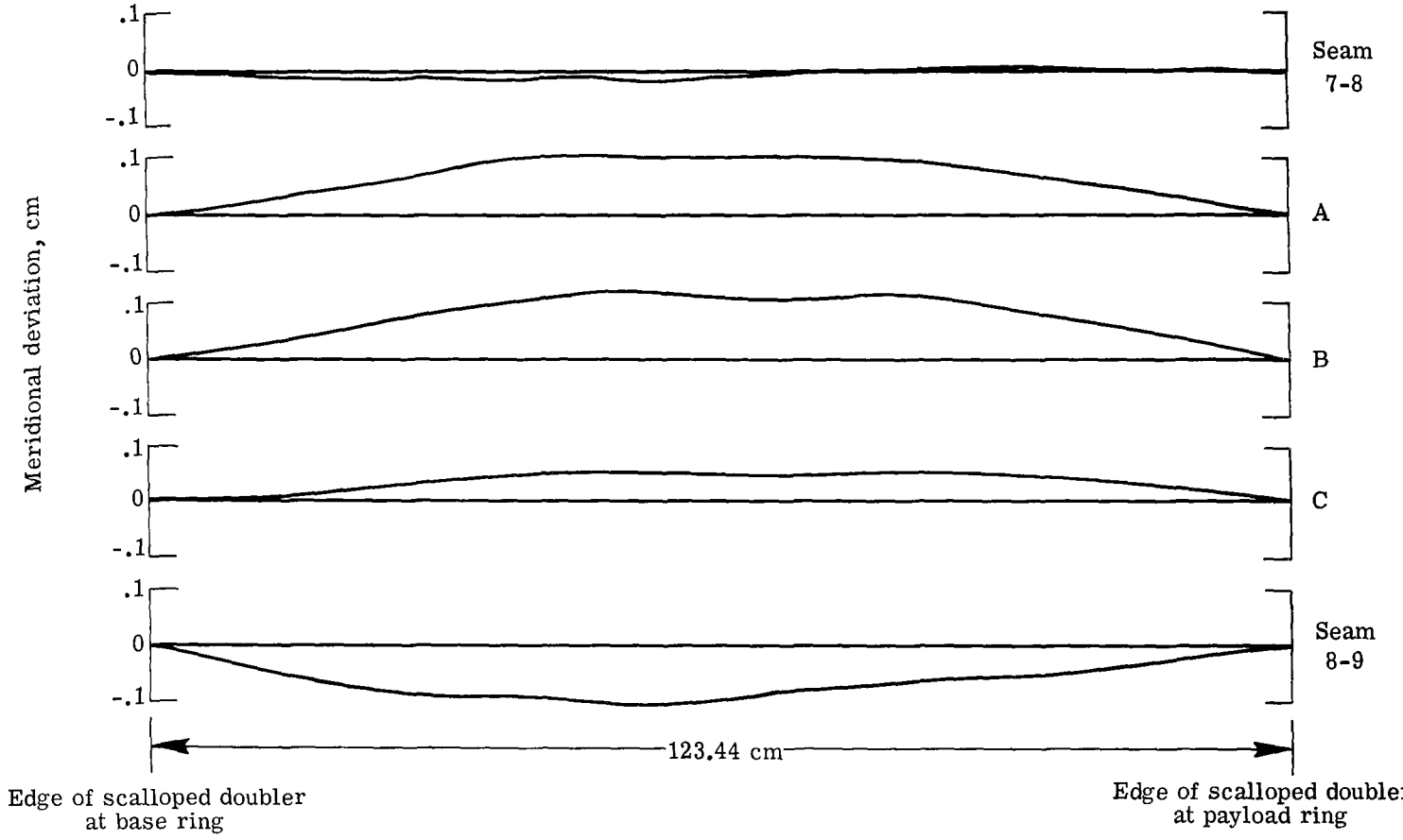

(h) Panel 8.

Figure 23.- Continued.

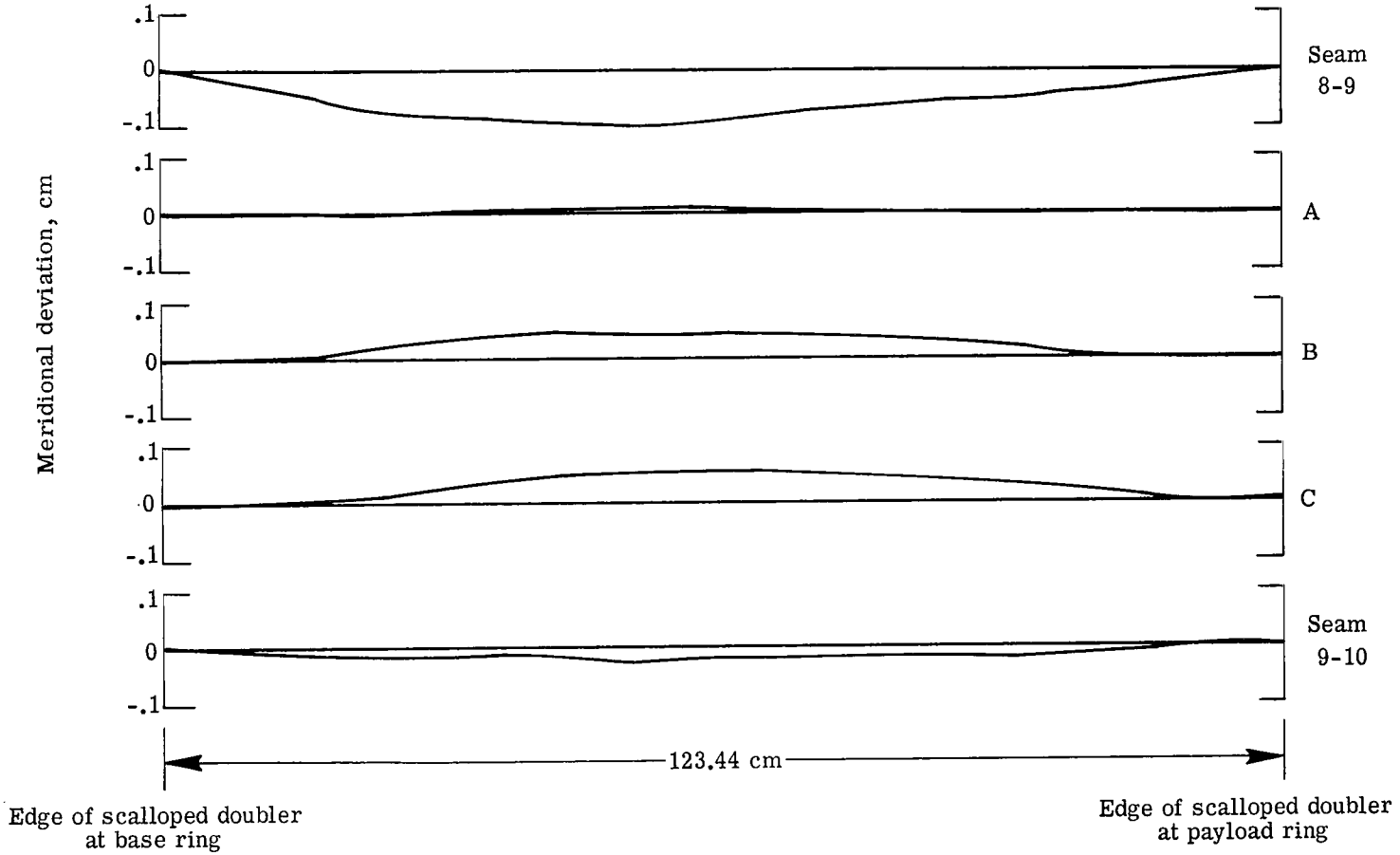

(i) Panel 9.

Figure 23.- Continued.

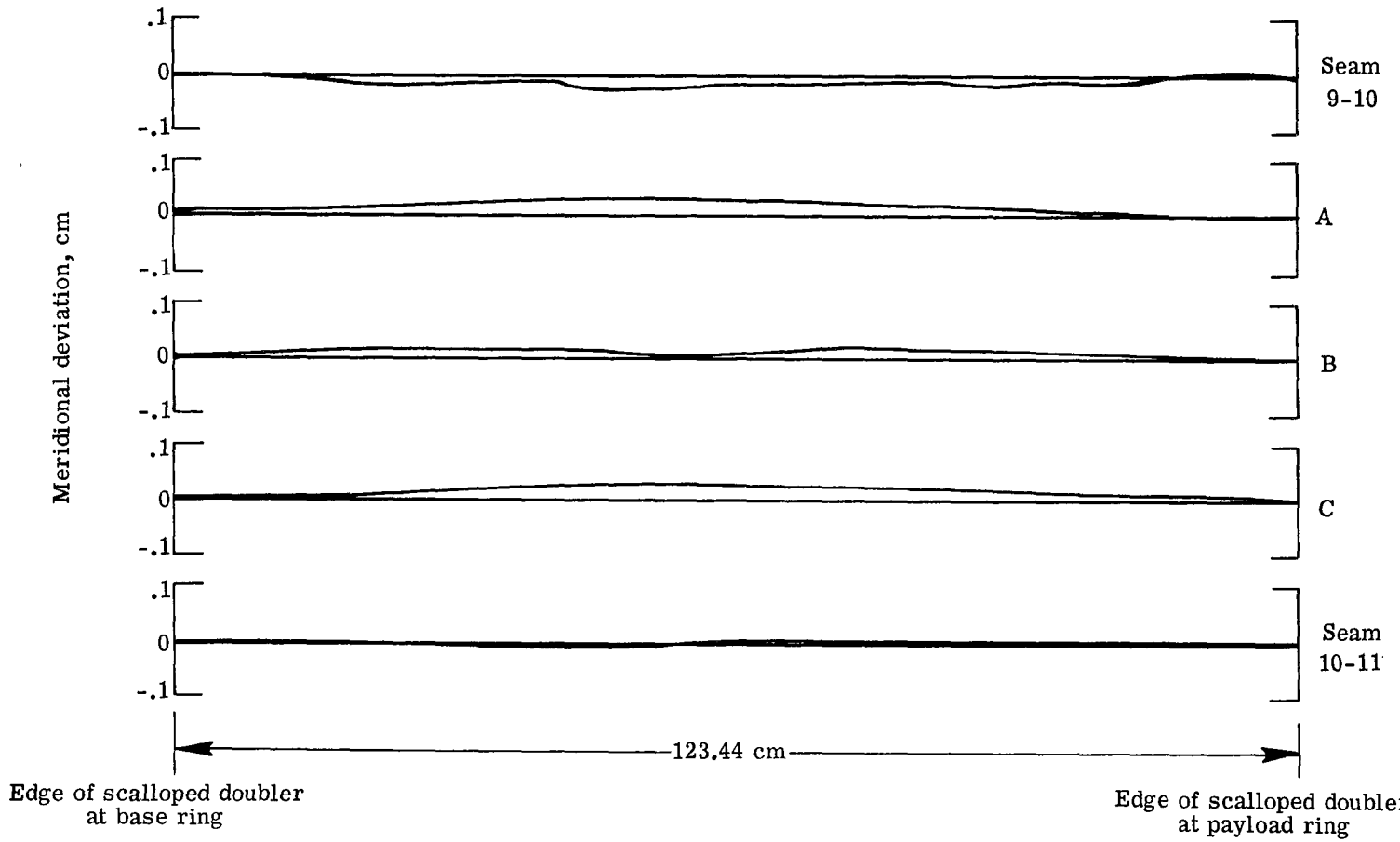

(j) Panel 10.

Figure 23.- Continued.

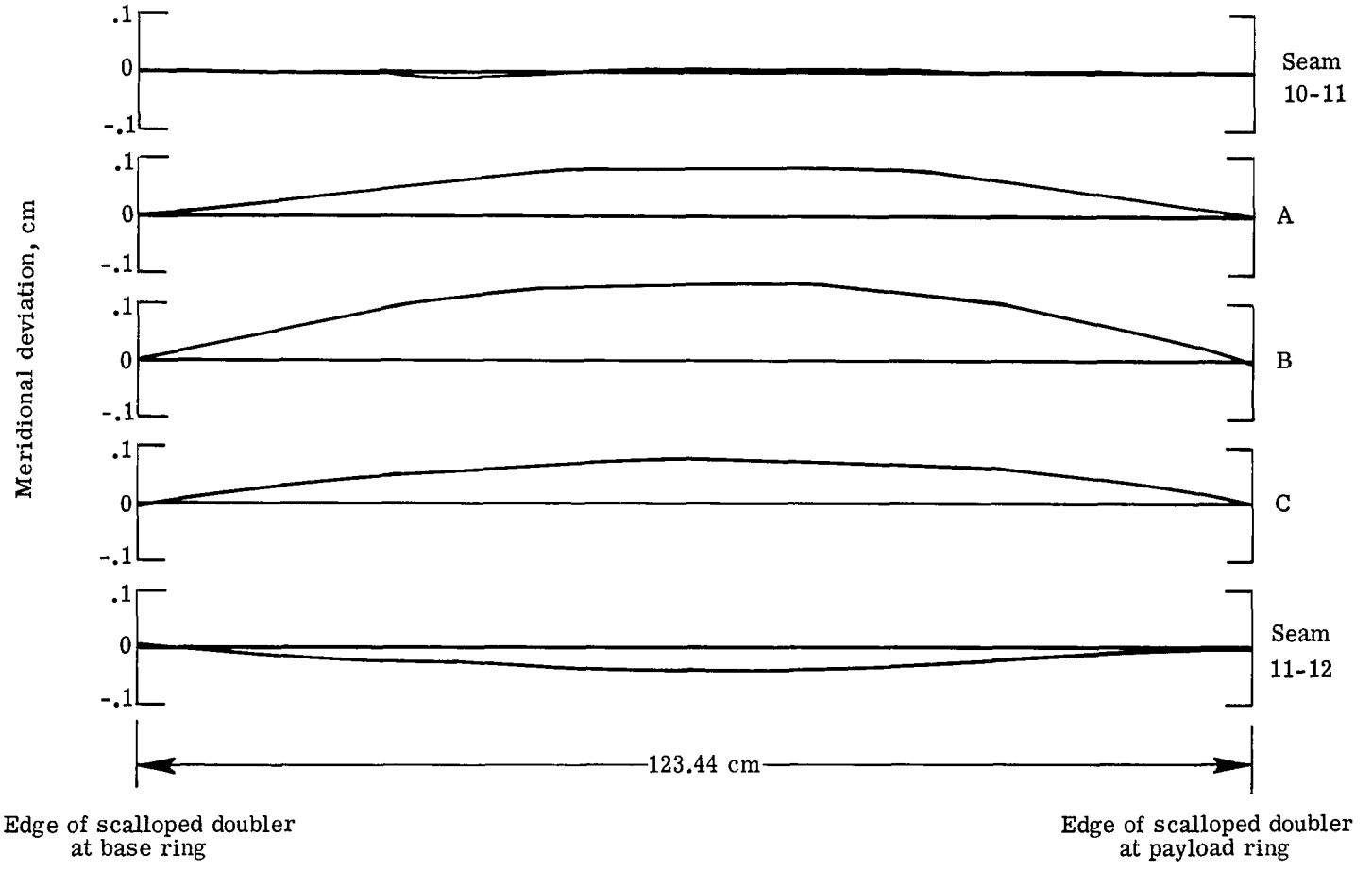

(k) Panel 11.

Figure 23.- Continued.

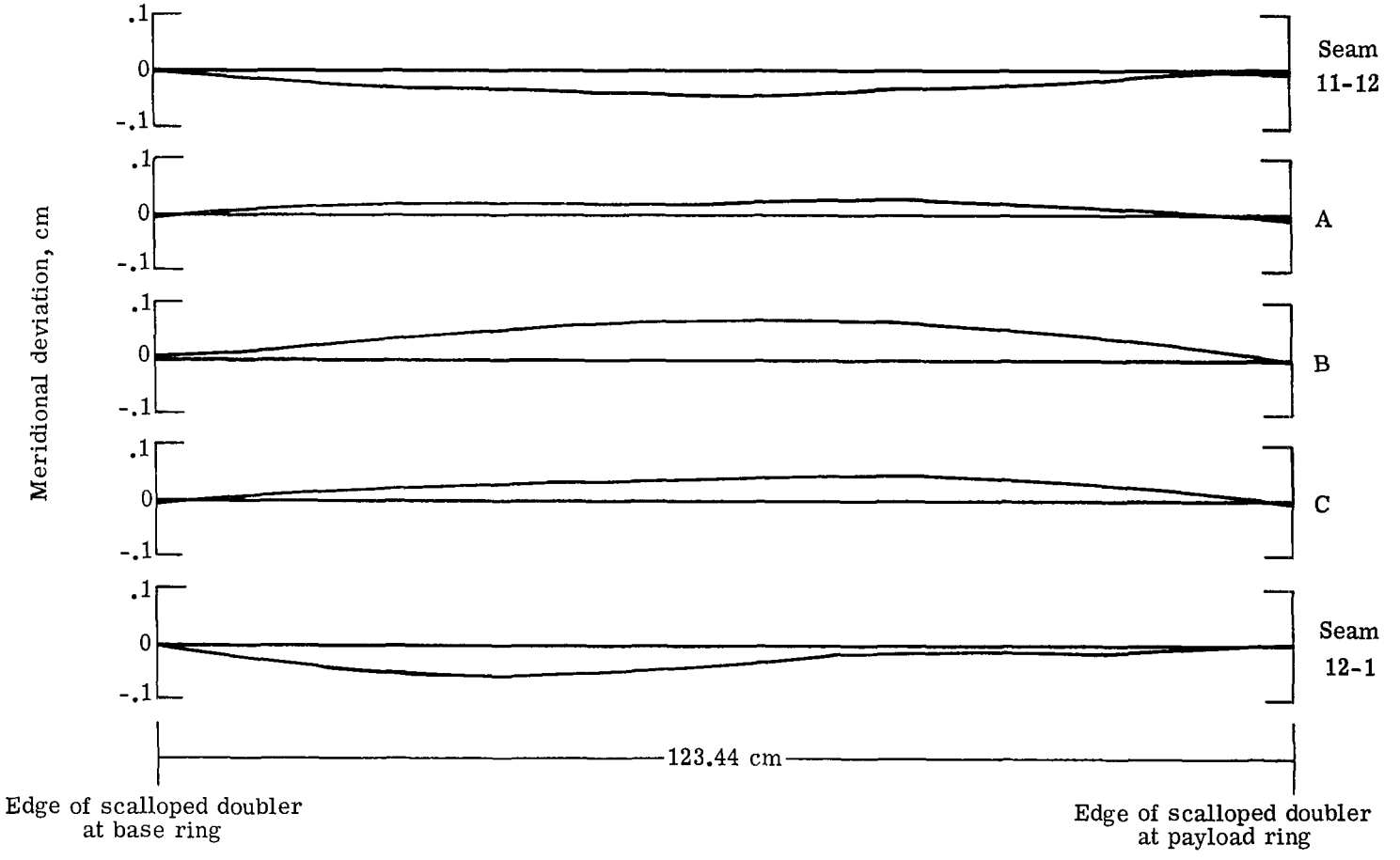

(l) Panel 12.

Figure 23.- Concluded.

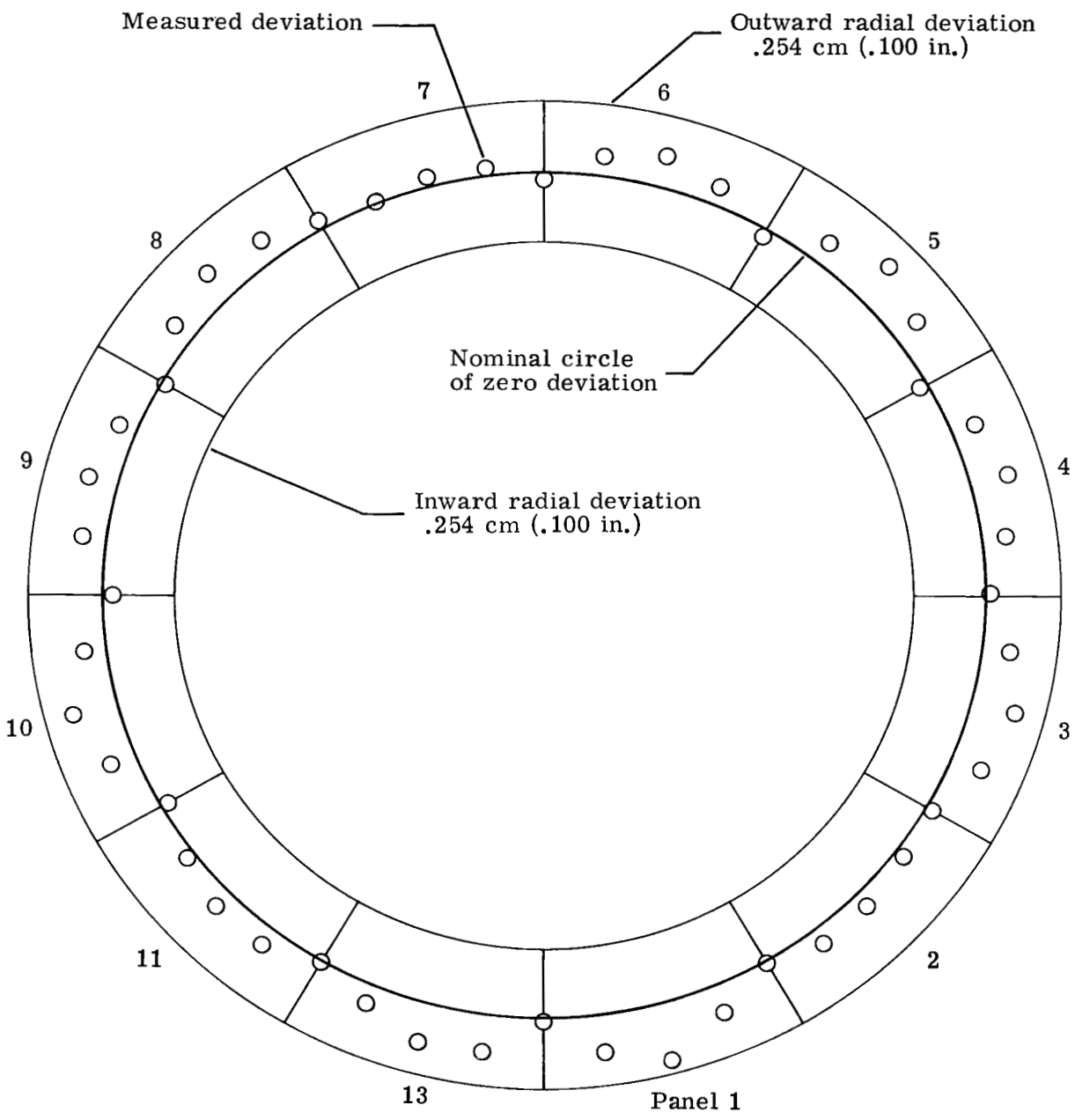

(a) Cone 1.

Figure 24.- Imperfection measurements at the meridional station.
s = 75.18 cm (29.60 in.).

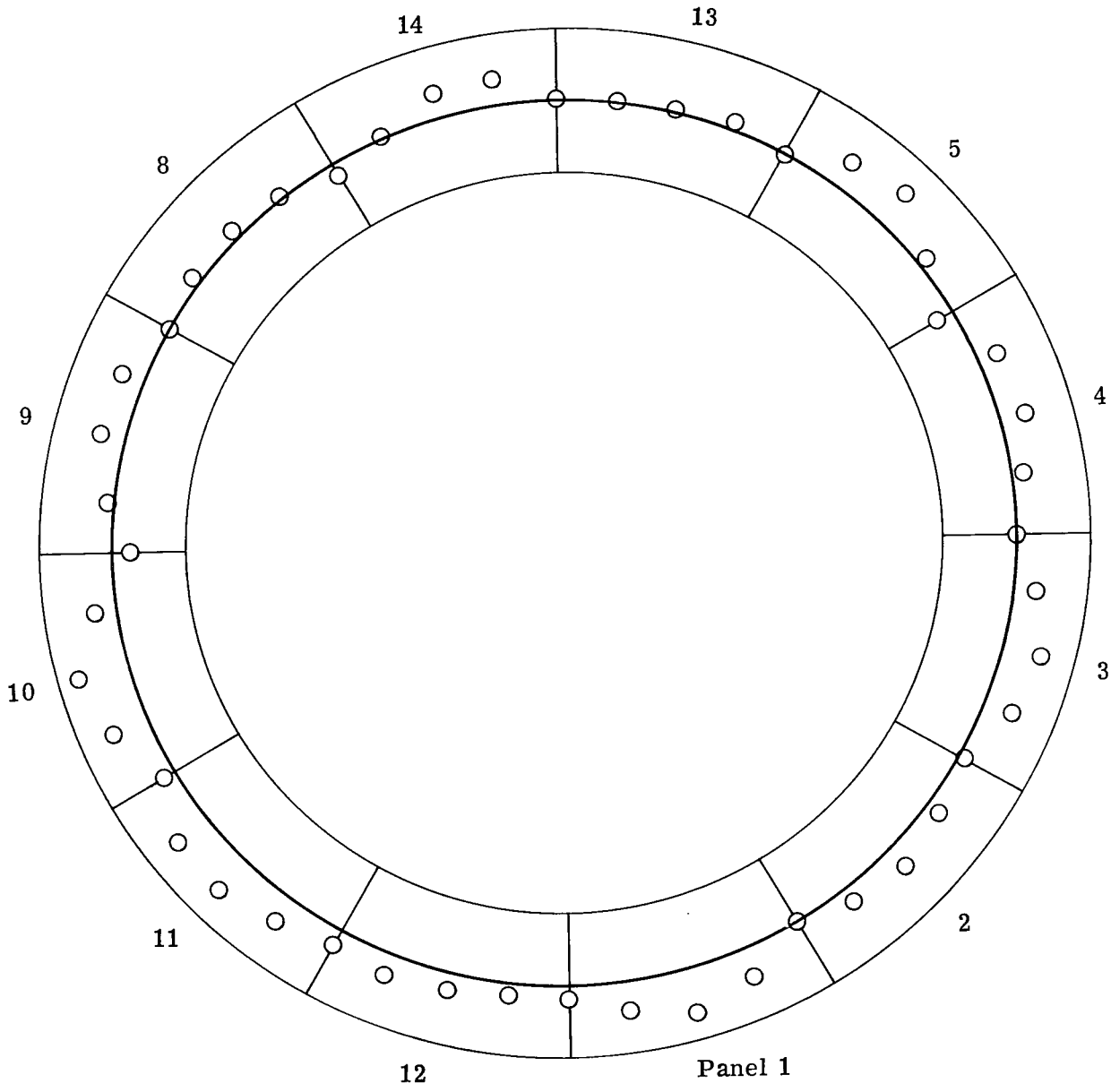

(b) Cone 2.

Figure 24.- Continued.

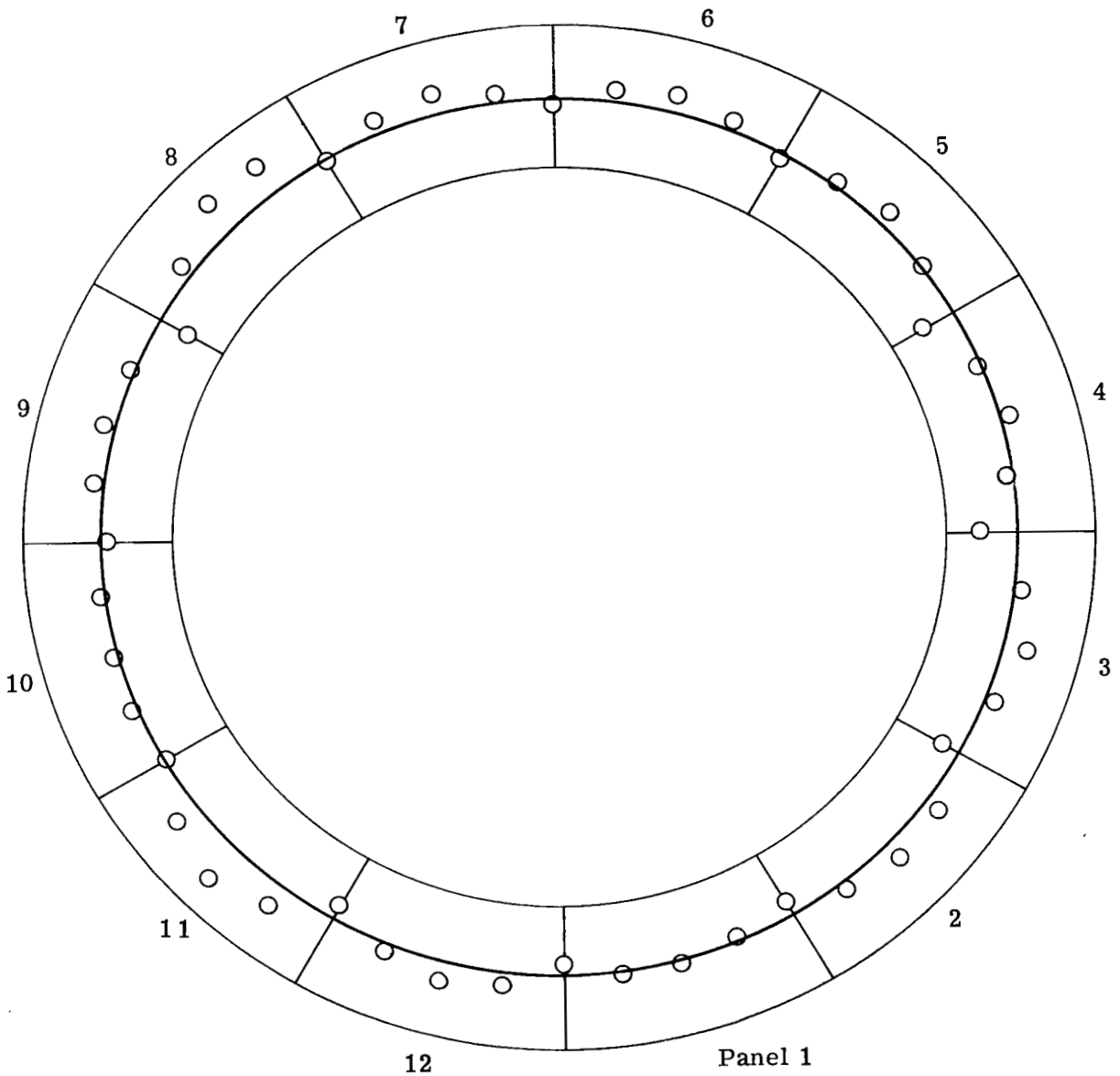

(c) Cone 3.

Figure 24.- Concluded.

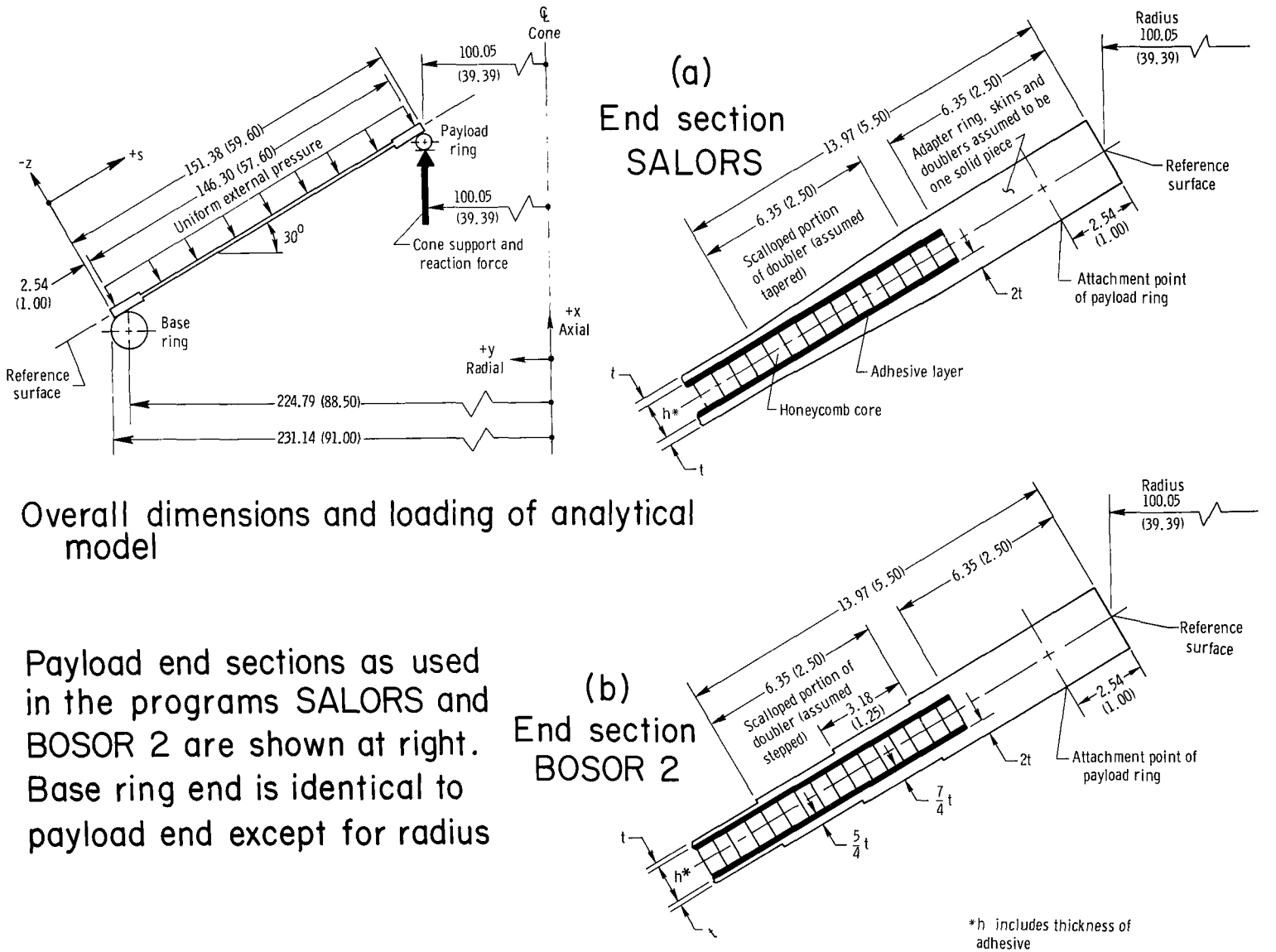

Figure 25.- Analytical models for program analyses. Dimensions given in cm (in.).

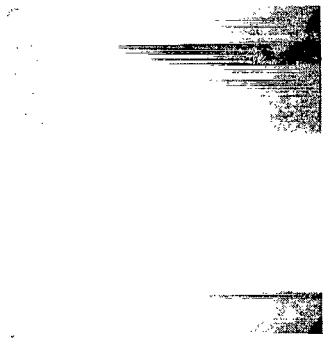

(a) Cone 1, panel 3.

(b) Cone 2, panel 13.

(c) Cone 3, panel 10.

L-75-151

Figure 26.- Photomicrographs of honeycomb sandwich walls. Magnification ×63.

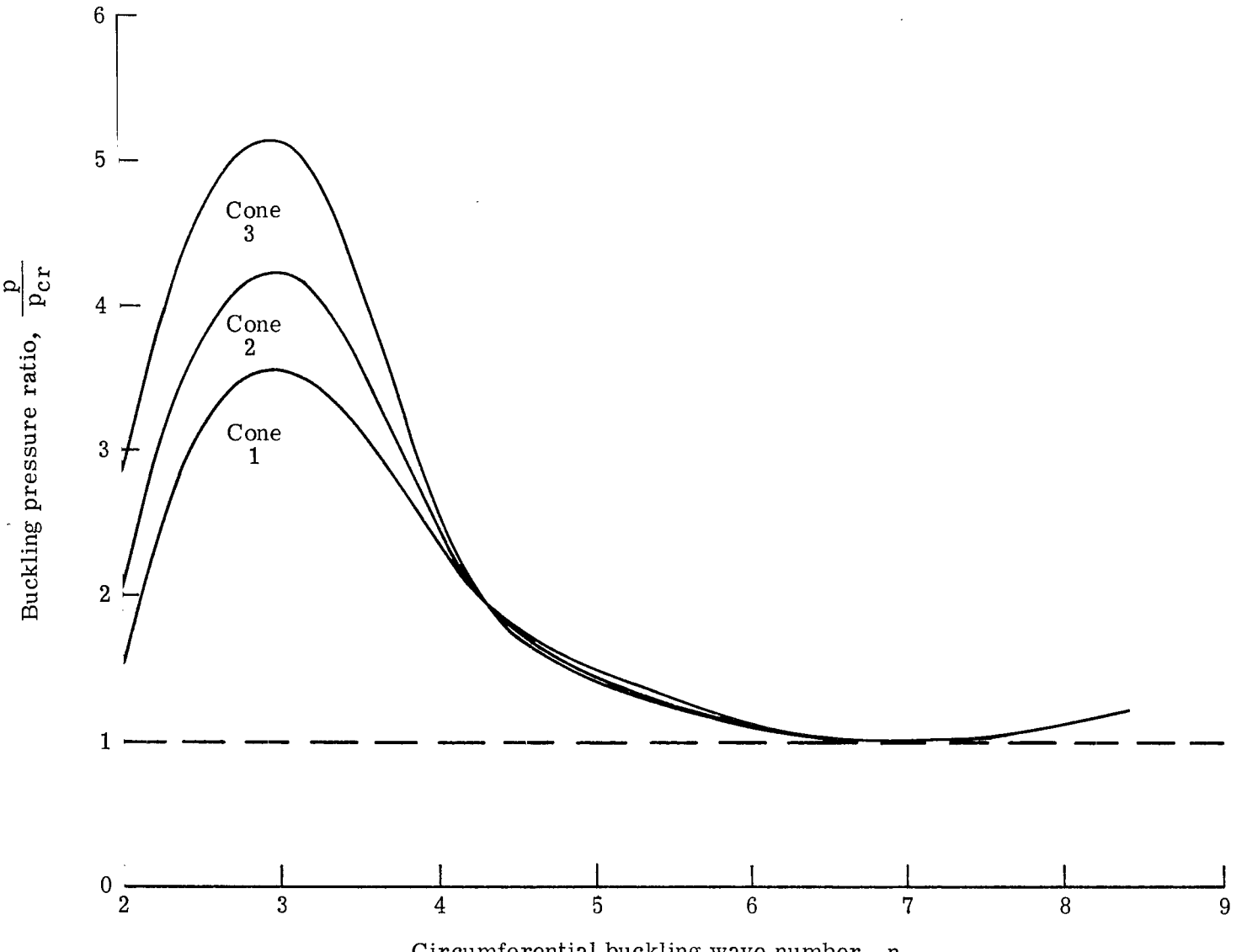

Figure 27.- Buckling pressure as a function of buckling mode, as computed by BOSOR 2.

"The aeronautical and space activities of the United States shall be conducted so as to contribute . . . to the expansion of human knowledge of phenomena in the atmosphere and space. The Administration shall provide for the widest practicable and appropriate dissemination of information concerning its activities and the results thereof."

—NATIONAL AERONAUTICS AND SPACE ACT OF 1958

NASA SCIENTIFIC AND TECHNICAL PUBLICATIONS

TECHNICAL REPORTS: Scientific and technical information considered important, complete, and a lasting contribution to existing knowledge.

TECHNICAL NOTES: Information less broad in scope but nevertheless of importance as a contribution to existing knowledge.

TECHNICAL MEMORANDUMS: Information receiving limited distribution because of preliminary data, security classification, or other reasons. Also includes conference proceedings with either limited or unlimited distribution.

CONTRACTOR REPORTS: Scientific and technical information generated under a NASA contract or grant and considered an important contribution to existing knowledge.

TECHNICAL TRANSLATIONS: Information published in a foreign language considered to merit NASA distribution in English.

SPECIAL PUBLICATIONS: Information derived from or of value to NASA activities. Publications include final reports of major projects, monographs, data compilations, handbooks, sourcebooks, and special bibliographies.

TECHNOLOGY UTILIZATION PUBLICATIONS: Information on technology used by NASA that may be of particular interest in commercial and other non-aerospace applications. Publications include Tech Briefs, Technology Utilization Reports and Technology Surveys.

Details on the availability of these publications may be obtained from:

SCIENTIFIC AND TECHNICAL INFORMATION OFFICE

NATIONAL AERONAUTICS AND SPACE ADMINISTRATION

Washington, D.C. 20546